Università degli Studi di Salerno

Dipartimento di Chimica e Biologia "A. Zambelli"

Corso di Dottorato di Ricerca in Chimica

Ciclo XXIX

Tesi di Dottorato in: **"Metathesis reactions catalyzed by ruthenium complexes for the self-healing of aeronautical materials"**

Tutor: Prof. Pasquale Longo

Co-tutor: Prof. Liberata Guadagno

Coordinatore: Prof. Gaetano Guerra

Candidato: Anna Agovino

Matr. 8880700208

Anno Accademico 2017/2018

A mia figlia Laura
e a Mariano, compagno di vita

Ci sono emozioni nel tuo cuore
di cui non conosci l'esistenza...
finchè non nasce un figlio

OUTLINE

This PhD thesis reports some advances in the field of aeronautical materials with self-repairing ability, in particular is investigated the design of new generation systems with healing properties.

The self-healing ability of the engineering material can prolong the life of the material itself thanks the repairing mechanisms that starts at the same moment in which the materials are damages.

In **Chapter 1**, the self-healing materials are described, as literature reports, focusing on their aeronautical application and several critical issue.

In **Chapter 2** are described the covalent functionalization of the carbon based nanomaterials with Ruthenium based catalysts. In the first part is reported the functionalization of graphene oxide and the protection of the catalytic site by a polymeric globular shell to make the catalyst more thermally stable. In the second part is reported the covalent functionalization of multi-walled carbon nanotubes and graphite by electrochemical modification and 1,3 dipolar cycloaddition at the aim to support the metathesis catalysts and at the same time preserve the chemical and physical properties of the pristine filler.

In **Chapter 3**, for the same purpose, is illustrated a non-covalent functionalization of the carbon based nanomaterials to support the Ruthenium based catalysts of several carbon nanofiller.

However, the carbon nanoparticles are used in the composite materials to improve the electrical, thermal and mechanical properties but shown the great problem of the aggregation, that can

be overcome using a polymer as compatibilizer. Through this functionalization, is possible obtain many polymers capable of linked on any filler able to establish π-stacking interaction, this aspect is described in the last section of this chapter.

Chapter 4 proposed a new generation system for the self-healing ability of the composite materials, based on Cu(0) catalysts active in the polymerization of styrene at room temperature, rarely reported in literature.

At the end of each chapter is reported the Experimental Part, the Conclusion and the References.

ABSTRACT

CHAPTER 1
AERONAUTICAL MATERIALS WITH SELF-HEALING ABILITY

CHAPTER 2

COVALENT FUNCTIONALIZATION OF THE CARBON NANOFILLER

CHAPTER 3

NON COVALENT FUNCTIONALIZATION OF THE CARBON NANOFILLER

CHAPTER 4

RADICAL POLYMERIZATION OF STYRENE WITH Cu-BASED CATALYST

ABSTRACT

In this work of PhD thesis, Ruthenium catalysts were covalently and non-covalently bound to carbon-based nanomaterials, in order to allow self-repairing reactions in aeronautical materials. These supported catalysts have been characterized and their activity has been evaluated in metathesis reactions.

The 1st and 2nd generation Grubbs and Hoveyda-Grubbs catalysts were covalently bonded to graphite oxide and tested in the ring-opening metathesis polymerization reaction of tensed monomers, and subsequently their catalytic activity was verified in the aeronautical composites. To optimize the performance of such supported catalysts, catalytic sites have been protected from the highly reactive environment by a polymeric globular shell.

These catalysts have been also supported on multi-walled carbon nanotubes and graphite by an alternative covalent synthetic approach that allows to preserve the chemical and physical properties of the carbon nanotubes employed, avoiding the initial oxidation step.

For non-covalent functionalization, the same catalysts were first linked to pyrene molecules and then, by π-stacking, anchored on graphite. Their activity was determined in metathesis reactions and the conductivity of modified nanofiller was estimated within aeronautical composites. Such complex pyrene-catalyst, highly versatile, have been used to synthesize polymers having a terminal pyrene capable of improving the dispersion of the same carbon nanotubes used in aeronautical materials in order to improve their

performance.

Lastly, was evaluated the possibility of self-repairing the aeronautical material through radical polymerization of monomers such as styrene, using Copper catalysts.

CHAPTER 1
AERONAUTICAL MATERIALS WITH SELF-HEALING ABILITY

1.1 Self-healing materials

The possibility of preserving the structural integrity of a material over time is a very important aspect that drives the research to focus attention in this direction. There is a possibility to associate this aspect at repair mechanisms that trigger at the same moment in which the material is damaged, rather at the characteristics of the material itself. This new idea in the '90s has stimulated the researcher in the application of self-healing materials.

In a self-healing material, following the formation of a fractures in the structure, triggered mechanisms that restore the structural integrity of the material before that the fractures can propagate and compromise its performance.

The application of these materials are very broad, ranging from building materials, to electronics, to transport. The materials that show self-healing properties are distinguished in extrinsic, whose self-healing ability is due to the addition of an external repair agent; and in intrinsic, whose repairing capacity is due to the chemical nature of the material itself.

The extrinsic materials are further distinguished for the catalytic and non-catalytic repair mechanism. In both cases the repair agent is

embedded in microcapsules or in a network of capillaries or empty channels (vascular networks, that can be made up of glass fibers or carbon fiber layers.), which can be interconnected in one, two or three dimensions, depending on the complexity of the system. In all systems the repair mechanism is triggered by the breakdown of the microcapsules or the network with subsequent release of the repair agent in the affected region.

A third option is to disperse particles of the repair agent into the matrix, however in this case it is necessary to provide heat to initiate the repair process.

The research over the last decades has focused on the use of microcapsules, as the design and production of vascular networks, although offering more contact points and hence better results, is too difficult.

Microcapsules can be used, beyond the self-healing, in almost limitless applications, such as agricultural, drugs delivery, food, paints and coatings and several other industries. Recently, explosives have been encapsulated to reduce their sensitivity.

Synthesis and production of microcapsules is quite complex because they must have different requirements: the synthesis procedure should be compatible with the core material, microcapsules must have long enough shelf lives and must not allow the diffusion of healing agent out of them (shell wall should not be porous), and shell wall must be well-built and adequately hard to survive the processing circumstances of the matrix composite, as well as maintaining good adhesion with the processed resin matrix [1].

Most of the microcapsules used for this purpose can be made up of

poly(urea-formaldehyde), poly(melamine-formaldehyde), poly(melamine-urea-formaldehyde), polyurethane and acrylates and are prepared by the in situ interfacial polymerization technique [2].

The self-repairing processes, proposed in the literature over the last few years, distinguish the materials with self-healing properties in two categories: non-autonomous systems, in which the repair process can be activated with external stimulation by using electric or magnetic fields, thermal treatments or chemistry; and in autonomous systems, in which the self-repair process is triggered automatically by the effect of cracking within the polymer matrix.

The application of self-healing materials is very important in the aeronautical field because the design and formulation of structural materials with self-repairing ability, is one of the most important objectives for the construction of structural aircraft parts. The use of this materials can avoid the inevitable process of deteriorating of the external structures of the planes subjected to the formation of cracks that originate to accidental events unobtainable to the naked eye caused by hail, stones on the keel during landing, accidentally contacted during maintenance and above all with flying birds. Thermo-hardening composite materials with self-healing capacity can cope these problems. Many realistic strategies have been formulated in the development of self-healing materials; a very promising system for thermosetting resin was proposed by White et al [3].

1.2 THE WHITE'S SYSTEM

The first thermosetting system with self-healing ability was proposed by White et al. which formulated and characterized a multifunctional extrinsic autonomically healing composite.

This formulation consists of incorporating a microencapsulated healing agent and a catalytic chemical trigger within an epoxy matrix. The self-repair function is based on the metathesis polymerization of a healing agent activated by the catalyst (*Fig. 1.1*).

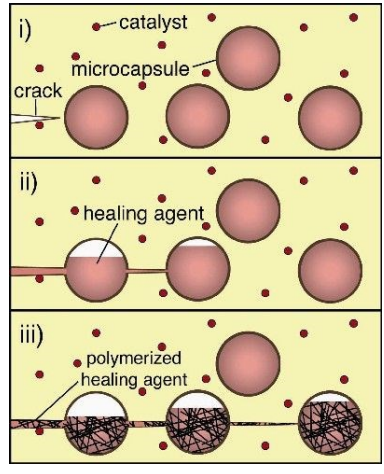

Figure 1.1: Step of the repairing mechanism that begins after a fractures.

An approaching crack ruptures embedded microcapsules releasing the curing agent into the crack plane through capillary action. Polymerization of the healing agent is triggered by contact with the embedded catalyst, bonding the crack faces. In these systems, the efficiency of self-repair function in terms of trigger, speed, and yield

is related to ring-opening metathesis polymerization (ROMP) of the healing agent by appropriate catalysts. The healing agent is a microencapsulated liquid monomer that must include a long shelf life, prompt deliverability, high reactivity, and low volume shrinkage upon polymerization [2], but also a high degree of crosslinking.

The catalyst employed by White is based on Ruthenium, it is active in the metathesis reaction, the benzylidene-bis(tricyclohexylphosphine)dichlororuthenium, known as Grubbs 1st generation (G1, *Fig. 1.2*), and the monomer was dicyclopentadiene (DCPD, *Fig. 1.3*).

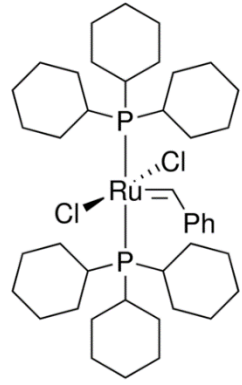

Figure 1.2: Grubbs catalyst first generation.

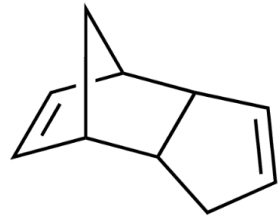

Figure 1.3: Dicyclopentadiene.

The reaction that leads at the repairing of the materials is a ring opening metathesis polymerization (ROMP, *Fig. 1.4*) that occur when the monomer comes out of the microcapsules and meets the catalysts.

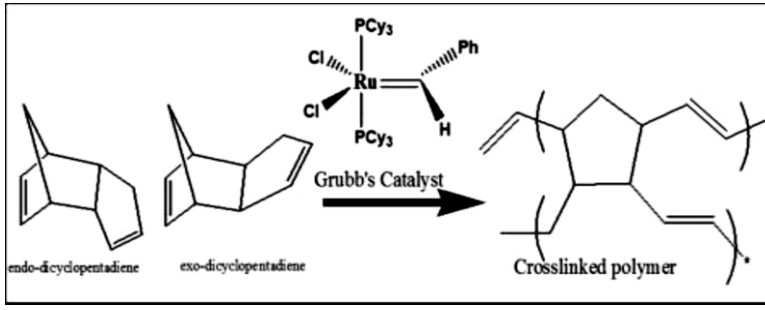

***Figure 1.4*:** ROMP reaction of DCPD catalyzed by first generation Grubb's catalyst.

1.2.1 THE METATHESIS

The olefins metathesis is a chemical reaction of exchange of substituents presents on two different olefins (*Fig. 1.5*). The reaction is catalyzed by metals such as nickel, tungsten, ruthenium and molybdenum.

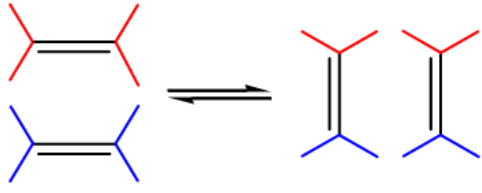

Figure 1.5: Metathesis of the olefins.

There are many different types of olefin metathesis, including:

- Cross metathesis (CM): involves the exchange of substituents on two olefins.
- Ring opening metathesis (ROM): allows the opening of cyclic olefins to form an open molecule with double bonds at the ends.
- Ring-closing metathesis (RCM): two double bonds on the same linear molecule reacts to form a cyclic molecule.
- Ring opening metathesis polymerization (ROMP, *Fig. 1.6*): is a ROM application, which consists of simultaneous opening with subsequent polymerization of the open olefin produced, all catalyzed by the same catalyst.

Figure 1.6: Ring opening metathesis polymerization (ROMP)

The ROMP mechanism (*Fig. 1.7*) is based on the one proposed by Chauvin: the mechanism involves the [2+2] cycloaddition of an alkene double bond to a transition metal alkylidene to form a metallacyclobutane intermediate. The subsequent opening of the cycle produces the polymer that retains monomer unsaturation and produces a new metal alkylidene. Interaction with the *d*-orbitals on the metal catalyst lowers the activation energy enough that the reaction can proceed rapidly at modest temperatures.

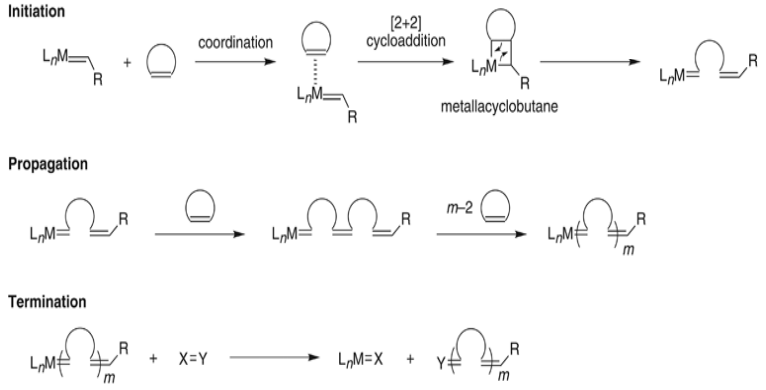

***Figure 1.7*:** Mechanism of ROMP reaction.

The ROMP reaction occurs for a cyclic and tensioned olefin structures, in fact the "*driving force*" of the reaction is the reduction of the ring tension. The reaction between the carbene and the double bond in the cyclic structure forms a highly reactive metallacyclobutane intermediate. The opening of the ring begins to polymerize, a double bond binds to the metal and the other becomes a terminal double bond. The new carbene obtained reacts with the double bond of the next monomer, so there is the propagation of the reaction. Termination takes place when non active catalytic species are formed.

1.3 SELF-HEALING MATERIALS FOR AERONAUTICAL APPLICATIONS

In the recent year, in the aeronautic field, new solutions have been proposed to improve safety and help to get, through fuel savings, environmental and economic benefits by use of lighter, stronger and more rigid polymer composites. These materials have already been applied in aircraft structures to replace the traditional metal alloys. However, in order to achieve the necessary mechanical strength for many structural applications, highly cross-linked polymeric materials are needed. Cross-linked polymers tend to be brittle and they are subject to structural weakening due to the impact damage that can lead to substantial matrix micro-cracking, delamination and fiber-matrix de-bonding, with a consequent reduction of the structural capability. Self-healing thermosetting resins are able to limit the fatigue damage and preserve their integrity, increase their lifespan, reduce maintenance costs, and ensure safety of passengers and staff [4].

White's system can be extended for the aeronautical purposes, but it is critical that self-healing activity functions at low working temperatures which can reach values as low as -55 °C, that is the minimum temperature reached during the flying [5]. Another problem concerns the components' stability of the composites which are compromised at the cure temperatures necessary, for good performance of the composite (> 180 °C).

The catalyst must survive in very reactive environments and at the curing temperature of the composite, whereas the monomer must

remain liquid in order to reach the catalyst at low temperature (-55 °C). Furthermore, also the microcapsules must resist under the same conditions.

These aspect was investigated by the research team of the Prof. Longo and Prof. Guadagno of the University of Salerno, in collaboration with the Alenia Aermacchi.

1.3.1 THE MONOMER

The monomer used in the White's system, the DCPD, is not suitable for this application because, despite having a T_b of 170 °C, solidifies at temperature below the 33 °C. Several monomers have been studied, but the monomer that satisfies all the required for the aeronautical applications is the 5-ethyliden-2-norbornene (ENB, *Fig. 1.8*) that have a T_b of 147 and a T_f of -80 °C. Though the T_b is lower to 180°C, when the monomer was encapsulated remains liquid up to the conditions of use.

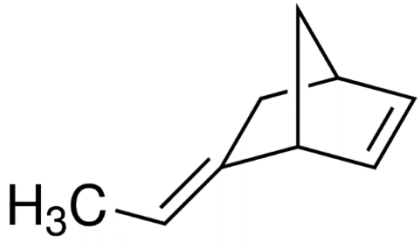

Figure 1.8: 5-ethyliden-2-norbornene.

In addition, the ENB has good compatibility with the walls of the

microcapsules, has a viscosity such as to allow it to flow into the vacuum crack and it converts in a polymer that have a high degree of crosslinking without substantial volume variations. At the aim to increasing the cross-linked fraction of the polymer products have been carried out several test on the blends of monomers formed by various percentage of ENB and DCPD. The best results were obtained for the blends ENB (95%)/ DCPD (5%), because at −50 °C after 4 h don't shows phase separation. These tests were also performed increasing the weight percentage of DCPD in the blends. The results have demonstrated phase separation after 1 h at −50 °C for ENB(85%)/DCPD(15%) and ENB(90%)/DCPD(10%) blends [6].

1.3.2 THE MICROCAPSULES

Once choice the monomer, need selected the microcapsules in order to satisfy all the necessary conditions to use. The prime function of microcapsules is to isolate the core material from surroundings to protect its functionality for a long period of time. The core material is released only when damage occurs in the matrix subsequently opening the microcapsule.

These micro-containers must be highly stable, both chemically and mechanically for use in the planes. In this respect, the shelf life of a microcapsule is as important as the capsule itself and the shorter life will reduce its efficacy in increasing the service life of materials. The stability of microcapsules depends upon a number of factors.

Normally polymers and composites for aeronautical application are

processed at elevated temperature. The durability of microcapsules requires considerable advancements for applications in self-healing composites at such harsh conditions. The strength of the shell wall is one factor that decides the mechanical properties of microcapsules. However, other factors like the chemical nature of core and shell wall, core to shell ratio, pH and temperature at which the capsules are produced, viscosity of core material, and probability of dissolution of shell wall in core material are the major aspects of shelf life determination of microcapsules [1].

The microcapsules selected for the encapsulation of the monomer, as in the White's system, are constituted by outer shell containing poly(urea-formaldehyde) and the inner shell of ethylene maleic anhydride copolymer. The capsules are prepared by in situ polymerization in an oil-in-water emulsion to modulate the dimension of the spheres and to obtain high yield.

In practice, the polymerization is carried out the in-water emulsion using a copolymer which has polar sites, compatible with an aqueous solvent, and non-polar sites, compatible with the healing agent; in this way a thin copolymer film incorporates the healing agent.

Then a condensation reaction leads to the formation of a polymer that grows at the interface of the emulsion. Finally, the microcapsules are washed and dried under vacuum [7]. It is possible to select a dimensional range (from a few μm up to 250 μm), modifying the conditions of process or by using sieves [8].

Once the microcapsules containing the monomer have been synthesized, another critical point to overcome has been to verify the resistance to 180 ° C (the maximum thermal treatment to which the

epoxy resin is subjected). The thermogravimetric analysis conducted up to 1000 ° C showed their explosion at 200 °C. Between 250 and 560 °C occur fragmentation of the polymer (urea-formaldehyde) and the elimination of ammonia, amine and carbon dioxide and the last stage of degradation involves the formation of thermally polycondensated structures more stable than the original one.

1.3.3 THE CATALYST

The last point to resolve for adapt the White's system at the aeronautical application, regards the efficiency of the catalyst at very low temperature and the thermal stability of this up to 180 °C.
The complexes that catalyzed the metathesis reaction are the metal alkylidene of nickel, tungsten, ruthenium and molybdenum.
Over the years, various metal complexes have been developed to catalyze olefin metathesis reactions. In the 1980s, Schrock developed synthesis to obtain highly reactive tungsten and molybdenum complexes. These catalysts, called "Schrock catalysts", are sensitive to air and water, and their use is limited to reactions in an inert atmosphere. A few years later Grubbs created a series of catalysts, called "Grubbs catalysts", based on ruthenium (II). This complexes containing a carbenic bond are selective to carbon-carbon double bonds and they are used in metathesis reaction. They offer several advantages including high activity, stability to air and water, tolerance to polar functional groups and possible use in protic polar solvents.

The researchers of UNISA have extended the application of White's system at Grubbs of 2nd generation catalyst ((1,3-Bis(2,4,6-trimethylphenyl)-2-imidazolidinylidene)-dichloro-(phenylmethylene)-(tricyclohexylphosphine)ruthenium(II), G2, *Fig. 1.9*) and at a new typology of catalysts called Hoveyda-Grubbs of 1st (Dichloro(2-isopropoxyphenylmethylene) (tricyclohexylphosphine)ruthenium(II) , HG1, *Fig. 1.10*) and 2nd generation ((1,3-Bis-(2,4,6-trimethylphenyl)-2-imidazolidinylidene)dichloro(o-isopropoxyphenylmethylene)ruthenium(II), HG2, *Fig. 1.11*). These last differ to the Grubbs for the substitution of the tricyclohexyl phosphine with a isopropoxy styrene group in which the oxygen coordinates the vacant site of the ruthenium. The catalyst of 2nd generation are characterized by the presence of a N-heterocyclic carbene instead of a tricyclohexyl phosphine, to obtain a catalyst more stable and more active.

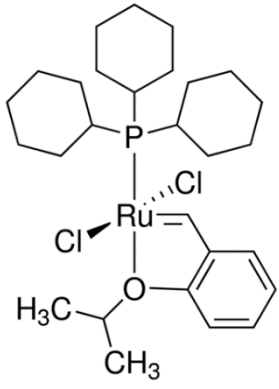

***Figure 1.9*:** Grubbs catalyst second generation.

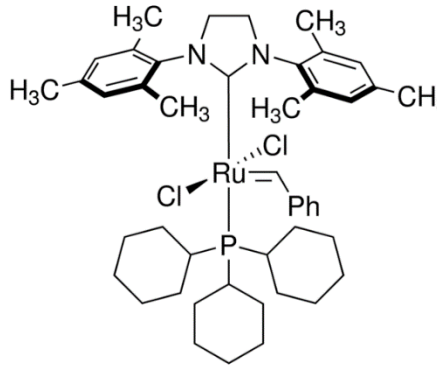

***Figure 1.10*:** Hoveyda Grubbs catalyst first generation.

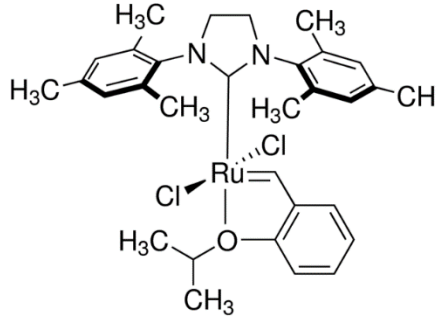

***Figure 1.11*:** Hoveyda Grubbs second generation.

The thermal stability and the activity at low temperature in the ROMP of the ENB of these catalysts was explored, moreover was evaluated the degree of crosslinking of the polymer obtained.

Thermal stability was evaluated testing the activity of the catalysts after treatment at different time and temperature, in nitrogen and air environment. Subsequently, the samples were characterized by ^{1}H-NMR for highlight possible changes. The results obtained showed

that the G1 was stable for 4 hours at 150 °C in nitrogen, decomposes after 2.5 hours at 150 °C in air; G2 was stable for 2 hours at 180 °C in nitrogen; the most stable ones were HG1 and HG2, in particular the 1st generation was stable 4 hours at 150 °C in nitrogen and stable 2.5 hours at 150 °C in the air; while that of the 2nd generation was stable for 2 hours at 180 °C in nitrogen.

The ROMP of the ENB at low temperature showed similar results, the Hoveyda-Grubbs catalysts gave at -50 °C a total conversion after 7 hours and 20 minutes, while G1 was active at -10 °C with a conversion of 16.8% after 60 minutes and G2 at -30 °C with a conversion of 74% after 24 hours. The exhaustive extraction in boiling cis-trans decahydronaphtalene of the polymers obtained allowed to evaluate the degree of crosslinking achieved. The best result was showed by the polymer obtained in the ROMP with the HG1 catalyst.

The test of the catalysts in the aeronautical materials is a crucial step to verify the stability of the catalysts at the thermal treatment of the epoxy mixture up to 180 °C. The results obtained were very promising for the application of this catalysts in the aeronautical materials, in particular for the Hoveyda-Grubbs catalysts. This tests showed that the G1 and G2 decompose at 150 °C, while HG1 and HG2 aren't subject at decomposition at the maximum temperature required; this is particularly advantageous, because it gives the possibility of conducting the hardening process at higher temperatures producing a material having better chemical, physical and mechanical characteristics [8].

However, there are still a number of unresolved problems: the high

amount of ruthenium based catalyst used in the formulation of the composite material (weigh upon for 5% by weight), its high market price and the need to impart additional functionalities to the epoxy matrix.

1.4 INNOVATIVE SELF-HEALING SYSTEM

In the attempt to significantly reduce the amount of metathesis catalyst and increase at the same time the properties of the epoxy matrix, we thought at several possible solutions.

At first, the ruthenium catalyst for ROMP can be supported on a substrate so to use a smaller amount of it, the interaction established between the catalyst and the filler can be covalent or non-covalent.

Initially, the ruthenium catalyst was covalently bond to a carbon nanofillers (graphite, graphene and carbon nanotubes), because many recent works highlight the significant benefits due to carbon nanoparticles embedded in the polymeric matrix of structural materials, although there are problems due to its non-homogeneous dispersion.

In a precedent work the multiwalled carbon nanotubes (MWCNTs) as the support to the Grubbs 1st generation catalyst was used, in order to obtain a homogeneous polymeric materials containing carbon nanotubes able to combine the mechanical strength and electronic conductivity of carbon nanotubes with the solubility and processability of the polymer [9]. The G1 was covalently bond to the

MWCNTs according to an "*grafting from*" approach which allows the polymer to be directly linked to nanotubes.

Subsequently, substituting the chemical arm pentaerythritol as arm with the ethylene or propylene glycol, the amount of polymer linked to the nanofiller was increased [10]. This improvement limits the "*chain leaking*" phenomenon attributed to cross-metathesis reactions between the ruthenium-alkylidene of the growing chain and a double bond C = C present within the chain itself or on a neighboring chain (*Fig. 1.12*).

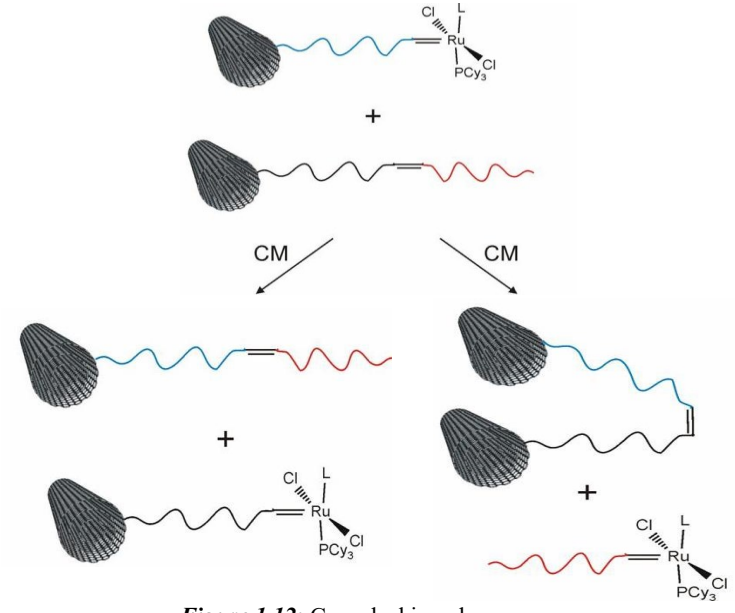

***Figure 1.12*:** Cross leaking phenomenon.

To support the Grubbs and Hoveyda-Grubbs catalysts was adopted the same synthetic procedure reported in this works and the filler choice was the graphene oxide (GO). The choice to use the graphene

depends on its extraordinary properties. Graphene exhibit fascinating physical properties such as thermodynamic stability, extremely high charge carrier mobility and mechanical stiffness, which are critical requisites for several applications [11,12]. Moreover, graphene based materials can activate self-assembling mechanisms able to improve gas barrier and mechanical properties of nanocomposites [13,14]. Furthermore, a large increases of the glass transition temperature of the nanocomposite in presence of GO can be observed [15].

GO was prepared by chemical oxidation of graphite and ruthenium based catalysts have been covalently bonded on oxidized graphene through four synthetic steps.

To bond covalently the catalyst to GO can allow for a catalyst savings while retaining the self-healing properties of the material, moreover the can have the beneficial effects on the properties of the epoxy matrix.

Ru catalysts covalently bonded to graphene oxide were tested in reactions of ROMP of 2-norbornene, that allow to evaluate the activity of the catalysts, and 5-ethylidene-2-norbornene. Graphene based catalysts were embedded in the epoxy precursors used for structural resins and several experiments for the evaluation of their activity were performed. Tests on the evaluation of the crack-healing efficiency of the developed self-healing materials, after the curing treatment, were carried out using Dynamic Mechanical Analysis (DMA). Very promising results were obtained for GO-HG1 and GO-HG2 catalysts, they result active in metathesis reaction at 90 °C. The amount of the ruthenium catalysts bonded to the GO used is lower than 0.5% wt of the epoxy mixture whereas, to achieve similar results

was utilizing powders of Grubbs' catalyst, a high amount (5% wt) was embedded in the epoxy formulation. This allows to considerably reduce the costs of the composite and to add the fascinating properties of GO.

As described so far, a better mechanical performance of the solidified resin is obtained by curing cycles at high temperatures, but this treatment can deactivate the ruthenium catalyst. Experiments performed in these last years to better understand the reason of the deactivation of ROMP catalysts highlighted that, when catalyst complex (Hoveyda-Grubbs'1st generation catalyst) is solubilized at molecular level, an equimolecular reaction between the epoxide ring of the matrix and the alkylidene of the ruthenium complex occurs determining its deactivation. In particular, the results demonstrated lower healing efficiency with respect to the more expensive self-healing system based on catalyst embedded in the form of solid particles in the microencapsulated epoxy resins. Experimental analysis has shown that solid catalyst particles in the epoxy mixtures, also at high temperature, retain an intact heart of active catalyst particles being the latter not to direct contact with the oxirane rings of the epoxy matrix. Instead, in the case of the catalyst particles solubilized at molecular level, the catalyst complex which is in contact with the oxirane rings is deactivated during the curing reactions, hence reducing the actual amount of catalyst active in the ROMP reactions [16]. Thus, in order to obtain high healing effectiveness a large amount of very expensive catalyst, introducing it as solid particles in the resin, is required.

The promising results obtained with GO-HG1 and GO-HG2 have suggested that it may be useful to protect the Ru-catalytic sites on graphene sheets, isolating them from the surrounding environment. This can be achieved forming a globular shell around the active catalytic site, obtainable by a short polymer chain.

Few units of 2-norbornene were polymerized around the GO-HG2, forming a globular shell that partially englobing the catalytic sites, to obtain the protected HG2-catalyst on graphene sheets.

The GO-HG2 protected with polymeric globular shell were tested after curing cycles up to 140 °C. The protection of the catalytic sites proved to be very effective in preventing catalyst deactivation during the curing cycle, even using a very low concentration of Ru-based catalyst (lower than 0.5% by weight).

Carbon based nano-materials (graphene or nanotubes), as already said, exhibit interesting structural, mechanical, electrical, and electromechanical properties, that are enhanced by the fact that all the atoms of the material are placed on the surface. It should be noted, however that the functionalization of this materials with the ROMP catalysts request a first step of oxidation and this involves in a modify of the graphitic planes; consequently, the sp^2 structure, responsible of remarkable electrical conductivity of this carbon materials, is partially destroyed. Instead, if the aromatic network remains intact, carbon nanoparticles can be used as filler and dispersed in the engineering materials to improve electrical conductivity, a fundamental requirement for several applications.

Therefore, the covalent modifications produce hybridized sp^3 carbon, resulting in loss of electrical conductivity of the nanofillers, so it

would be important to functionalize the carbon nano-filler in noncovalent ways to preserve the sp^2 structure and thus their electronic characteristics.

For these purposes, we explored the functionalization of the MWCNTs via electrochemical modification and functionalization of the MWCNTs and graphite via 1,3-dipolar cycloaddition reaction, that produce formation of covalent bonds. The catalysts supported through this alternative covalent functionalization of the carbon nanofiller shown an activity lower than the activity of the catalysts supported on the GO, probably for the nearness of the catalyst at the filler.

Thus, at the purpose of didn't modify the graphitic plane, a non-destructive modification of the carbon filler structure that always allowing to support the ROMP catalysts and at the same time leave intact the conductivity of the filler was studied. To realize this system we used a molecule that interacted whit the aromatic ring of the graphitic sheet without establishing a covalent bond. This was achieved through π-stacking interaction between, aromatic rings of the filler and of a suitable ligand.

The pyrenyl group (*Fig. 1.13*), which has a highly aromatic nature, is known to interact strongly with the basal plane of graphite and sidewalls of nanotubes via π-stacking [17,18].

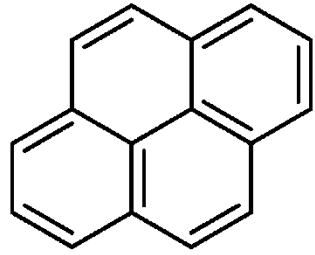

Figure 1.13: Pyrene.

To bond the Ruthenium catalyst on the carbon nanoparticles, the pyrene butyric acid was functionalized, in a similar manner as previously reported for the GO. The final reaction gives the catalyst linked to the pyrene and this system can interact not only on the graphite, graphene or nanotubes, but also on any filler able to give the π – stacking interaction [19]. This is an important goal in the field of the self-healing materials because it allows to functionalize the filler without alter the characteristics of the nanofiller itself, and furthermore, one times synthetized the catalytic complex pyrene-catalyst, this is available to link it on any filler, saving considerable time of reaction and costs.

In addition, the pyrene-catalyst can be used to synthesize, through ROMP, a wide range of polymers with a terminal pyrene, allowing them to bind to many substrates thus favoring a homogeneous dispersion of the filler in the materials.

1.4.1 SELF-HEALING VIA RADICAL POLYMERIZATION OF STYRENE

The critical issue of the high costs of Ruthenium catalysts moves the research towards alternative solutions to have materials with self repairing ability through the use of less expensive systems. What described up to now concerns the repair of materials via metathesis reactions promoted by Ruthenium complexes. It was thought to the possibility of a different healing mechanism which excludes the use of such expensive complex. The new idea is to replace the expensive Ru catalyst with a Cu(0) based catalyst, and thus also utilize a different mechanism of healing respect to considered until now. The new proposal mechanism of healing is a radical polymerization of the mixture styrene-divinylbenzene, with the catalytic system formed by Cu(0)- N,N,N',N'',N''-pentamethyl-diethylentriamine (PMDETA) and methyl-2-bromopropionate as initiator. The Cu(0) is much cheaper than Ru catalyst.

1.4.1.1 RADICAL POLYMERIZATION

The polymerizations depending on the mechanism involved are distinct in addition and step polymerization. The step polymerization is often a condensation polymerization because involved with expulsion of a low molecular weight molecule, called "condensate". The features of the step polymerization are that the start and

propagation reactions occur with approximately the same speed, you do not need to activate the system with an initiator, the macromolecule is formed in a relatively long time and the degree of polymerization increases over time and the conversion to polymer remains constant. The monomers that give this type of polymerization are characterized by two or more functional groups.

The chain polymerization, instead, is carried out for successive additions, therefore it is said addition polymerization. In this kind of reactions each step depends on the previous one and allows the next and don't form byproduct; they involved vinyl monomers, or monomers in which is present a double bond C = C.

The different types of chain polymerization depending on the active species:

- radical polymerization
- ionic polymerization
    - cationic polymerization
    - anionic polymerization

In radical polymerization reactive molecules are the radicals, while in ionic polymerization the reactive molecules are carbocations or carbanions for respectively cationic and anionic polymerization. They differ in the mode of bond cleavage.

The radical polymerization is carried out in three steps:

1. activation
2. propagation
3. termination

The activation process is obtained starting from a free radical initiator. The initiator is a molecule able to decompose by homolytic

breakage of a link, with the corresponding formation of the radical, according to a reaction of the type:

$$I_2 \rightarrow 2I \bullet$$

Where with I_2 indicates the initiator and I • indicates the radical.

The radical (I •) presents a remarkable reactivity, for which it can join a monomer (M) leading to the formation of a primary radical (• P_1):

$$\bullet I + M \rightarrow P_1 \bullet$$

The activation of a molecule can take place via thermal, chemically or electromagnetic radiation. The generation reaction of the radicals is a slow reaction, because it leads to the formation of an unstable compound. The initialization is affected by temperature and is slow enough to ensure that in general the speed of the entire process of polymerization is controlled by the only chemical activation reaction: in fact, other reactions are relatively fast and are not influenced by temperature.

In the process of propagation, the primary radical (• P_1) reacts with more monomers subsequently, forming a radical compound having a number of repeating units higher.

$$\bullet P1 + nM \rightarrow P_n\bullet$$

where "n" is the number of monomers that are added to the chain and (P_n•) represents a chain composed of a number "n" of repeating units.

The attack can occur in different types:

- tail-head attack
- head-tail attack
- tail-to-tail attack.

The polymer product present only isotacticity in the case in which

the propagation takes place through the head-tail attack.

The termination process take place when a polymer chain (P_n•) meets another polymer chain which is also in the propagation phase (P_m•). The reaction between these two radicals leads to the formation of a polymer (P) with a number of repeating units equal to the sum (m + n) of the repeating units that made up the single chains.

$$• P_n + P_m• \rightarrow P$$

The previous reaction corresponds to a termination reaction for coupling. There is also the possibility that two chains react in a termination reaction by disproportionation, giving rise to the formation of chains having a terminal unsaturation:

$$R\text{-}CH_2\text{-}CH_2 • + R'\text{-}CH_2\text{-}CH_2 • \rightarrow R\text{-}CH_2\text{-}CH_3 + R'\text{-}CH = CH_2$$

The initiators of these reactions can be divided according to their greater solubility in water or in organic solvents.

The initiators soluble in organic solvents: the most used are benzoyl peroxide (BPO), the azodiisobutyronitrile (AIBN) and hydroperoxides.

The initiators soluble in water: are the Fenton reagent, which exploits the redox reaction between the persulfate and bisulfite (or metabisulphite) catalyzed by Fe^{3+} ions.

Other types of initiators are those activated by heat or by electromagnetic radiation.

1.5 CARBON NANOFILLER

Materials with layers of sp^2-bonded carbon atoms exhibit a large variety of structures characterized by different degree of structural order and morphologies. These materials, principally, differ for their degree of order perpendicular to the graphitic layers, out-of-plane order, and in the graphitic layers, in-plane order (*Fig. 1.14*). The most disordered graphitic structures are coals, cokes and carbon blacks.

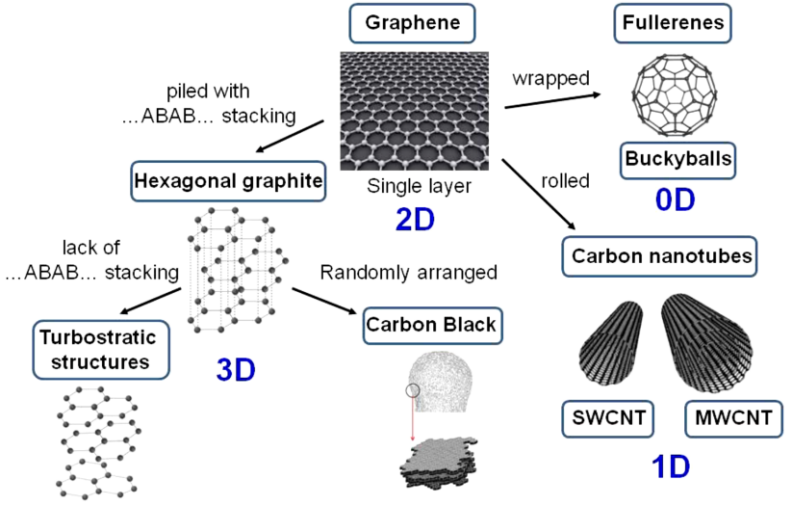

***Figure 1.14*:** All graphitic allotropes.

The carbon nanofillers used in the epoxy matrix both to support the Ruthenium catalyst for self-healing and to improve the properties are graphene, graphite and nanotubes.

1.5.1 GRAPHENE

Recently, applied research interest has been focused on the production of graphene, the basic building block for all graphitic materials. Graphene is a two-dimensional sheet of sp^2-hybridized carbon. Its extended honeycomb network makes it the basic of other important allotropes; it can be stacked to form 3D graphite, generally consisting of more than ten graphene layers; rolled to form 1D nanotubes, further categorized into single- or multi- walled depending on the number of graphene layers present (SWCNT/MWCNT respectively); and wrapped to form 0D fullerenes, a spherical buckyballs (*Fig. 1.15*). Consequently, graphene can be considered the "*mother of all carbon forms*".

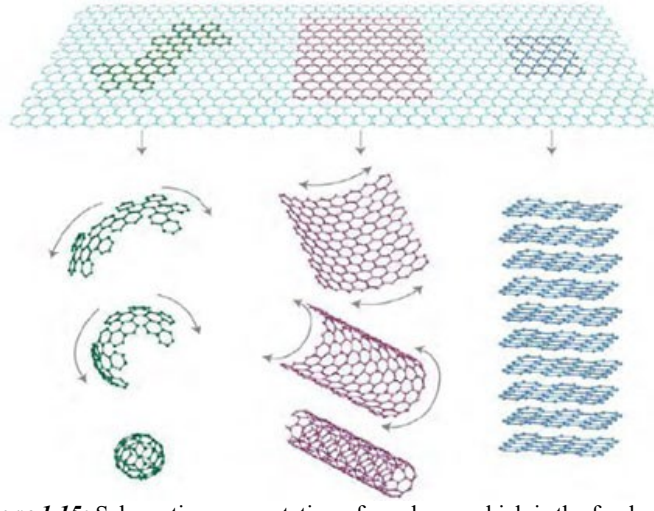

Figure 1.15: Schematic representation of graphene, which is the fundamental starting material for a variety of fullerene materials; buckyballs, carbon nanotubes, and graphite**.**

Long-range π-conjugation in graphene yields extraordinary thermal, mechanical, and electrical properties. While studies of graphite have included those utilizing fewer and fewer layers for some time, the field was delivered a jolt in 2004, when Geim and co-workers at Manchester University first isolated single-layer samples from graphite [20]. Until 2004, 2D crystals like graphene were considered to be thermodynamically unstable and hence theoretically impossible to exist in the free state and were passed off as mere "academic" materials. However, the discovery of free-standing graphene in 2004 changed the scenario and spurred the interests of material scientists and condensed matter physicists. For their discovery, Geim and Novoselov received the 2010 Nobel prize in physics. The routes available for the preparation of graphene are the chemical vapor deposition (CVD) of monolayer of graphite on transition metal surfaces; the micromechanical exfoliation of graphite that involves peeling of the graphene from graphite using "*Scotch*" tape; the epitaxial growth of graphene on sonication in aqueous media, GO exfoliates readily into colloidal suspensions of single graphene oxide layers and thermal reducing of GO [21].

Pristine graphene is a hydrophobic material, and has no appreciable solubility in most solvents. Nevertheless, the processing of graphene composites concerns itself foremost with the solubilization of graphene. To improve the solubility of graphene, different functional groups have been attached to the carbon backbone by chemical modification, both covalent or noncovalent.

Graphene combines the peculiarity of being an extremely lightweight material with exceptional mechanical strength properties, for this

reason the applications are really varied.

A successfully investigated of the graphene is the preparation of polymeric nanocomposites for which remarkable improvements of various properties such as electrical conductivity, thermal stability, elastic modulus or traction resistance are observed following insertion into the polymer matrix of graphene or other graphene-based nanostructures [22].

The use of graphene in electronics is very promising due to the high mobility of chargers and low noise, properties that are well exploited in the manufacture of high performance field transistors and battery applications [22], supercondensers, cells fuel, photovoltaic devices, photocatalysts and more [23]. Moreover, the extraordinary thermal, chemical and mechanical stability combined with transparency and monoatomic thickness make graphene a new generation of transparent electrode materials. As describe above, the recent application of this materials are to support the metathesis catalysts in self-healing materials.

1.5.2 GRAPHITES

Graphite (*Fig. 1.16*) is a crystalline, polymorphic form of elementary carbon with ordered layers.

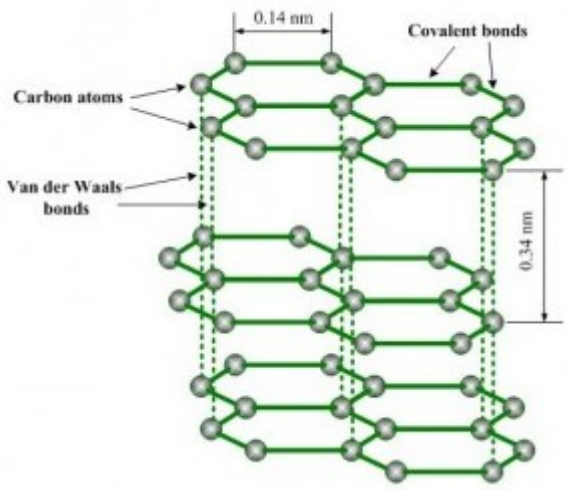

Figure 1.16: Structures of the Graphite.

It is the 3D carbon allotrope and is made of graphene sheets piled on top of each other with …*ABABAB*… stacking and separated by 0.335 nm. Each carbon atom in the graphite crystal is hybridized trigonally, forming three σ and one π bonds. The hybridized orbitals of the sp^2 type give σ bonds of a length of 1.42 Å, arranged at 120° angles with respect to one another, with sheets made up of regular hexagons. The fourth electron of each atom, being in the p orbital, forms π bonds with all the neighboring atoms. The structure of graphite consists of six-membered rings in which each carbon atom has three near neighbors at the apices of an equilateral triangle. Within the large

planar layers, there are linkages intermediate between atomic and metallic bonds. The layers in the crystal are held together by van der Waals bonding forces. Weak bonding perpendicular to the layers gives rise to easy gliding parallel to the sheets [24].

1.5.3 NANOTUBES

The carbon nanotubes are obtained rolled the graphene sheet to form one dimensional carbon material. The discovery of carbon nanotubes (CNTs) in 1991 opened up a new era in materials science by Lijima [25]. These incredible structures have an array of fascinating electronic, magnetic and mechanical properties. CNTs are at least 100 times stronger than steel, but only one-sixth as heavy, so nanotube fibers could strengthen almost any material [26]. Nanotubes can conduct heat and electricity far better than copper. CNTs are already being used in polymers to control or enhance conductivity and mechanical properties. Carbon nanotubes are composed of carbon atoms linked in hexagonal shapes, with each carbon atom covalently bonded to three other carbon atoms. Carbon nanotubes have diameters as small as 1 nm and lengths up to several centimeters. Although, like buckyballs, carbon nanotubes are strong, they are not brittle. They can be bent, and when released, they will spring back to their original shape. Carbon nanotubes can occur as multiple concentric cylinders of carbon atoms, called multi-walled carbon nanotubes (MWCNTs) and as one cylinder which are called single-walled carbon nanotubes (SWCNTs) (*Fig. 1.17*). Both

MWCNTs and SWCNTs are used to strengthen composite materials [27, 28].

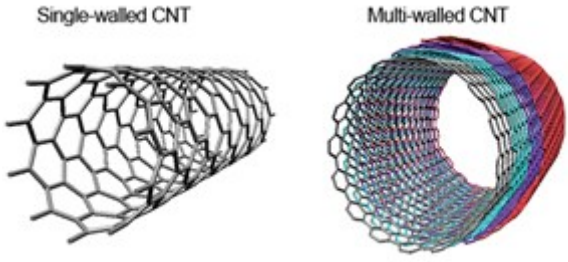

***Figure 1.17*:** Structure of Single Walled Carbon Nanotubes (SWCNTs) and Multi Walled Carbon Nanotubes (MWCNTs).

REFERENCES

[1] H. Ullah, K. A. M. Azizli Z. B. Man, M. B. Che Ismail, and M. Irfan Khan; POLYMER REVIEWS, ***2016***, VOL. 0, NO. 0, 1-57.

[2] S. Billiet, X. K. D. Hillewaere, R. F. A. Teixeira, F. E. Du Prez; Macromolecular Rapid Communication 2013, 34, 290−309, chemistry of crosslinking processes for self-healing materials;

[3] S. R. White, N. R. Sottos, P. H. Geubelle, J. S. Moore, M. R. Kessler, S. R. Sriram, E. N. Brown, S. Viswanathan; Nature, 2001, 409, 794;

[4] B. J. Blaiszik, S. L. B. Kramer, S. C. Olugebefola, J. S. Moore, N. R. Sottos NR, S. R. White. *Selfhealing polymers and composites*. *Annu Rev Mater Res* ***2010***; 40, 179-211.

[5] Guadagno L., Mariconda A., Longo P. et al. U.S. Pat. Appl. Publ. 2011, US 20110118385 A1 del 19/05/2011.
"Process for preparing self-healing composite material of high efficiency for structural applications.";
Guadagno L., Longo P., Mariconda A., et al. US 2010168280 A1 del 01/07/2010.
"Process for preparing self-healing composite material.";
Guadagno L., Longo P., Mariconda A., et al. WO 2009/113025 A1 International Application No.: PCT/IB2009/051005 del 17/09/2009.
"A composite material which is self-reparing even at low temperature";

[6] M. Raimondo, P. Longo, A. Mariconda and L. Guadagno. *Advanced Composite Materials,* ***2014***, 1-11.

[7] S. R. White, N. R. Sottos, P. H. Geubelle, J. S. Moore, M. R. Kessler, S. R. Sriram, E. N. Brown, S. Viswanathan, Autonomic healing of polymer composites. Nature 2001; 409:794-7; E. N. Brown, M. R. Kessler, N. R. Sottos, S. R. White; Journal of Microencapsulation, ***2003***, 20 N0 6, 719-730;

[8] L. Guadagno, P. Longo, M. Raimondo, A. Mariconda et al.; US 6518330 del 13/3/2008

"Materiale composito autoriparantesi anche a bassa temperatura";

[9] Y. Liu, A. Adronov; *Macromolecules;* ***2004***, 37, 4755-4760;

[10] C. Costabile, F. Grisi, G. Siniscalchi, P. Longo, M. Sarno, D. Sannino, C. Leone, P. Ciambelli; *Journal of Nanoscience and nanotechnology*, ***2011***, 11, 1.

[11] A. K. Geim, K. S. Novoselov. *Nat Mater,* ***2007***; 6, 183-191.

[12] T. J. Echtermeyer, M. C. Lemme, M. Baus, B. N. Szafranek, A. K. Geim, H. Kurz; *Electron Devices Lett*, ***2008***, 29, 952-954.

[13] N. Yan, G. Buonocore, M. Lavorgna, S. Kaciulis, S. K. Balijepalli, Y. Zhan, et al.; *Compos Sci Technol,* ***2014***, 102,74-81.

[14] G. Scherillo, M. Lavorgna, G. G. Buonocore, Y. H. Zhan, H. S. Xia, G. Mensitieri, et al.; *ACS Appl Mater Interfaces,* ***2014***, 6, 2230-2234.

[15] M. Mauro, M. R. Acocella, C. E. Corcione, A. Maffezzoli, G. Guerra; *Polymer,* ***2014***, 55, 5612- 5615.

[16] M. Raimondo, P. Longo, A. Mariconda, L. Guadagno; *Adv Compos Mater,* ***2015***, 24(6), 519-529.

[17] Katz, E. J. Electroanal. Chem. 1994, 365, 157.

[18] H. Jaegfeldt, T. Kuwana, G. J. Johansson; *J. Am. Chem. Soc.,* ***1983***, 105, 1805.

[19] F. J. Gómez, R. J. Chen, D. Wang, R. M. Waymouth, H. Dai; *The Royal Society of Chemistry,* ***2003***, 190-191.

[20] M. J. Allen, V. C. Tung, R. B. Kaner; *Chemical Reviews*, ***2009.***

[21] R. Sengupta, M. Bhattacharya, S. Bandyopadhyay, Anil K. Bhowmick; *Progress in Polymer Science,* ***2011,*** 36, 638–670.

[22] G. Di Francia, E. Massera, M. Miglietta, I. Nasti, T. Polichetti; *Energia Ambiente e Innovazione*, ***2011***, 3, 59-67.

[23] X. Huang, X. Qi, F. Boeyab, H. Zhang; Chem Soc Rev, 2011, 1-21;

[24] S. Park and R. S. Ruoff; *Nat. Nanotechnol.,* **2009**, 5, 217–224.

[25] S. Lijima. *Nature* **1991**, 354, 56 – 58.

[26] M. Treacy, T. W. Ebbesen, J. M. Gibson. *Nature,* ***1996***, 381, 678–680.

[27] E. Flahaut, R. Bacsa, A. Peigney, C. Laurent. *ChemComm,* ***2003***, 12 1442–1443.

[28] Cumings, J.; Zettl, A; *Science,* ***2000***, 289 (5479): 602–604.

CHAPTER 2

COVALENT FUNCTIONALIZATION OF THE CARBON NANOFILLER

2.1 FUNCTIONALIZATION OF GRAPHENE OXIDE WITH CATALYSTS ACTIVE IN THE METATHESIS POLYMERIZATION

2.1.1 GRAPHENE OXIDE (GO)

Graphene oxide (GO, *Fig. 2.1*) is a layered material, which can be obtained by chemical oxidation of graphite. Graphene oxide can be prepared by reaction of graphite with strong mineral acids and oxidizing agents, typically via treatment with a mixture of sulfuric and nitric acid, using potassium chlorate, as in the Staudenmaier's [1] methods, or with a mixture of sodium nitrate and concentrated sulfuric acid, using potassium permanganate, as in the Hummers' method [2].

The precise structure of GO remains a matter of debate [3] and, according to model of Lerf et al. [4], the GO obtained consists of oxidized sheets having oxygen containing functional groups, that confer polar surface properties and a strong hydrophilic character. At the surface of the basal planes there are hydroxyl and epoxide groups

and at the edges there are carbonyl and carboxyl groups.

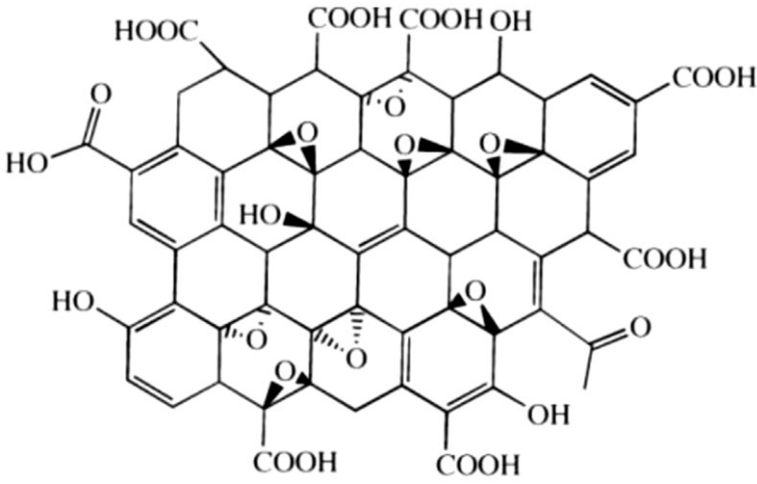

Figure 2.5: Schematic picture of GO.

The acidity of the GO was determined performing a typical acid-base titration. Amount of carboxyl and total acidic site on the GO were quantitatively chemical analyzed by titration. The acid group was basified with a strong base NaOH, and then the NaOH in excess was titrated with the strong acid HCl. The equivalent volume that allows to determine the title was obtained from the point of inflection. The title obtained for difference was 14.1 mmol/g.

$$GO - OH \ + NaOH \ \rightarrow GO - O^{-}Na^{+} + H_2O + \ NaOH_{exc}$$
$$NaOH_{exc} \ + \ HCl \ \rightarrow NaCl + \ H_2O$$

FT/IR spectra in *Fig. 2.2* show the presence of oxygenated functional groups on the layers of GO, whose concentration is negligible in the

starting graphite sample (G). Absorption bands of carboxyl groups (1730 cm^{-1}), hydroxyl groups (stretching at 3420 cm^{-1} and bending at 1385 cm^{-1}) and epoxide groups (1145-1065 cm^{-1}) are observed [5].

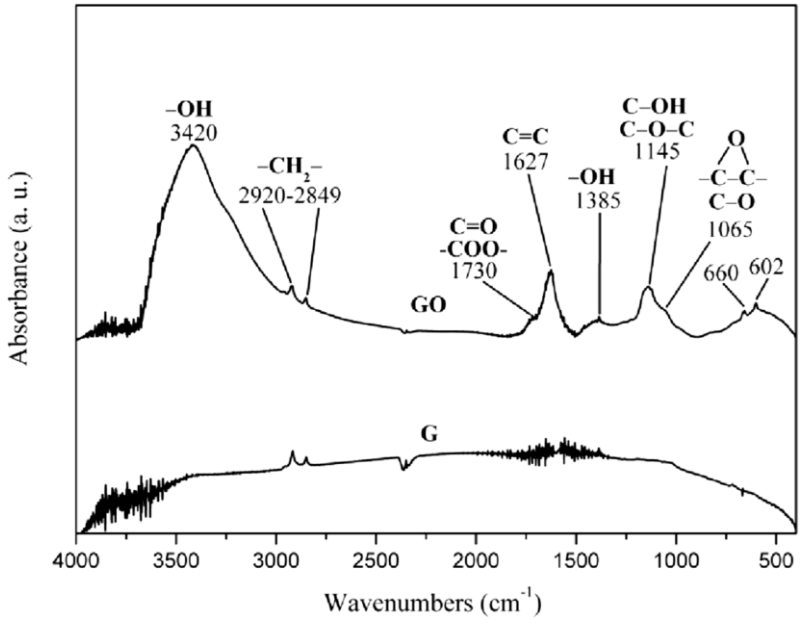

Figure 2.6: FT/IR spectra in the range 4000-400 cm^{-1} of the starting high surface area.

The GO thermogram (*Fig. 2.3*) shows a loss of about 10 % between 20 °C and 150 °C due to the evaporation of the interlaced water. In the range of 150 °C to 350 °C there is a loss of 28 % due to the degradation of the carboxy functions and between 350 °C and 650 °C instead regards the rest of the structure corresponding to 62 % of weight loss.

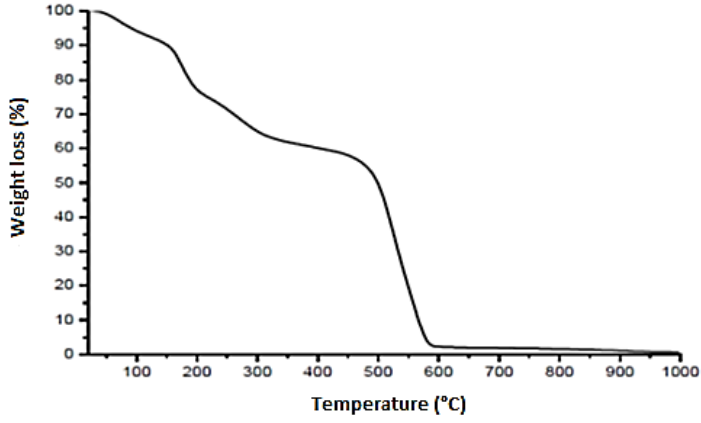

Figure 2.7: Thermogram of GO in air.

The oxidation of G produces an oxidized layered material with increased interlayer distance. This distance can be evaluated by X-ray diffraction pattern. X-ray diffraction patterns of the starting graphite (G) and of the derived GO are shown in *Fig. 2.4*.

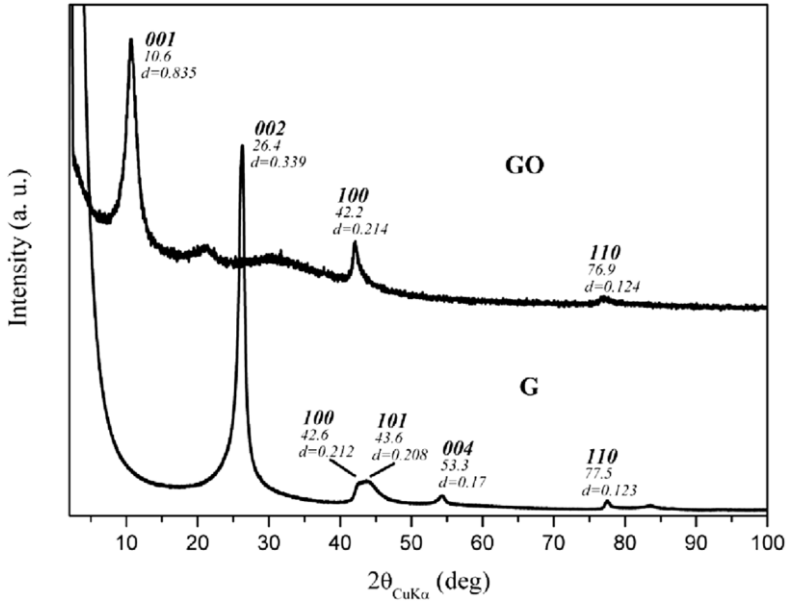

Figure 2.8: X-ray diffraction patterns (Cu Kα) of the starting high surface area graphite (G) and of graphene oxide (GO).

The pattern of GO reveals a broad 001 reflection, corresponding to an interlayer distance of 0.84 nm. The pattern of G shows an intense 002 reflection, corresponding to an interlayer distance of 0.339 nm. Hence, the value of interlayer distance of GO is higher than the interlayer distance observed in the starting graphite, as represented in *Scheme 1*.

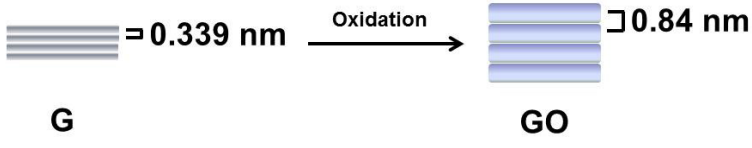

Scheme 2.1: Schematic representation of the increasing of the interlayer distance in GO after oxidation of graphite G.

All the observed reflections are indicated in *Table 2.1* in which the observed XRD peak d-spacings are compared to the expected hexagonal graphite [6].

Table 2.1: Observed XRD reflection d-spacings of sample G and comparison to the expected hexagonal graphite.

Experimental d-spacings (nm)	***(hkl)***	***Theory***	***Difference***
0.339	(002)	0.338	0.01
0.212	(100)	0.214	-0.02
0.208	(101)	0.204	0.04
0.170	(004)	0.168	0.02
0.123	(110)	0.123	0

Data shown in *Table 2.1* indicate that the starting graphite is the most common form of graphite in nature. In fact, the values in the column of the "difference" indicate that it is hexagonal graphite with ABAB stacking of layers. The correlation length (D_{002}) of sample G was determined using Scherrer's equation:

$$D = \frac{K\,\lambda}{\beta \cos\theta}$$

where K is the Scherrer constant, assumed = 1, λ is the wavelength of the incident X-rays, θ is the diffraction angle and β is the corrected integral breadth. The value obtained for D_{002} was 10 nm. From

Scherrer's equation, the number of layers can be obtained using the below equation [7].

$$\text{Number of layers} = \frac{D_{002}}{d_{002}}$$

Considering the value of 0.339 nm for the d-spacing of the reflection (002), a number of about 30 layers was calculated. As shown in *Fig. 2.4*, while the WAXD pattern of G shows the intense 002 reflection, corresponding to an interlayer distance of 0.339 nm; this reflection disappears in the diffraction spectrum of GO which shows the most intense reflection at 2θ = 10.6°. This last reflection corresponds to a value of the inter-layer spacing of 0.835 nm. A typical broad reflection near 10.21° of 2θ was observed for GO powder prepared by other research groups [8, 9].

2.1.1.1 MORPHOLOGICAL INVESTIGATION

FESEM images of the starting graphite G and the derived graphene oxide GO are shown in *Fig. 2.5*.

FESEM images reveals that the GO material consists of randomly aggregated, thin, crumpled sheets, closely associated with each other. Many block sheets show a number of layers consistent with the observed diffractogram for which a number of layers less than 10 was calculated.

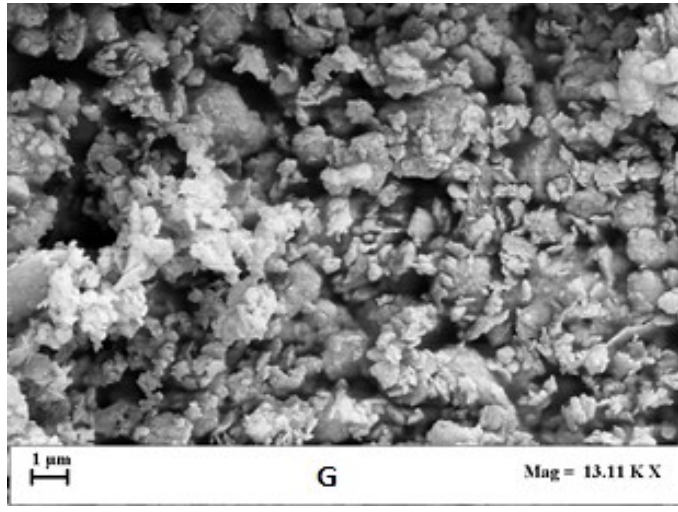

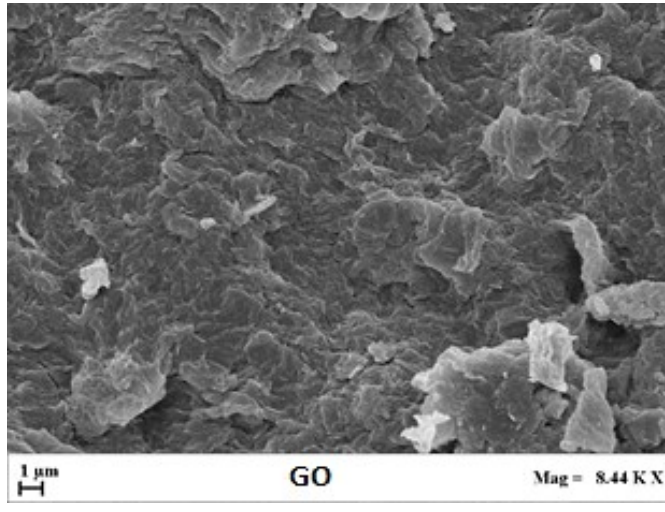

Figure 2.5: FESEM pictures of graphite (G) and graphene oxide (GO).

2.1.2 PROCEDURE

Carboxylic groups on GO sheets were used in the first step of the functionalization. The concentration of carboxylic groups on GO sheets was determined by titration [10].

A second titration was conducted at the aim of evaluate the only carboxylic acid groups using a weak base $NaHCO_3$. In this case, the excess of HCl was titrated in a second acid-base titration with NaOH. The value of the title was found to be 5.5 mmol/g.

$$GO - COOH + HCO_3Na$$
$$\rightarrow GO - COO^-Na^+ + H_2O + CO_2 + NaHCO_{3\,exc}$$
$$NaHCO_{3\,exc} + HCl \rightarrow (H_2O + CO_2) + NaCl + HCl_{exc}$$
$$HCl_{exc} + NaOH \rightarrow NaCl + H_2O$$

The functionalization of GO with ROMP catalysts was carried out through a series of four reaction steps (see *Scheme 2.2*). This procedure was a slightly modification of one recently reported for the functionalization of multi-walled carbon nanotubes [11].

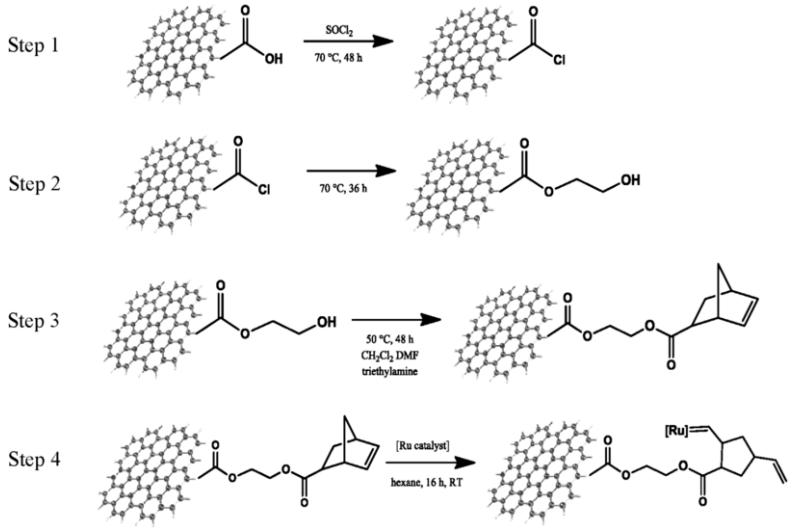

Scheme 2.2: Functionalization of GO with Ru-based catalysts.

Carboxylic groups on GO sheets were first reacted with thionyl chloride, resulting in the corresponding acyl chloride (GO-Cl), step 1, esterified with ethylene glycol (GO-Gly), step 2 and then reacted with 5-acid chloride 2-norbornene (GO-Nor), step 3. The metathesis reaction between GO-Nor and catalyst produced Grubbs or Hoveyda-Grubbs catalyst-functionalized graphene oxide layers step 4.

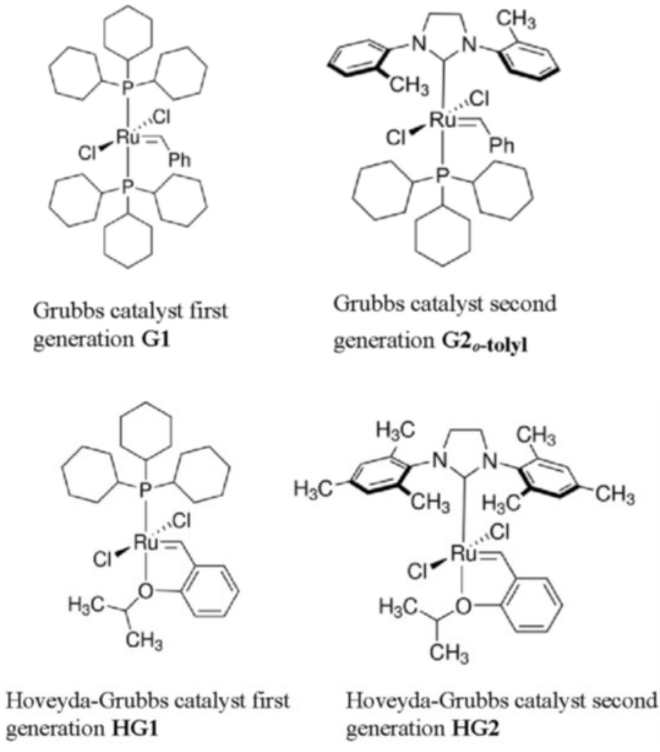

Figure 2.9: Grubbs and Hoveyda-Grubbs of I and II generation.

The intermediate products of each step have been characterized by X-ray diffraction and FT/IR analysis. *Fig. 2.7* and *Fig. 2.8* shows respectively the X-ray diffraction patterns (CuKα) and the FT/IR spectra of GO, of the intermediate products for each functionalization step GO-Cl (1), GO-Gly (2) and GO-Norbornene (3) and of the covalent functionalized graphene oxide layers with G2 (4).

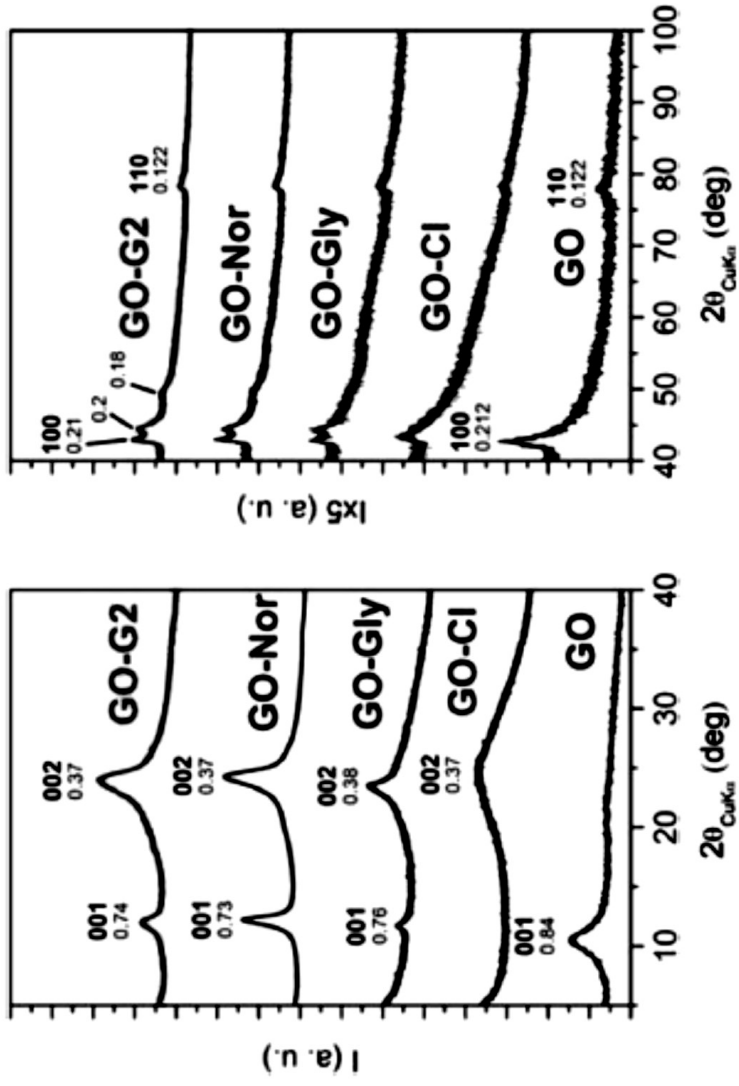

Figure 2.7: X-ray diffraction patterns (Cu Kα) of: L-GO, the intermediate products of each functionalization step (GO-Cl, GO-Gly and GO-Nor) and the covalent functionalized graphene.

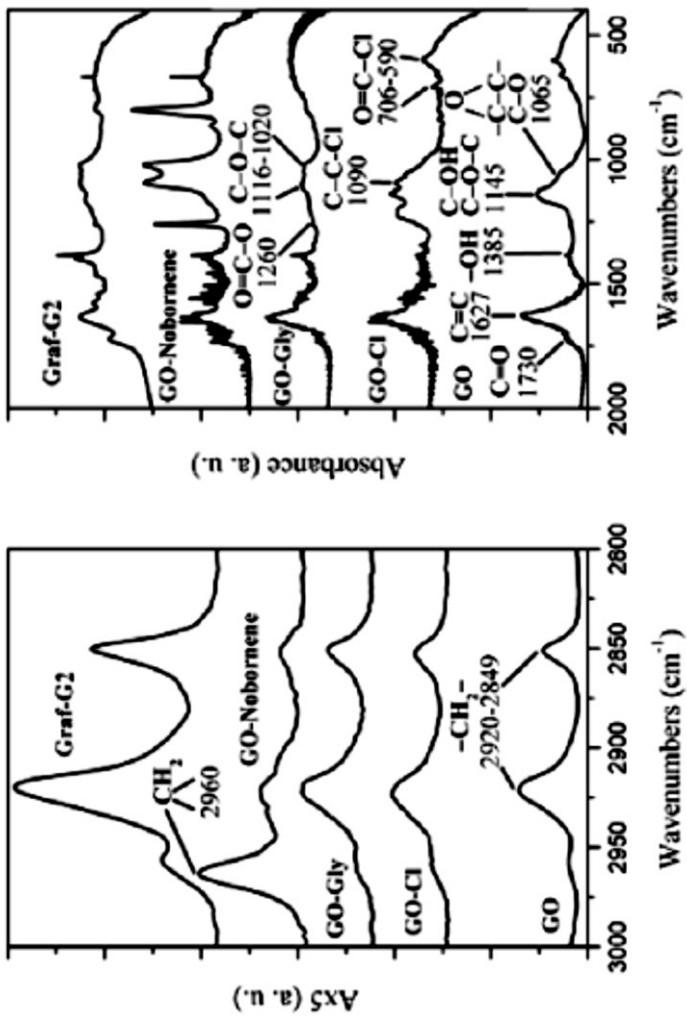

Figure 2.8: FT/IR spectra of: GO, the intermediate products of each functionalization step (GO-Cl, GO-Gly and GO-Norbornene) and the covalent functionalized graphene oxide layers.

2.1.2.1 SYNTETIC STEPS OF FUNCTIONALIZATION

- **First step:** ***formation of graphene acyl chloride***

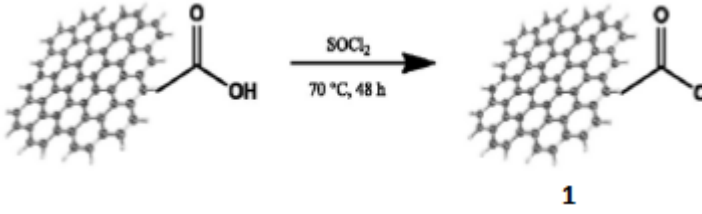

Figure 2.9: Chlorination of GO.

The first step of functionalization of GO consist in the formation of product (1), the corresponding chloride of the starting GO in which the carboxylic groups was converted in the corresponding acyl chloride. The treatment of GO with thionyl chloride causes the complete exfoliation of GO particles, in fact the pattern of GO-Cl in *Fig. 2.7* shows a very broad halo, centered at d = 0.37 nm with a correlation length of about 1 nm. In the FT/IR spectrum (*Fig. 2.8*) it was observed the absorption peaks at 1090 cm^{-1} and 790 cm^{-1} (C-Cl stretching) and the carbonyl peak at 1720 cm^{-1} confirm the formation of -COCl groups on graphene oxide layers.

- **Second step:** ***esterification reaction***

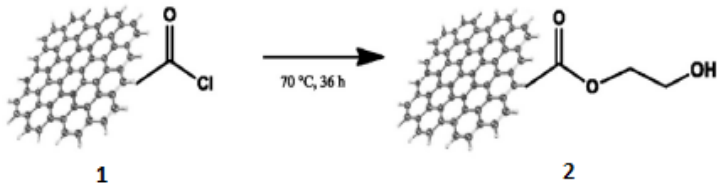

Figure 2.10: Esterification of GO-Cl.

The reaction of GO-Cl (product 1) with ethylene glycol leads to the formation of an ester, which furthermore generates an ordered intercalate crystalline phase with periodicity d = 0.76 nm and a correlation length of about 16 nm (*Fig. 2.7*). The FT/IR spectrum of *Fig. 2.8* shows the shift of the position of the absorption band of the carbonyl groups at 1743 cm^{-1} and the absorption peaks at 1260 cm^{-1} (related to the groups O=C-O) and 1116 cm^{-1} and 1020 cm^{-1} (C-O-C stretching).

- **Third step:** ***functionalization of GO with 5-acid chloride 2-norbornene***

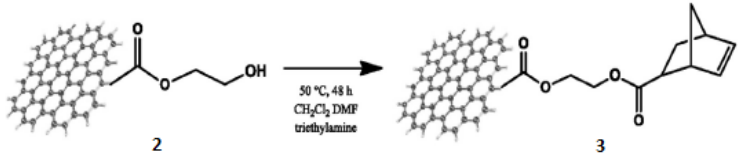

Figure 2.11: Esterification of GO-Gly with norbornene.

Also this reaction is an esterification, the product (3) leads another bond C-O-C by reaction with 5-acid chloride 2-norbornene. The

FT/IR spectrum (*Fig. 2.8*) shows the same profile of product (3) confirming the esterification reactions. These further treatments of GO-Gly disturb the out-of-plane order of the intercalate crystalline phase ($D^{\perp}$ = 8 nm in GO-G2), while maintaining about the same periodicity (as see in the *Fig. 2.7*).

- **Fourth step:** ***functionalization of GO with Ru-based catalysts***

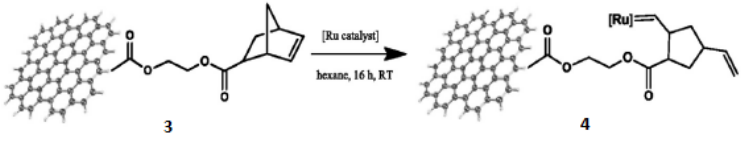

Figure 2.12: Metathesis reaction with Ru-based catalyst.

The last step consists in the metathesis reaction of the product (3) with the ROMP catalysts. For examples are show only the characterization of the GO-Norbornene with G2-*o*-tolyl catalysts. From the *Fig. 7* can be deduced that the product (4) are consistent with an intercalated structure with ethylene glycol, covalently functionalized at the edges and on the surfaces of the crystalline domains with G2-*o*-tolyl. In the FT/IR spectrum of *Fig. 2.8* are present similar absorption peaks of the product (3).

2.1.3 EVALUATION OF THE AMOUNT OF Ru-BASED CATALYSTS LINKED TO GRAPHENE OXIDE

The amount of Ru linked to graphene was evaluated by thermogravimetric analysis (TGA). The analyses were conducted in air flow up to 1000 °C to allow the Ru to oxidize in the form of ruthenium oxide (RuO_2). Ruthenium (IV) oxide is a purple crystalline solid at room temperature. It can be prepared by direct synthesis at 1000 °C from the elements, or by pyrolysis of halides of ruthenium. From the residue was possible to calculate the moles of RuO_2 and therefore the amount of bonded catalysts.

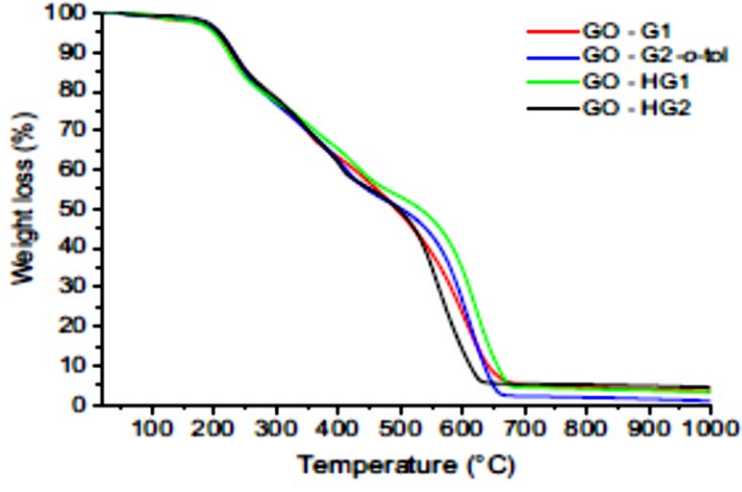

Figure 2.13: Thermogram in air at 1000 °C of the Ru-based catalysts covalently bonded to the GO.

Thermogravimetric analysis of the Ru-based catalysts bonded to the GO (*Fig. 2.13*) shows a loss of water at about 100 °C; between 120 °C and 300 °C there is a loss of about 20 % and between 300 °C and 400 °C a second loss by about 20 %. This is due to phenomenon of decarboxylation of ester function -COO- labile groups. The last loss to 650 °C is due to the degradation of the structure with a loss of approximately 68 %.

The residue at 1000 ° C allows to estimate the amount of ruthenium present, corresponding to RuO_2, is in percentage 3.0% for G1, 2.9% for G2$_{o\text{-tol}}$, 6.0% for HG1 and 5.0% for HG2, while the residuals in mol/mg are shown in the *Table 2.2*.

Table 2.1: Residual at 1000 °C (mol/mg) for all the functionalized catalysts.

GO-catalyst	**Residual at 1000°C (mol/mg)**
GO-G1	$2.96 \cdot 10^{-7}$
GO-G2$_{o\text{-tol}}$	$2.86 \cdot 10^{-7}$
GO-HG1	$5.95 \cdot 10^{-7}$
GO-HG2	$4.94 \cdot 10^{-7}$

The amount of ruthenium linked to GO has also been determined by ICP-OES (Inductively coupled plasma and optical emission spectrometry) analysis, the results obtained are substantially the same as those obtained via TGA (differences of less than 5%).

2.1.4 EVALUATION OF THE CATALYTIC ACTIVITY OF Ru-BASED CATALYSTS

The catalytic activity of the Ru-based catalysts covalently bonded on the GO was evaluated trough the Ring Opening Metathesis Polymerization (ROMP) of 2-norbornene and 5-ethylidene-2-norbornene. The ROMP of 2-norbornene, shown in *Scheme 2.3,* was carried out using THF as solvent.

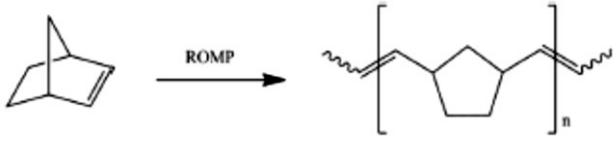

Scheme 2.3: Ring Opening Metathesis Polymerization of 2-norbornene.

The results of these polymerizations were compared with polymerization performed in the presence of ungrafted Ru-based catalysts. Data shown in *Table 2.3* summarize the results of the ROMP of 2-norbornene with catalysts supported on GO, while data shown in the *Table 2.4* summarize the results of the ROMP of 2-norbornene with catalysts not bonded to the nanofiller.

Table 2.2: ROMP of 2-norbornene in the presence of Ru-based catalysts covalently bonded to GO.

Catalyst	**2-norbornene (mol)**	**Catalyst ($mol \cdot 10^{-7}$)**	**Time (h)**	**Yield (g)**	**Conversion (%)**	**Activity** [a]
GO-G1	$1.03 \cdot 10^{-2}$	4.03	0.033	0.271	28	$1.96 \cdot 10^{6}$
GO-$G2_{o\text{-tol}}$	$9.97 \cdot 10^{-3}$	3.86	0.022	0.207	22	$2.15 \cdot 10^{6}$
GO-HG1	$1.03 \cdot 10^{-2}$	2.94	0.330	0.036	3.7	$3.68 \cdot 10^{4}$
GO-HG2	$9.71 \cdot 10^{-3}$	5.45	0.006	0.538	59	$1.83 \cdot 10^{6}$

***Table 2.3*:** ROMP of 2-norbornene in the presence of Ru-based catalysts.

Catalyst	***2-norbornene (mol)***	***Catalyst ($mol \cdot 10^{-6}$)***	***Time (h)***	***Yield (g)***	***Conversion (%)***	***Activity*** [a]
G1	$9.99 \cdot 10^{-3}$	3.64	0.008	0.269	29	$8.88 \cdot 10^{6}$
$G2_{o\text{-}tol}$	$1.01 \cdot 10^{-2}$	3.97	0.001	0.344	36	$1.54 \cdot 10^{6}$
HG1	$9.92 \cdot 10^{-3}$	5.49	0.140	0.061	6.5	$8.03 \cdot 10^{4}$
HG2	$9.67 \cdot 10^{-3}$	5.27	0.001	0.902	99	$3.46 \cdot 10^{6}$

[a] calculated in $\frac{Kg_{(polymer)}}{mol_{(monomer)} * mol_{(catalyst)} * h}$

All the runs were carried out a RT in 99 ml THF.

The data in *Table 2.3* highlight that Grubbs and Hoveyda Grubbs catalysts covalently bonded to the GO are active in the ROMP of 2-norbornene. A comparison of the activity values shown in *Table 2.3* with those of *Table 2.4* highlights that the catalyst covalently bonded to the nanofiller show catalytic activity very similar to that observed for the catalyst alone, demonstrating that the "grafting from"

approach did not cause significant reduction of the pristine catalytic activity when located on GO. An exhaustive extraction of the samples of GO-grafted-polynobornene obtained in this reactions of ROMP, with chloroform ($CHCl_3$), that totally dissolves ungrafted polynorbornene, lead to a residue of about 30-60 % of GO-grafted-polynobornene, indicating that part of the polymer is certainly grafted to the GO.

The ungrafted polynorbornene chains are probably generated by side cross metathesis (CM) reactions, sketched in *Fig. 2.14*. Indeed, the Ru-alkylidene, bound to a polymer terminal growing chain, can react, besides with the monomer, with whatever double bond along another growing chain present on the same as well as on another GO. This kind of CM can generate crosslinks between GO as well as ungrafted polymer growing chains [12].

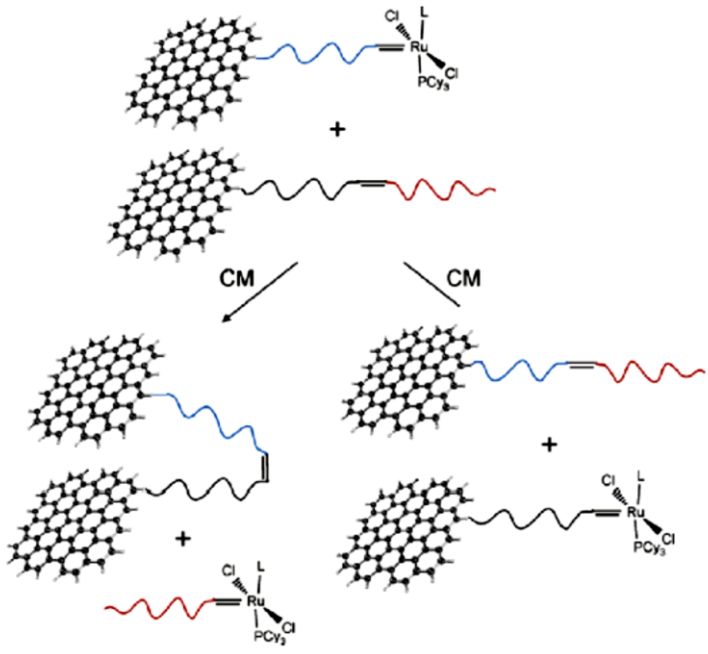

Figure 2.14: Cross metathesis (CM) reactions.

The Ru-based catalysts covalently bonded on the GO was tested also in the ROMP of 5-ethylidene-2- norbornene, the monomer used in the self-healing system. This polymerization was performed in bulk at the aim to replicate the inner part of the aeronautic systems. The results are summarized in the *Table 2.4* and the reaction was shown in the *Scheme 2.4*.

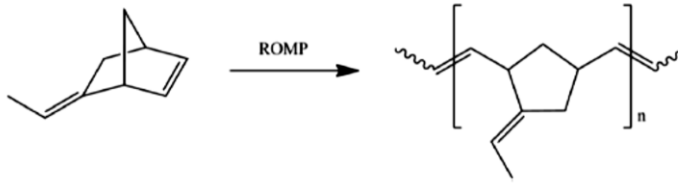

Scheme 2.4: Ring Opening Metathesis Polymerization of 5-ethyliden-2-norbornene.

The obtained products are completely insoluble in boiling decaline, probably due to the crosslinking among the polymer chains, in fact, the same results were found for the Grubbs and Hoveyda Grubbs catalysts not bonded to carbon nanofiller.

Table 2.4: Polymerization of 5-ethylidene-2-norbornene in the presence of Ru-based catalysts covalently bonded to GO.

Catalyst	***ENB (mol)***	***Catalyst ($mol \cdot 10^{-6}$)***	***Time (h)***	***Yield (g)***	***Conversion (%)***	***Activity*** [a]
GO-G1	$8.74 \cdot 10^{-3}$	1.13	$3.2 \cdot 10^{-2}$	0.400	38	$1.26 \cdot 10^{6}$
GO-G2$_{o\text{-}tol}$	$9.24 \cdot 10^{-3}$	1.19	$3.5 \cdot 10^{-2}$	0.970	87.4	$2.52 \cdot 10^{6}$
GO-HG1	$8.66 \cdot 10^{-3}$	2.25	$4.2 \cdot 10^{-3}$	0.995	96	$3.01 \cdot 10^{6}$
GO-HG2	$9.16 \cdot 10^{-3}$	1.84	$4.2 \cdot 10^{-3}$	1.010	92	$1.43 \cdot 10^{7}$

[a] calculated in $\frac{Kg_{(polymer)}}{mol_{(monomer)} * mol_{(catalyst)} * h}$

All the runs were carried out an RT in bulk.

2.1.5 EVALUATION OF THE CATALYTIC ACTIVITY INSIDE THE LIQUID EPOXY MIXTURE

In the development of the self-healing epoxy resins, the evaluation of the catalytic activity was investigated for the epoxy matrix composite without microcapsules. The epoxy mixture chosen was prepared by mixing an epoxy precursor (Bisphenol A diglycidyl ether, E) with a reactive diluent (1,4-Butanediol-diglycidyl ether, B) at a concentration of 80%: 20% (by wt) epoxide to flexibilizer giving the EB2 sample. This reactive diluent has proven to be effective to reduce the viscosity of epoxy precursors [13,14] allowing to improve handling and ease of processing and to optimize consequently performance properties. The curing agent investigated for this study was an anionic initiator Phenol-2,4,6-tris[(dimethylamino)-methyl] (Ankamine, A). The curing agent Ancamine was added at a concentration of 10% (by wt) with respect to the mixture EB2 giving the sample EB2A [15,16]. The catalysts G1, G2$_{o\text{-tol}}$, HG1 and HG2 covalently bonded to the GO were dispersed by mechanical agitation in the liquid epoxy mixture (EB2) composed of epoxy precursor (E) and reactive diluent (B). This mixture was filled with two different percentages of each functionalized nanofiller (GO-G1, GO-G2$_{o\text{-tol}}$, GO-HG1 and GO-HG2). In particular, the chosen percentages were 0.5% and 5% by weight of functionalized nanofiller (G1 0.015%, G2$_{o\text{-tol}}$ 0.0145%, HG1 0.030% and HG2 0.025%) with respect to the epoxy mixture EB2. The functionalized nanofillers were embedded

into the epoxy mixture EB2 at the temperature of 90 °C and kept at this temperature for 1 h using an oil bath. To verify the catalytic activity of each catalyst covalently bonded to the GO, spectroscopic investigation was carried out. For this purpose, the mixtures containing functionalized GO were stratified on a slide for light microscopy. Subsequently, two drops of ENB were added to the stratified mixtures. The control of the catalytic activity was performed by evaluating the formation of the metathesis product. For the catalysts bonded to the GO active in the Ring opening metathesis polymerization (ROMP) of ENB a thin solid film of metathesis product was obtained.

FT/IR spectra obtained for GO-HG1 and GO-HG2 (5% wt) show a peak at 966 cm^{-1} (see *Fig. 2.15*), characteristic of ring-opened poly(ENB). This peak is attributable to trans-substituted alkenes, characteristic of the ring-opened cross-linked product [poly(ENB)] providing evidence that the catalyst is active and that the activity was not compromised by the chemical nature of the environments, by the temperature and by the mechanical mixing.

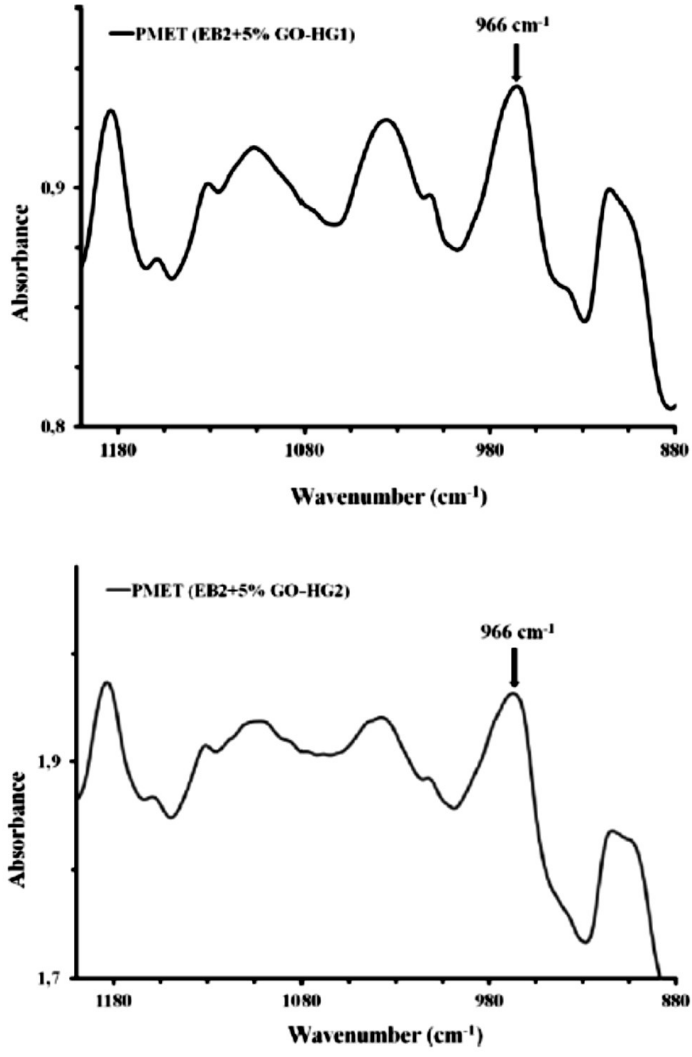

Figure 2.15: FT/IR spectra of the solid films (metathesis product) obtained by polymerization

Similar results were obtained with for GO-HG1 and GO-HG2 (0.5% wt). No catalytic activity was observed for GO-G2$_{o\text{-tol}}$. Concerning

the functionalized GO-G1 a very weak activity was observed. In particular, the metathesis product was obtained only after 2 days. Probably, Grubbs catalysts bonded to the graphene oxide (GO-G2$_{o\text{tol}}$ and GO-G1) deactivates during the process of preparation of the self-healing epoxy mixtures, maybe by reaction with oxirane rings. It is very likely that G1 and G2$_{o\text{-tol}}$ undergo deactivation by oxirane rings already at room temperature, while HG1 and HG2 are deactivated only at temperatures above 90 °C. A possible explanation for the different behavior of G1 and G2 with respect to HG1 and HG2 consists in the fact that the former two complexes, in order to react with the norbornene chemically bonded to GO, must lose the coordinated phosphine, and therefore the ruthenium compound becomes a complex to 14 electrons (see *Fig. 2.16 a*), so easily attacked by coordinating compounds, e.g. oxirane rings, while the latter two compounds may still coordinate oxygen of group isopropoxide, maintaining a configuration with 16 electrons (see *Fig. 2.16 b*) which is more stable than the 14 electron complexes of GO-G1 and GO-G2 catalysts.

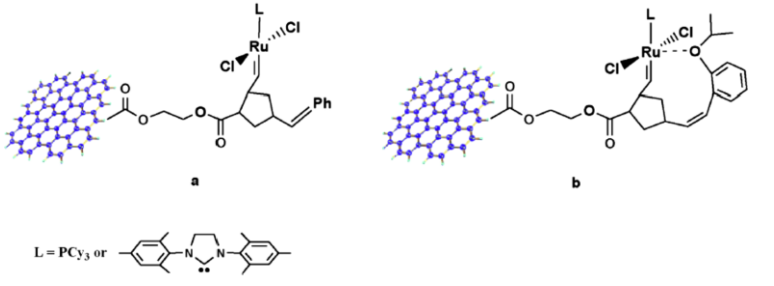

Figure 2.16: Possible structure of G1 and G2 (a) and HG1 and HG2 (b) ruthenium catalysts after reactions to chemically bind them to GO.

It worth noting that at higher temperature HG1 and HG2 solubilized at molecular level are deactivated by reaction with oxirane rings during the curing reactions of the resins. The catalysts covalently bonded to GO are exposed to contact with the rings of the epoxy resin and capable of giving reaction.

2.1.6 STUDY OF THE CATALYTIC ACTIVITY OF HG1 IN PRESENCE OF OXIRANE RINGS

HG1 catalyst powder was solubilized at molecular level in cyclohexene oxide to test HG1 reactivity with the epoxy groups in high concentration (without other components of the resin) [17]. To better analyze the behavior of the epoxides with the catalyst, we have used a simpler monomer as an epoxide: the cyclohexene oxide. The reactivity of this monomer with the catalyst was analyzed at different concentration and temperature by means of ^{1}H NMR. The ^{1}H NMR spectra of Hoveyda-Grubbs I, cyclohexene oxide, and of mixtures containing both HG1 and cyclohexene oxide in a molar ratio 1/1 were recorded at room temperature; the δ values were given in ppm, on samples dissolved in 1,1,2,2-tetrachloroethane-d2 (TCDE). *Figure 2.17* shows the spectra of Hoveyda-Grubbs I and cyclohexene oxide recorded at room temperature.

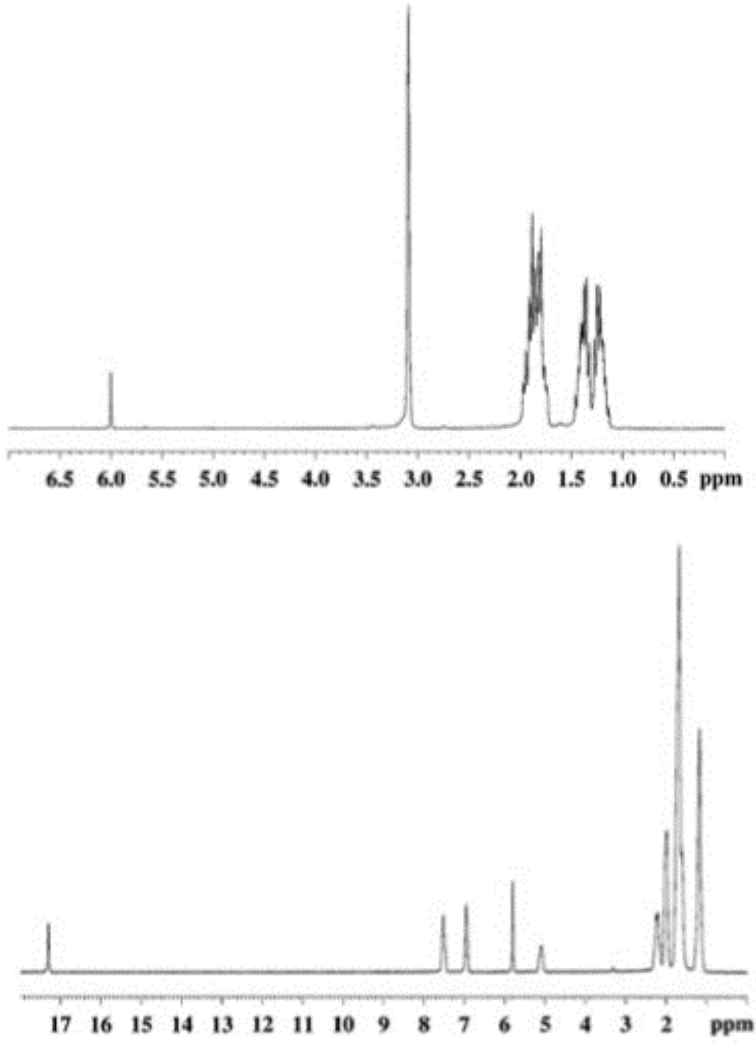

Figure 2.17: ^{1}H NMR spectra of Hoveyda-Grubbs I catalyst (above) and cyclohexene oxide (below) dissolved in 1,1,2,2-tetrachloroethane-d2 TCDE.

In *Figure 2.18*, variable-temperature (VT) ^{1}H NMR experiments in the range 80 < T < 140 °C of the mixture containing HG1 and cyclohexene oxide in a molar ratio 1:1 are reported. Spectrum at 80 °C (*Fig. 2.18* (a)) shows all the signals characteristics of HG1 and cyclohexene oxide, highlighting that no reaction take place between these two compounds. At higher temperatures, the signal at 17.45 ppm due to proton on alkylidene carbon of HG1 decreases, as well as the signal at 3.09 ppm attributable to protons of methine carbons of cyclohexene oxide, evidently because a reaction occurs between the alkylidene and the epoxide ring. At 140 °C (*Fig. 2.18* (d)), the reaction is practically completed, being the signals of the proton on alkylidene carbon of HG1 and the signal of protons of methine carbons of cyclohexene oxide barely noticeable.

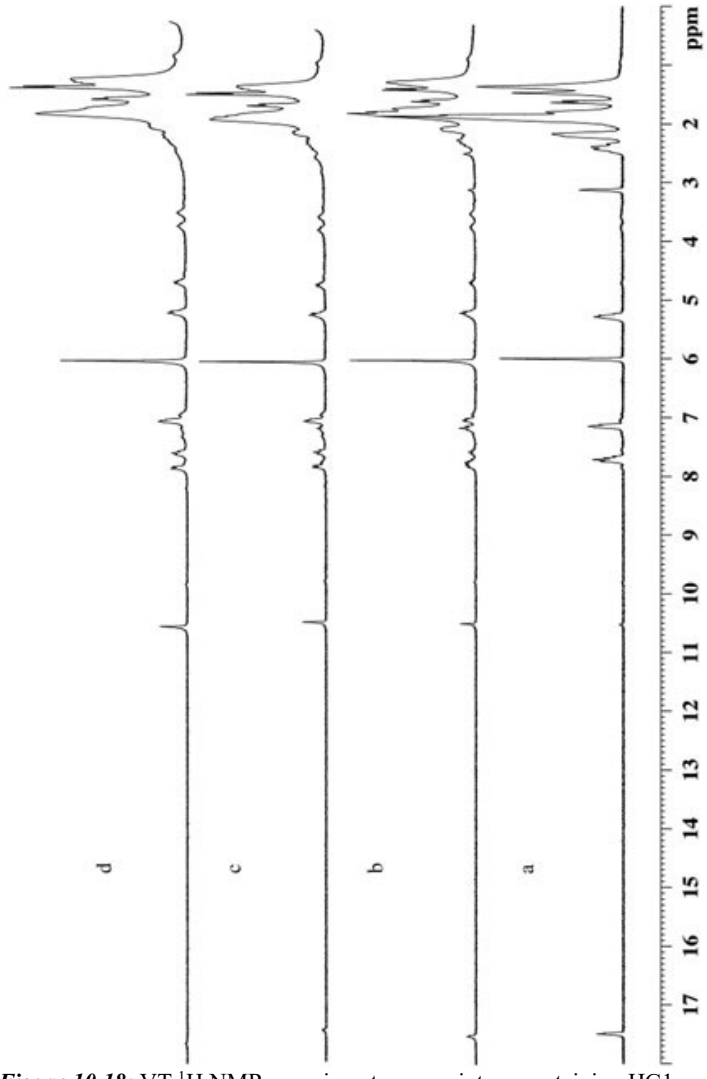

Figure 10.18: VT ^{1}H NMR experiments on a mixture containing HG1 and cyclohexene oxide in a molar ratio 1:1 ((a) 80 °C, (b) 100 °C, (c) 120 °C, and (d) 140 °C).

It is worth to note that NMR spectra of both the HG1 catalyst and cyclohexene oxide kept for 35 min at 140 °C show all the

characteristic signal indicating that no thermal decomposition occurs. The effect of the concentration on the ^{1}H NMR results with increasing the epoxy compound has also been analyzed and ^{1}H NMR spectrum of a mixture of Hoveyda Grubbs I catalyst with cyclohexene oxide (molar ratio 1/35) after a permanence for 1 hour at 140 °C is shown in *Figure 2.19*.

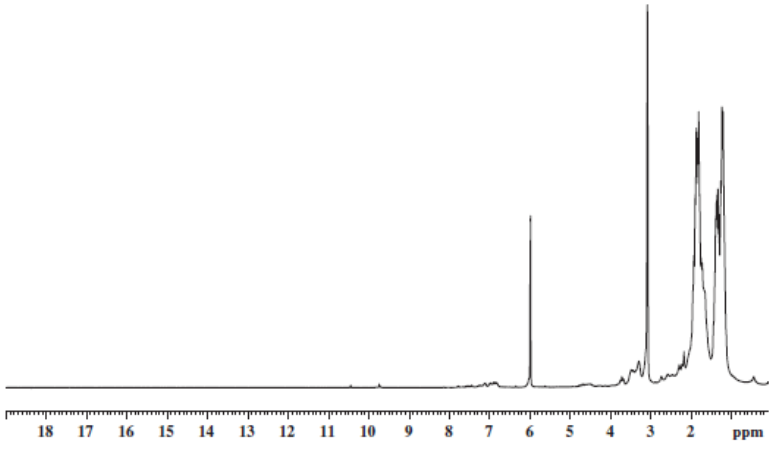

Figure 2.19: ^{1}H NMR spectra of HG1 and cyclohexene oxide in TCDE kept for 35 min at 140 °C.

In this case, we observe the absence of the characteristic resonance signal of the benzylidene proton (Ru = CH-Ph) at 17.45 ppm. Moreover, we again observe the resonance signal at 3.09 ppm due to the protons on the epoxy carbons; this result is obvious considering that the cyclohexene oxide is in large excess. Evidently, the reaction between epoxide ring and alkylidene of rutenium compound is equimolecular. The addition of a drop of healing agent (5-ethylidene-2-norbornene – ENB) to this mixture shows that the catalyst is

deactivated, as can be seen from the absence of the solid film formation due to the metathesis reaction. Consistently it was observed catalyst deactivation with the complete disappearance of the alkylidene signal in the ^{1}H NMR spectrum. Thus, the last results highlight that a deactivation of the HG1 catalyst occurs at 140 °C due to a reaction between the catalyst and the cyclohexene oxide. Of course, the deactivation of the catalyst due to the oxirane rings is facilitated in the mixture HG1/cyclohexene oxide with respect to the deactivation of the catalyst due to the contact with oxirane rings in the mixture HG1/ epoxy mixture, due to the higher concentration of oxirane rings in the mixture with cyclohexene oxide.

It is worth noting that when the powder catalyst is used in the epoxy mixture, a part can survive up to 170 °C, due the accidental lack of direct contact between molecules of the complex (catalyst) and oxirane rings of the epoxy mixture. Therefore, even if the deactivation of the HG1 catalyst occurs at 130 °C due to a reaction between the catalyst and the oxirane rings, for the catalyst molecules for which the contact does not occur, the self-healing mechanisms may still be active until at 170 °C with reduced self-healing efficiency due to the reduction in the actual amount of catalyst.

2.1.7 MICROCAPSULE MANUFACTURE

Microcapsules containing as “healing agent” a blend of two olefins 5-ethylidene-2-norbornene (ENB) and dicyclopentadiene (DCPD), with the outer shell composed of poly(ureaformaldehyde) and the

inner shell of ethylene maleic anhydride (EMA) copolymer, were prepared by in situ polymerization in an oil inwater emulsion (the name used was capED5) [16]. DCPD was added to ENB with the aim of increasing the crosslinked fraction of the metathesis products [18]. The composition of the microcapsules was ENB (95%)/DCPD (5%). The morphology of the microcapsules was obtained by FESEM investigation (*Fig. 2.20*).

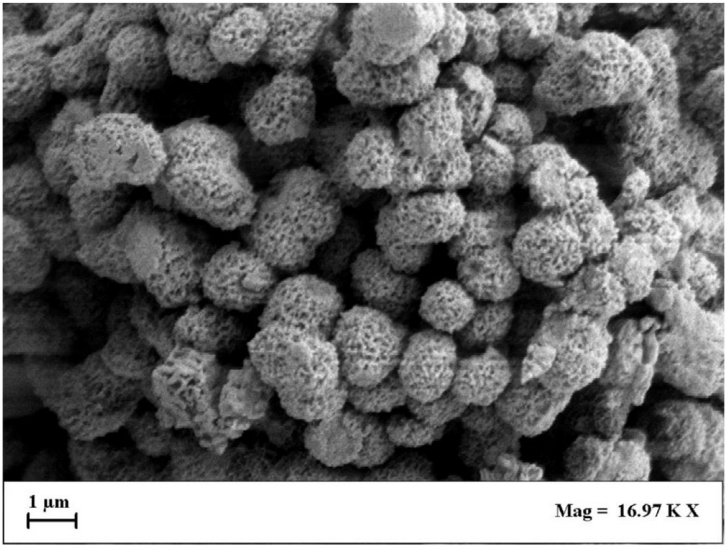

Figure 2.20: FESEM image of the microcapsules (capED5) in the form of spherical snarls.

The histogram of diameter of microcapsule used for the manufactured self-healing specimens is shown in *Fig. 2.21*. It yields a mean diameter of 1.5 µm.

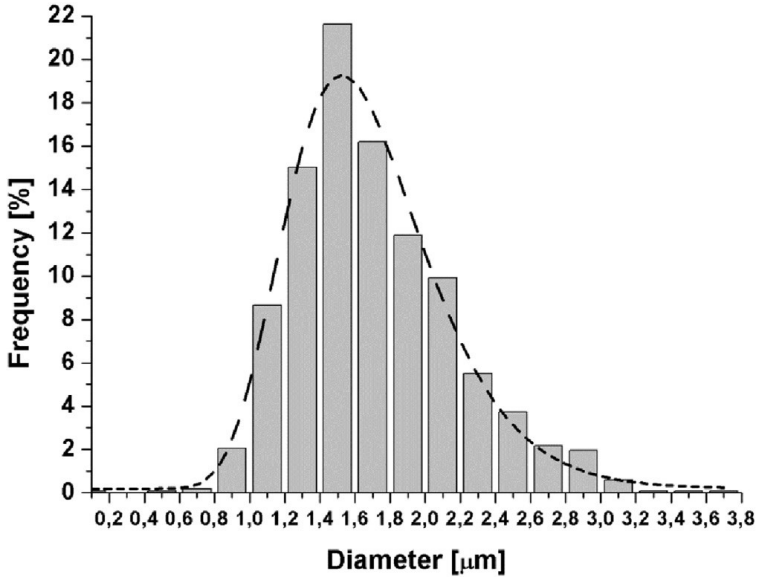

Figure 2.21: Histogram of the microcapsule diameter.

2.1.8 EVALUATION OF THE SELF-HEALING ACTIVITY IN THE SOLID EPOXY SAMPLES

The dynamic test defines mechanical behavior responding to a continuously deformation, and it can be used to identify the recovery time and the amount mechanical healing. The self-healing sample was prepared mixing the epoxy matrix EB2A, 0.5% of GO-Ru catalyst (HG1 and HG2) and 5% of microcapsules capED5.

The relative elastic modulus evolution of the self-healing samples is shown in *Fig. 2.22* for the sample containing GO-HG1 and in *Fig.*

2.23 for the sample containing GO-HG2.

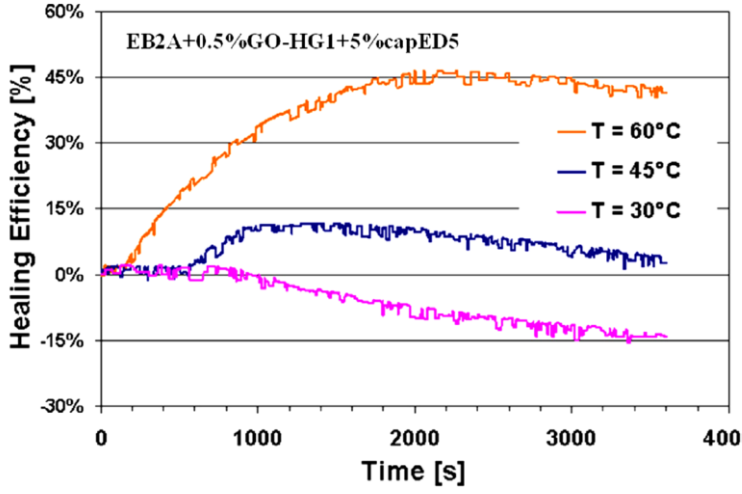

Figure 2.22: Time evolution of the relative elastic modulus of the EB2A+0.5%GO-HG1+5% capED5 sample at different temperature.

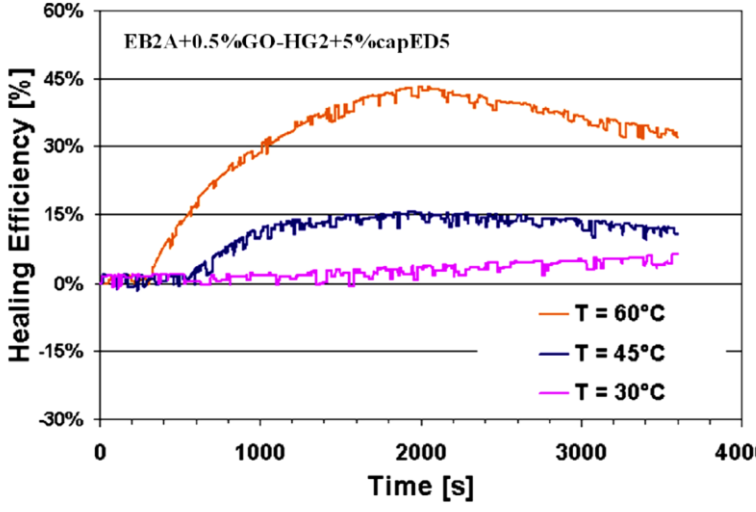

Figure 2.23: Time evolution of the relative elastic modulus of the EB2Aþ0.5%GO-HG2+5% capED5 sample at different temperature.

The behavior is quite similar for both samples and seems to depend by the test temperature. In particular, the samples show a maximum in the healing efficiency, followed by a drop probably due to the crack propagation caused by the cyclic fatigue stress. The time at which crack healing starts, was found to be a complex function of both the test temperature and the crack geometry/ dimension. On the contrary, the healing efficiency, defined as the percentage of elastic modulus recovered, was found to be less sensitive by the crack formed by the initial impulsive load.
In this specific case, at 60 °C the sample with GO-HG1 shows a higher healing efficiency (about 47%) with respect to the other sample (about 43%). The sample with GO-HG1 at 30 °C does not show any evidence of healing.

2.2 PROTECTION OF THE CATALYTIC SITE WITH POLYMERIC GLOBULAR SHELL

The satisfactory results obtained for the healing of the materials promoted to the Grubbs and Hoveyda Grubbs catalysts supported on functionalized GO have inspired a new approach that involves the use of this supported catalysts [19]. The deactivation of the catalysts supported on graphene sheets at temperature above 90 °C could be overcome through the preservations the catalytic sites, composed of Ru preventing contact with the surrounding environment.
We have explored the protection of the catalytic sites polymerizing 2-norbornene with ruthenium complex, to form a globular shell

around the active catalytic site.

The protection mechanism proposed is based on the formation of a micrometric globular shell that partially englobed the catalytic site, causing hindrances for the deactivation of the catalyst, preventing equimolecular reaction between the catalyst complex and the oxirane ring. Several steps were used to obtain the Protected Ru-functionalized Graphene Sheets (Poly-NBE-GO-HG2): 1) Graphene Oxide (GO) was prepared by chemical oxidation of high surface area graphite; 2) GO was used to support ruthenium catalysts for Ring Opening Metathesis Polymerization (ROMP); 3) few units of 2-norbornene were polymerized by Hoveyda Grubbs II (HG2) complex covalently bound to the graphene layers (GO-HG2), forming a globular shell which partially englobe the catalytic sites thus producing Protected Ru-complex on graphene sheets (PolyNBE-GO-HG2).

The ruthenium catalyst bonded to the graphene oxide (GO-HG2) and protected by polynorbornene is able to trigger self-healing reaction based on the ROMP of 5-ethylidene-2-norbornene (ENB) which can be used as healing agent in auto-repair composites. This system enables an efficient transfer of the graphene properties to the polymer matrix and allows a significant reduction in the amount of ruthenium complex to be used for self-healing reactions in highly reactive matrices, with substantial cost savings; it can be used for self-healing resins cured up to 140 °C [20].

2.2.1 SELECTION OF THE RATIO GO-HG2/ENB TO OBTAIN THE BEST DISPERSION IN THE EPOXY MATRIX

PolyNBE-GO-HG2 catalyst was prepared by ROMP of 2-norbornene using Hoveyda Grubbs II generation catalyst covalently bonded to graphene sheets (GO-HG2) (see section 2.1.2.1). The molar ratio of GO-HG2 and 2-norbornene initially used was 1:50. The protection of catalytic sites was conducted mixing the 2-norbornene and the in the CH_2Cl_2 (*Fig. 2.24*). Then, the solvent was removed. Despite the high molar ratio of gHG2 and 2-norbornene used, the protected catalyst showed a very good performance in the activation of ROMP reaction, but, probably due to the high amount of polymer around the catalyst, it did not give a good dispersion in the epoxy matrix. Instead, using molar ratio of 1:10 of gHG2 and 2-norbornene this critical point was eliminated.

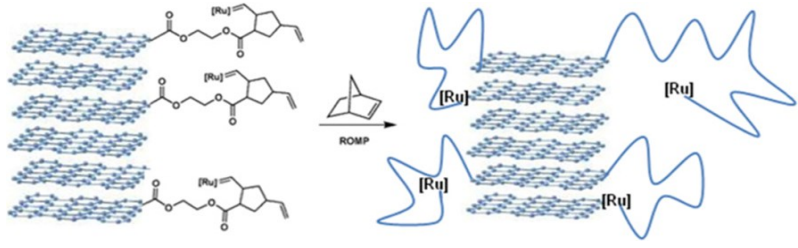

Figure 2.24: Scheme of the reaction for the protection of catalyst.

2.2.1.1 MORPHOLOGYCAL CHARACTERIZATION

FESEM images of GO-HG2 sample are shown in *Fig. 2.25* for two different zones of the functionalized nanofiller. FESEM images reveal that the gHG2 functionalized material consists of randomly aggregated, thin, crumpled graphene sheets.

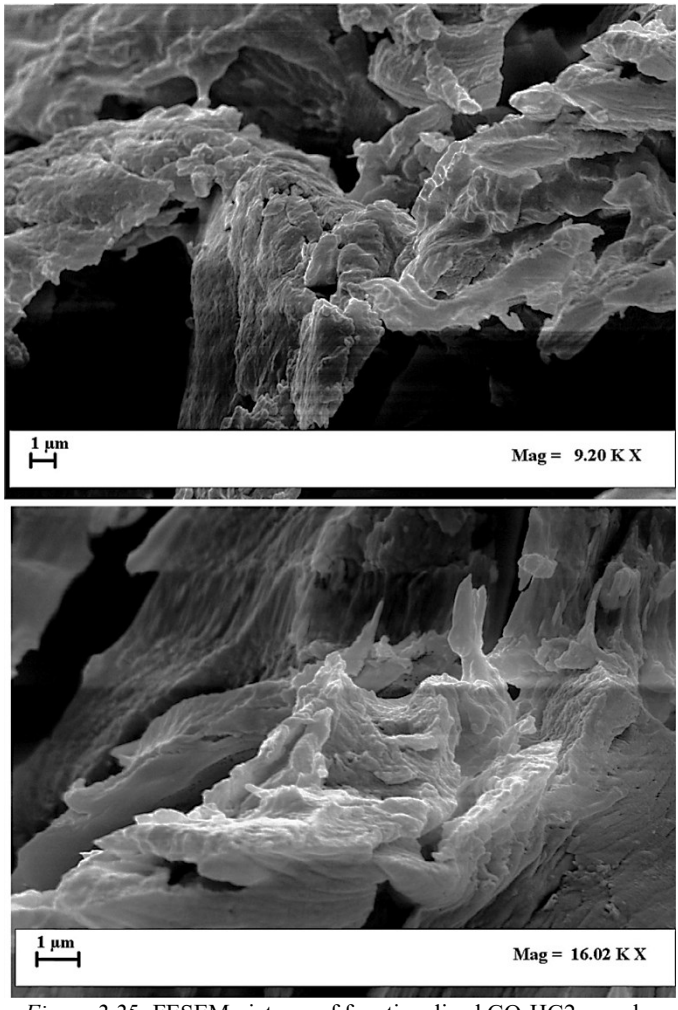

Figure 2.25: FESEM pictures of functionalized GO-HG2 sample.

Fig. 2.26 shows FESEM images of the protected Ru-functionalized graphene sheets (PolyNBE-GO-HG2). Indeed, units of monomers around the ruthenium atoms were polymerized forming an open globular shell around the catalytic sites, as evident in the FESEM image at two different magnifications.

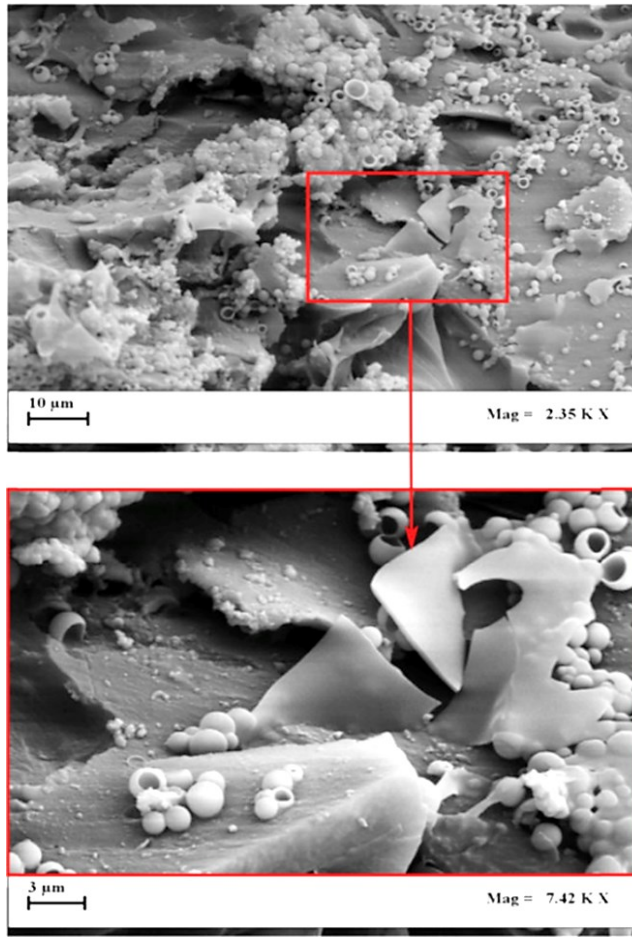

Figure 2.26: FESEM images of the globular shell around the catalyst sites attached on graphene sheet (PolyNBE-GO-HG2sample).

2.2.2 EVALUATION OF THE CATALYTIC ACTIVITY INSIDE THE LIQUID EPOXY MIXTURE

In the development of the self-healing epoxy resins, the evaluation of the catalytic activity was investigated for the epoxy matrix without microcapsules to avoid confusion between globular shells surrounding the catalytic sites and the microcapsules.

The epoxy mixture chosen on the basis of considerations reported in previous papers was EB2 [21-22]. PolyNBE-GO-HG2 were dispersed by mechanical agitation in the liquid epoxy mixture (EB2) composed of epoxy precursor (E) and reactive diluent (B) (*Fig. 2.27*). This mixture was filled with a low percentage of PolyNBE-GO-HG2 (0.326% by weight) with respect to the epoxy mixture EB2.

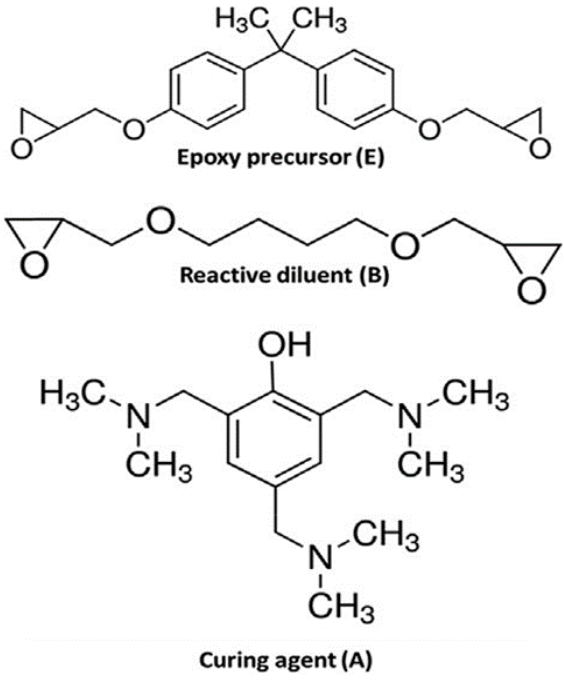

Figure 2.27: Chemical formulas of the compounds used for the mixture EB2A.

PolyNBE-GO-HG2 were embedded into the epoxy mixture EB2 at the temperature of 90 °C and kept at this temperature for 1h using an oil bath. To verify the catalytic activity of this catalyst, spectroscopic investigation was carried out. For this purpose, the fluid mixture containing PolyNBE-GO-HG2 was stratified on a slide for light microscopy. Subsequently, two drops of 5-ethylidene-2-norbornene (ENB) were added to the stratified mixtures. The control of the catalytic activity was performed by evaluating the formation of the metathesis product. PolyNBE-GO-HG2 dispersed in the epoxy mixture showed high ROMP activity, in fact a thin solid film of

metathesis product was obtained immediately.

The FT/IR spectrum of the polymeric film obtained for EB2-0.326% PolyNBE-GO-HG2 (*Fig. 2.28*) showed the characteristic peak at 966 cm^{-1} which is due to ring-opened poly(ENB). This peak is assigned to the trans substituted alkenes; it is characteristic of the ring opened product [poly (ENB)] and provides direct evidence that the embedded protected catalyst is active.

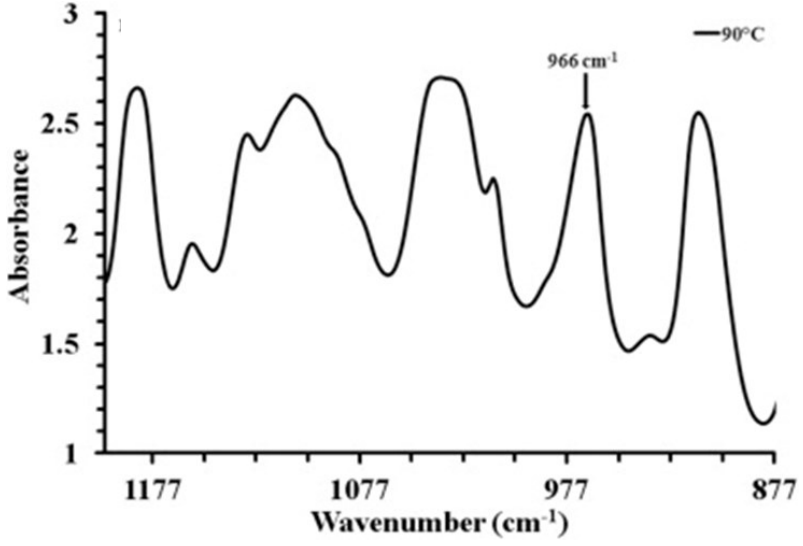

Figure 2.28: FT/IR spectrum of the solid film (metathesis product) obtained by polymerization of ENB with PolyNBe-GO-HG2 (0.326 wt %) dispersed in the EB2 mixture at 90 °C.

2.2.3 EVALUATION OF THE SELF-HEALING ACTIVITY IN THE SOLID EPOXY SAMPLES

Similar results were also obtained for the solidified sample EB2A -

0.326% PolyNBE-GO-HG2 cured up to 140 °C.

Indeed, *Fig. 2.29* shows FT/IR spectra of the metathesis products of the cured material respectively after the intermediate stage at 110 °C and the second stage carried out up to 140 °C. The samples EB2A - 0.326% PolyNBE-GO-HG2 cured up to 110 °C and 140 °C were cut by a serrated blade; the powders produced from the samples were collected in a mortar and a drop of healing agent (5-ethylidene-2norbornene - ENB) was added before dispersing the sample powder into the KBr disks for FT/IR investigation.

The presence in all cases of the strong peak at 966 cm^{-1}, indicating formation of the metathesis product, proved the catalytic activity of the PolyNBE-GO-HG2 embedded in the solid epoxy matrix. The mixture can be cured up to 140 °C for 2h without compromising the catalytic activity.

Self-healing samples containing embedded unprotected HG2 catalyst bonded to the graphene sheets (GO-HG2) were previously analyzed [19]. The absence of protection of the catalytic sites imposed limits on the curing temperatures of the self-healing samples (90 °C was the max. value of temperature used for the curing reactions). So, mild curing conditions were used with respect to the self-healing samples of the present work in which curing temperatures up to 140 °C have been reached.

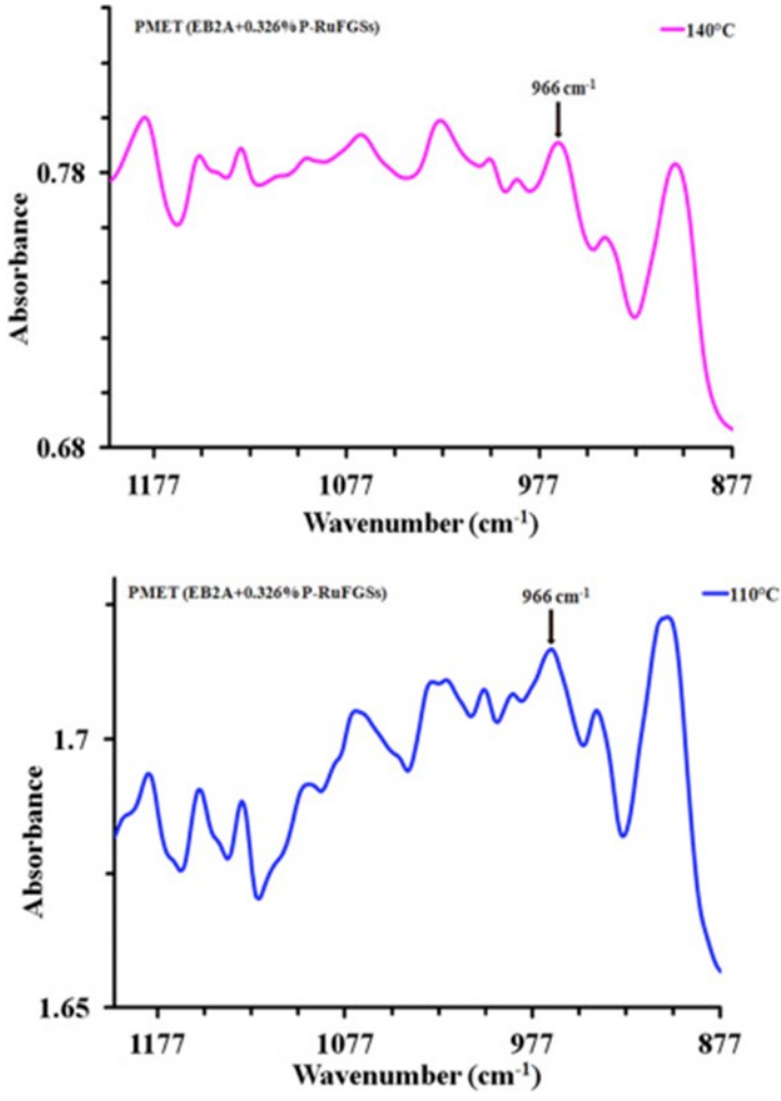

Figure 2.29: FT/IR spectra of the solid film (metathesis product) obtained by polymerization of ENB with PolyNBe-GO-HG2 (0.326 wt %) dispersed in the EB2A mixture cured up to 110 °C (graph on the bottom) and cured up to 140 °C (graph on the top).

2.3 ALTERNATIVE APPROACHES FOR THE COVALENT FUNCTIONALIZATION OF THE CARBON NANOFILLER

Carbon-based nanomaterials have become important due to their excellent combinations of chemical and physical properties (i.e., thermal and electrical conductivity, high mechanical strength, and optical properties), and extensive research efforts are being made to utilize these materials for various industrial applications, such as high-strength materials and electronics.

The method of functionalization descried above requested a preliminary step of oxidation of graphite to graphite oxide for the purpose to create the support that, through sequential reactions, bind the metathesis catalysts. This procedure modifies the graphitic plane and compromise the final performance of the material. At the aim to preserve the intrinsic properties of the pristine carbon filler was evaluated alternative approaches that don't request the oxidation of the filler. Those methods are the functionalization of the multiwalled carbon nanotubes (MWCNTs) via elettrochemical modification and functionalization of the MWCNTs and graphite with 1,3-dipolar cycloaddition reaction.

2.3.1 FUNCTIONALIZATION OF THE MULTIWALLED CARBON NANOTUBES (MWCNTs) WITH ARYLDIAZONIUM SALTS VIA ELECTROCHEMICAL MODIFICATION

The graphitic materials conduct electricity, by the delocalization of π electrons forced to move above and below the planes of the carbon atom. These electrons are free to move, so they are able to conduct electricity. However, electricity is only conducted along the plane of the layers.

In this materials each carbon atom uses only 3 of its 4 electrons in the outer energy level in the bond covalently to three other carbon atoms. Each carbon atom contributes an electron to an electron delocalized system which is therefore a part of the chemical bond. The delocalized electrons are free to move around the floor. For this reason, graphite conducts electricity along the planes of carbon atoms, but does not conduct between the planes.

As described so far, our work was particularly focused to the use of these carbon nanomaterials as a support for metathesis catalysts in materials with self-repairing ability. For these purposes carbon nanomaterials were properly functionalized at the aim to bond the metathesis catalysts.

However, these nanomaterials must undergo a preliminary step of oxidation to be able to bind the catalysts, in this way the structure of the graphitic plane is modified resulting in drastic reduction of the conductivity of the carbon material.

For this purpose, you can think an alternative approach for the functionalization of these carbon nanomaterials that allows at the same time to bind the metathesis catalysts and leave intact the structure of the carbon material [25].

In recent literature is reported that the MWCNTs, due to their excellent structural and electronic properties [26], have emerged as an attractive material for various applications including molecular electronics [27,28] and field emission devices [29]. A variety of devices have been realized with MWCNTs, such as single electrode transistor operating at very low temperatures, field-effect transistor, chemical sensor and logic circuits. Moreover, the electrochemistry approach is a well-suited tool for controlled modification of MWCNTs. The work reported below regards the functionalization of multiwalled carbon nanotubes (MWCNTs) through an electrochemical modification [30] that allows to link the metathesis catalyst.

2.3.1.1 FUNCTIONALIZATION OF MWCNTs WITH RU-BASED CATALYST

The functionalization of MWCNTs was obtained through four synthetic step. The first step consists in the electrochemical modification of the MWCNTs, at the aim to create a support for the next steps of functionalization, using a reductive coupling approach.

- **First step: electrochemical modification of the MWCNTs with 4-bromobenzenediazonium salt**

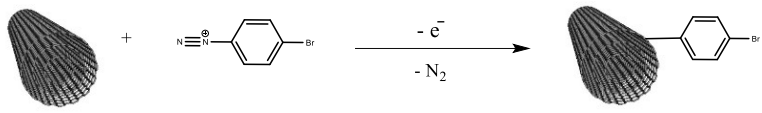

MWCNTs (1)

Figure 2.30: First step: electrochemical modification of the MWCNTs with 4-bromobenzenediazonium salt.

The reduction of a 4-bromobenzenediazonium salt was used to attach 4-bromophenyl group covalently to MWCNTs (*fig. 2.30*). The electrochemical modification was carried out in a microcell with platinum counter and pseudoreference electrodes. A tungsten needle probe was used to make contact with the electrodes on the substrate surface, which enabled the functioning of the MWCNTs as the working electrode. Reductive coupling of 4-bromobenzenediazonium tetrafluoroborate ($BrC_6H_4N_2^+BF_4^-$), was performed with lithium perchlorate ($LiClO_4$) in N,N-dimethylformamide (DMF)[25]. The reaction has been monitored by voltammogram (*fig. 2.31*). Data were acquired after 1 minute, 3 minutes, 1 hour and 3 hours. The voltammogram show an increment over time of the signal at -1.3 V, to associate with the electrochemical modification of MWCNTs, as reported in literature [1]. The product (1) was characterized by FT/IR analysis (*Fig. 2.37*).

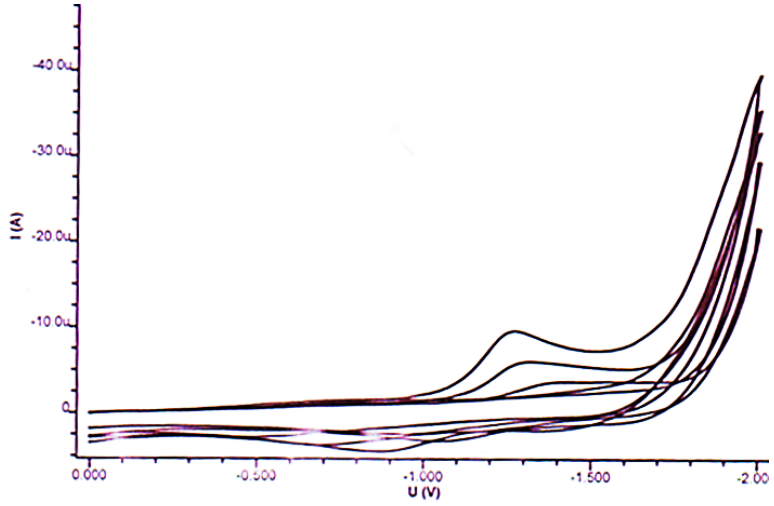

Figure 2.31: Voltammogram of electrochemical modification of the MWCNTs with 4-bromobenzenediazonium salt.

The formation of product (1) was confirmed through test that highlights the bromine presence. The alkaline fusion is a drastic treatment that frees Br^- ions (*Fig. 2.32*), which are then reacted with $AgNO_3$ to allow the precipitation of AgBr. The product (1) was treated with metallic Na according to the reaction:

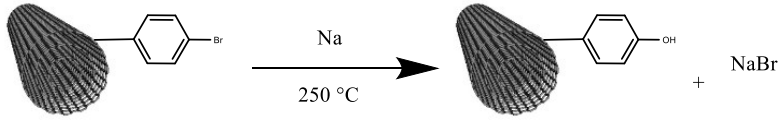

(1)

Figure 2.32: The alkaline fusion of MWCNTs-Ph-Br.

At the product obtained by alkaline fusion (1) was added $AgNO_3$ at

the aim to form AgBr, that looks like a yellow-white solid precipitate. This highlights the presence of Br^-.

$$Br^- + AgNO_3 \leftrightarrow AgBr \downarrow + NO_3^-$$

- **Second step: formation of lithium organic derivate of MWCNT**

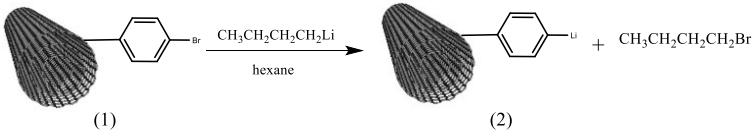

Figure 2.33: Second step: formation of lithium organic derivate of MWCNTs.

The lithium organic derivate of the MWCNTs was formed by reaction with *n*-butyl lithium reagent ($CH_3CH_2CH_2CH_2Li$, *n*-BuLi) in hexane (*Fig. 2.33*). The reaction was a metal-halogen exchange between an organic halide (usually a bromide or an iodide) and a organo-lithium species (usually *n*-BuLi, *s*-BuLi, *t*-BuLi). This is an equilibrium reaction, and then is successful only if the format lithium reagent has a more stable carbanion of the starting one. This method is often used to prepare reagents of vinyl lithium, aryl and primary alkyl.

The product (2) was characterized by FT/IR analysis (*Fig. 2.37*). The success of the reaction was confirmed by the formation of byproduct bromobutane. The solution recovered from the reaction was characterized by ^{1}H-NMR (*Fig. 2.34*) to verify the presence of bromobutane, confirmed by the signal at 2.55 δ.

The ^{1}H spectrum of *n*-BuLi shows the signal related to the H bonded on the CH_2-Li at about 1.3 δ, this signal shifts at lower fields due to the bond with electronegative Br that shields the proton and the signal appears at 2.55 δ. The spectrum shows the signals at 0.9 δ, related to the terminal -CH_3, 1.3 δ related to the CH_3-CH_2-CH_2-CH_2-Br and 1.6 δ CH_3-CH_2-CH_2-CH_2-Br.

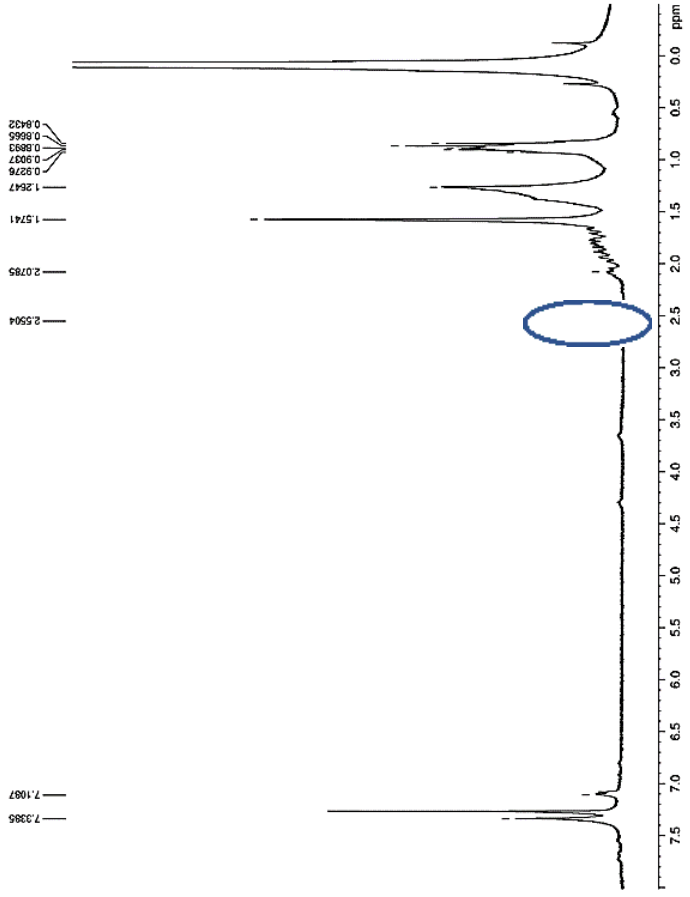

Figure 2.34: ^{1}H-NMR spectrum of bromobutane.

- **Third step**: ***functionalization of the MWCNTs with 5-norbornene-2-carboxaldehyde***

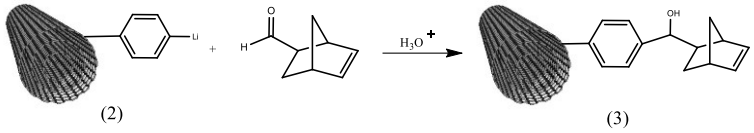

Figure 2.35: Third step: functionalization of the MWCNTs with 5-norbornene-2-carboxaldehyde.

The organometallic reagents such as organic lithium, Grignard reagents and sodium acetylides react with aldehydes and ketones in a nucleophilic addition in order to forming an alcohol with a more C. In this way by formaldehyde primary alcohols, by other aldehydes secondary alcohols and by ketones tertiary alcohols are obtained, respectively.

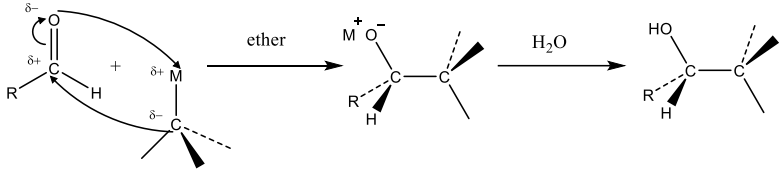

The reaction evolves in two steps. The mechanism starts with a nucleophilic attack on the carbonylic site of the organometallic compound, which is a carbanion with a negative charge on the C. This reaction forms an alkoxide intermediate that for treatment with acidified water produces the corresponding alcohol with an additional carbon atom than the carboxyl of start. This step of functionalization of the MWCNTs gives the addition of 5-

norborbornene-2-carboxaldehyde to product (2), the organic lithium derivate of the MWCNTs, to yield the secondary alcohol, according to the mechanism above reported. The product (3) obtained then was characterized by FT/IR spectroscopy: the signal characteristic of C=O of the aldehyde, stretch (1630 cm^{-1}), was decreased (*Fig. 2.37*), confirmed that the secondary alcohol was obtained.

- **Fourth step**: ***functionalization of the MWCNTs with Ru-based catalyst***

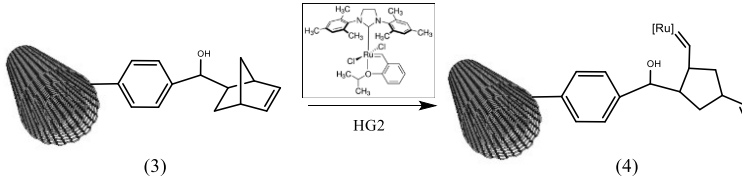

(3) (4)

Figure 2.36: Fourth step: functionalization of the MWCNTs with Ru-based catalyst.

The product of the third reaction step was reacted with (1,3-Bis-(2,4,6-trimethylphenyl)-2-imidazolidinylidene)dichloro(*o*-isopropoxyphenylmethylene)ruthenium(II) (HG2 catalyst). The synthetic procedure used was the same reported for to bind the catalyst on the GO functionalized. The product (4) was subjected to FT/IR (KBr pellet) spectroscopy (*Fig. 2.37*) and showed no significant differences compared with that obtained with the previous product (3).

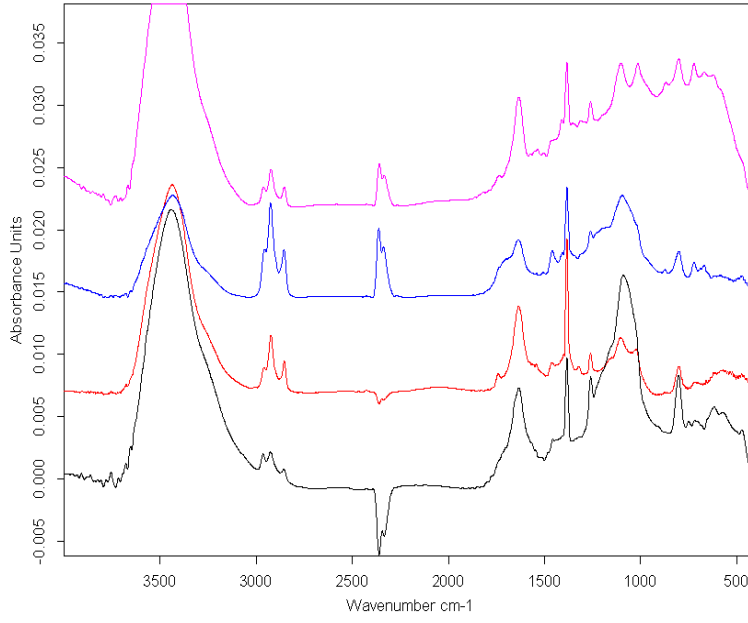

Figure 2.37: FT/IR analysis of product of (1), (2), (3) and (4).

The product (4) was characterized by thermogravimetric analysis (*Fig. 2.38*) to evaluate the residue at 1000°C in air related at RuO_2 and to calculate the amount of Ru bonds to the MWCNTs. The value

obtained was 2.5 %, corresponding to 0.0188 mmol/g of Ru.

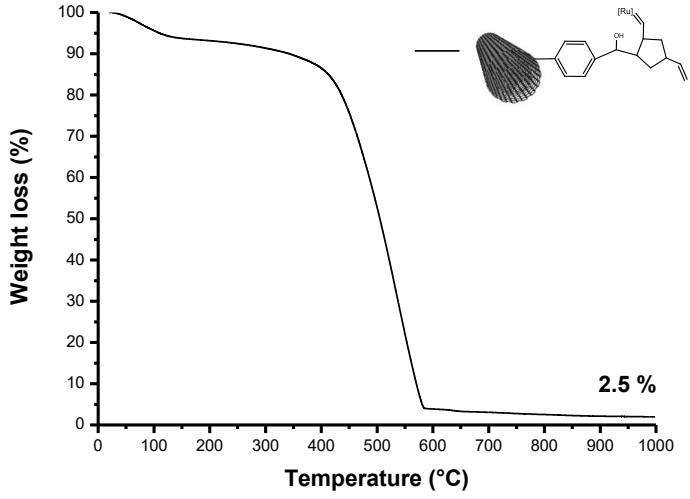

Figure 2.38: Thermogravimetric analysis of product (4).

The functionalized nanotubes with the catalyst was tested in reactions of ring opening metathesis polymerization (ROMP) of 2-Norbornene and 5-Ethylidene-2-norbornene.

2.3.1.2 EVALUATION OF THE CATALYTIC ACTIVITY OF THE MWCNTs/Ru-BASED CATALYST

- **ROMP of 2-norbornene**

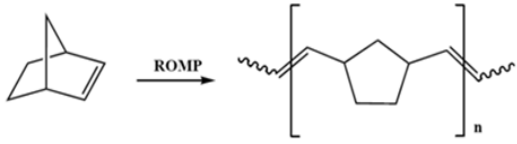

The activity of catalyst supported on MWCNTs (product (4)) was evaluated by ROMP of 2-norbornene. The polymerization was conduct with 9.8 mmol of 2-norbornene and $6.02 \cdot 10^{-1}$ mmol of HG2 supported on MWCNTs functionalized, in tetrahydrofuran (THF) for 1 hour. The product obtained was 68 mg. The activity of the catalyst was $1.12 \cdot 10^{4} \frac{Kg}{mol^2 * h}$.

- **ROMP of 5-etiliden-2-norbornene**

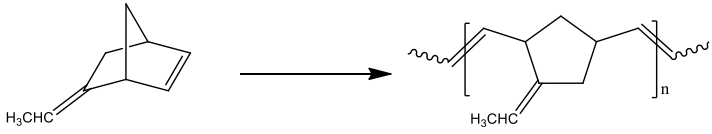

The polymerization of 5-ethyliden-2-norbornene was conduct with $1.0 \cdot 10^{-3}$ mmol of catalyst (product (4)) and 9.3 mmol of 5-ethilyden-2-norbornene in bulk for 24 h. The polymer obtained was about 33 mg.

The low activity of the catalyst obtained can be related to the nearness between the catalytic site and the MWCNTs. The literature reports that this factor may influence the access of the monomer at the catalytic site, leading to the formation only of a low quantity of polymer [31]. For this reasons the test in the self-healing mixture were not done.

2.3.2 FUNCTIONALIZATION OF THE FILLER WITH 1,3-DIPOLAR CYCLOADDITION REACTION

In this section was described the functionalization of MWCNTs and graphite through 1,3-dipolar cycloaddition reaction of azomethine-ylides to the graphitic surface, to give pyrrolidine fused ring [32,33].

2.3.2.1 FUNCTIONALIZATION OF THE MWCNTs

The MWCNTs used for the functionalization were subjected to FT/IR analysis, which display the presence of oxygenated functional groups in the material. In fact, absorption bands of carboxyl groups (1741 cm^{-1}), hydroxyl groups (bending at 1385 cm^{-1}) and epoxide groups (1145-1065 cm^{-1}) were observed.

The large IR band at ca. 3400 cm^{-1} and the weak one at 1627 cm^{-1} are attributed to the asymmetrical stretching and scissoring vibrations, respectively, also due to traces of water in the KBr pellet used for the analysis. The trace water could not be removed even with extensive drying of the KBr at elevated temperatures and prolonged purging of the instrument with a stream of nitrogen gas.

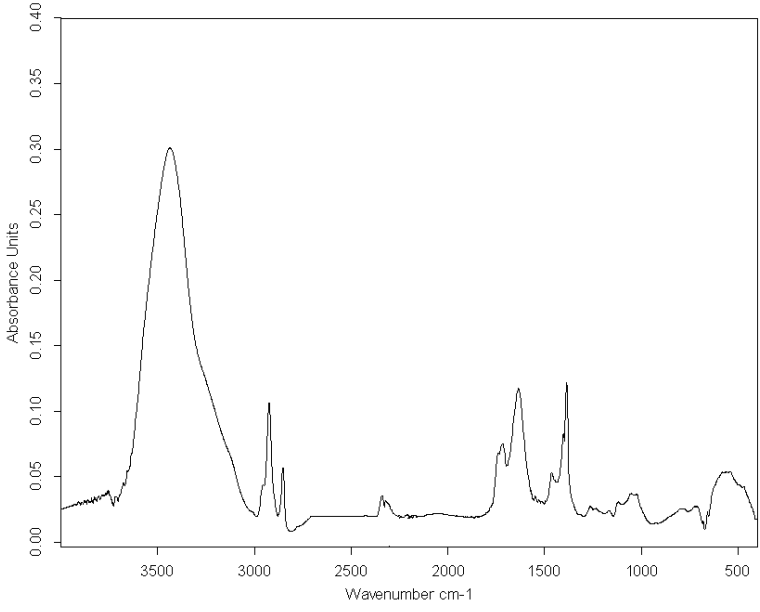

Figure 2.39: Spectrum FT/IR of MWCNTs.

- **First step**: ***functionalization of the MWCNTs with 4-hydroxyphenyl glycine and octyl aldehyde***

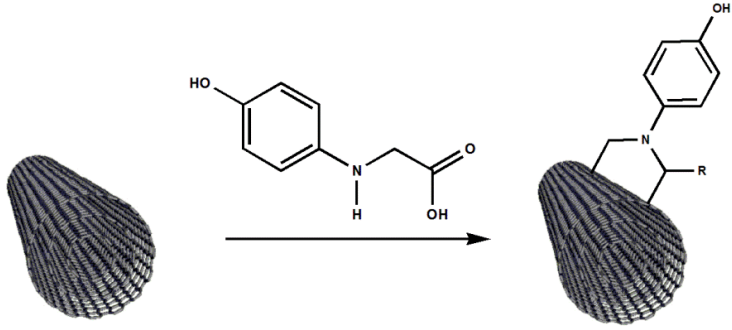

MWCNTs (1)

Figure 2.40: First step: functionalization of the MWCNTs with 4-hydroxyphenyl glycine and octyl aldehyde.

Addition of 4-hydroxyphenyl glycine and octyl aldehyde to a suspension of MWCNTs in DMF, followed by heating at 130 °C for 5 days, resulted in the incorporation of phenol-functionalized pyrrolidine rings on the surface of the MWCNTs.

The product of this procedure was characterized by FT/IR spectroscopy and exhibited the expected aromatic C-C stretch at 1634 cm^{-1} and the signal at 2900 cm^{-1} due to the alkyl portions of the attached unit and aromatic C-C bending at 715 cm^{-1}.

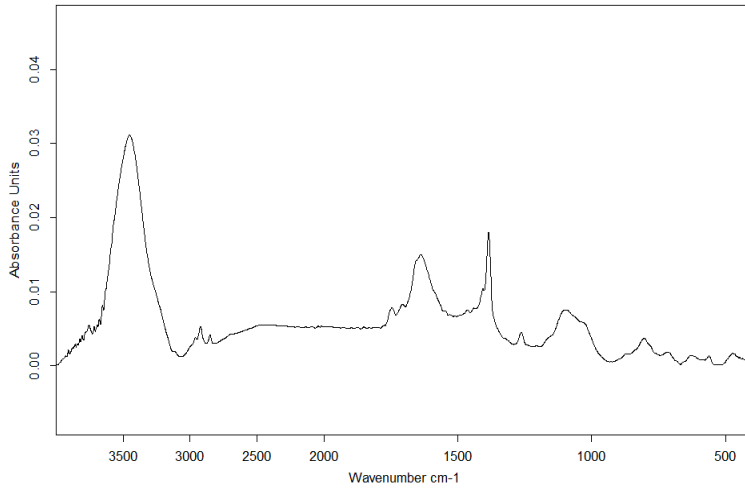

Figure 2.41: Spectrum FT/IR of functionalization MWCNTs with 4-hydroxyphenyl glycine and octyl aldehyde.

The thermogravimetric analysis (TGA) in air, is used to estimate the thermal stability of functionalization MWCNTs with 4-hydroxyphenyl glycine and octyl aldehyde (1). The important parameters of TGA curves are the initiation temperature, the final temperature and the residual mass percent [34]. As can be seen from *Fig. 2.42*, the initiation temperature, the final temperature and the residual mass percent of (1) are 520.3 °C, 580 °C and 0.4 % respectively.

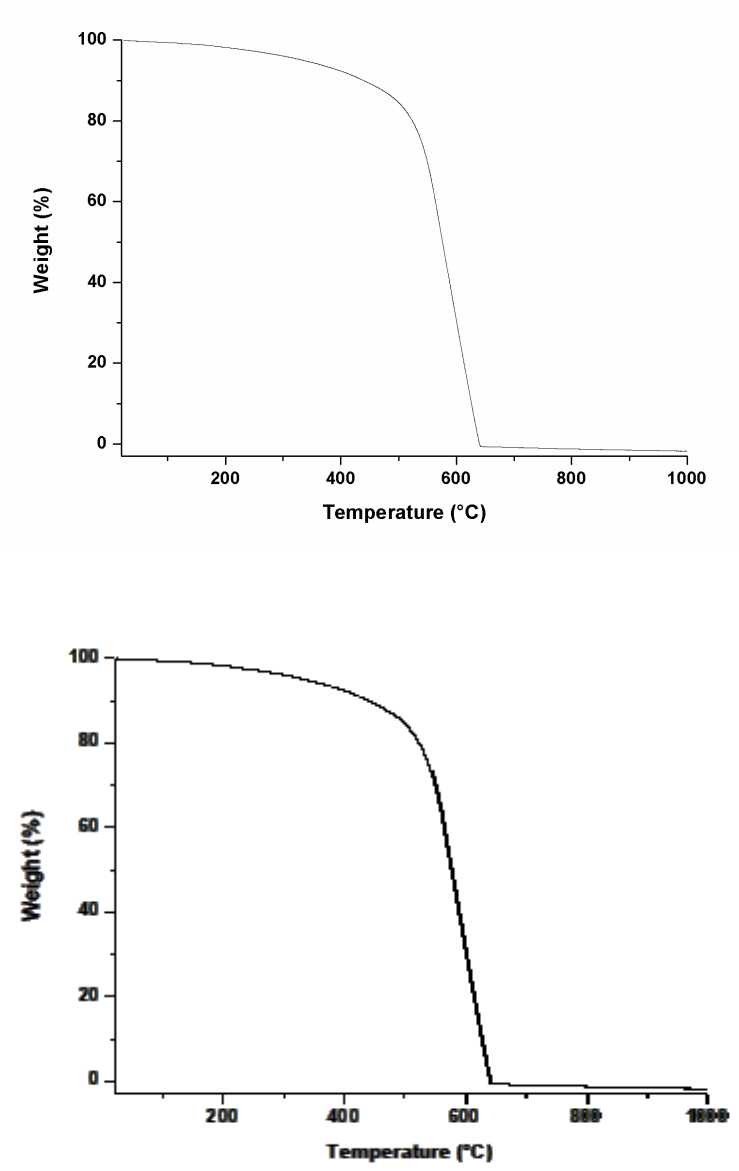

Figure 2.42: TGA curve of functionalization MWCNTs with 4-hydroxyphenyl glycine (above) and octyl aldehyde (below).

Elemental analysis of (1) revealed the presence of nitrogen (1.1%).

- **Second step**: ***functionalization of the MWCNTs with 5-norbornene-2-carboxylic***

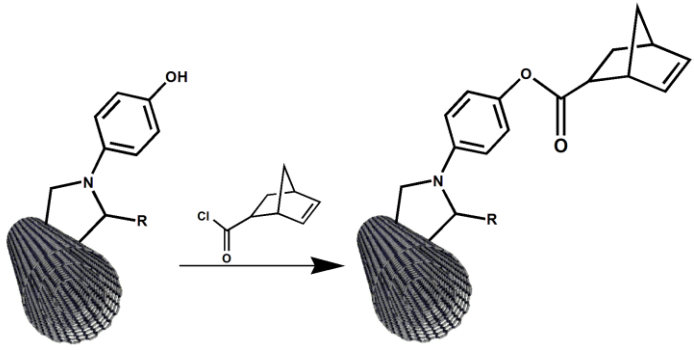

1 2

Figure 2.43: Functionalization of the MWCNTs with 5-norbornene-2-carbonyl chloride.

The other reagent for the second step: the 5-norbornene-2-carbonyl chloride was prepared by reaction of 5-norbornene-2-carboxylic acid and thionyl chloride under nitrogen in Schlenk flask and stirred at reflux for 24 h. The excess of thionyl chloride was evaporated in vacuum and was obtained the chlorinated product (5-norbornene-2-carboxyl chloride). The surface phenol functionalities were treated with 5-norbornene-2-carbonyl chloride in CH_2Cl_2 dry with anhydrous dimethylformamide and triethylamine for 48 h at reflux. The profile of the TGA of the product (2) is practically identical to the product obtained previously.

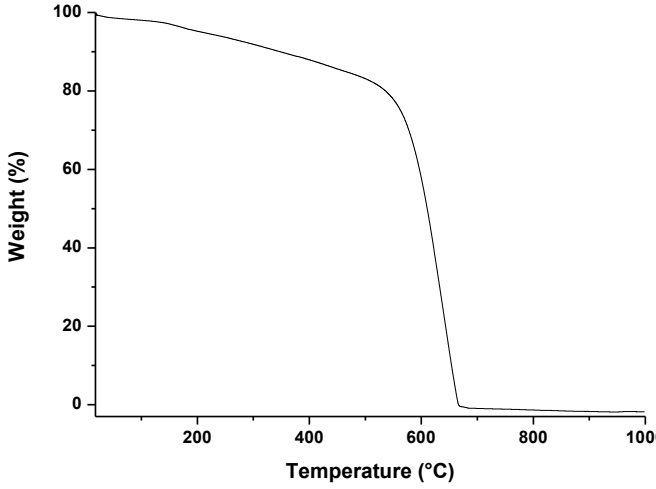

Figure 2.44: TGA curve of functionalization MWCNTs (2).

- **Third step**: ***functionalization of the MWCNTs with Ru-based catalyst***

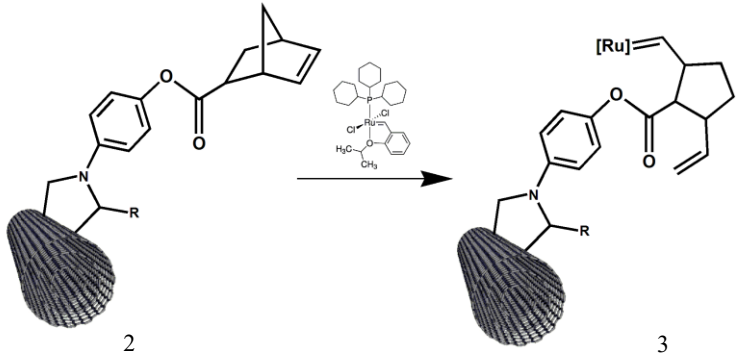

Figure 2.45: Third step: functionalization of the MWCNTs with HG1 catalyst.

The product obtained from the second reaction step was reacted with

dichloro(*o*-isopropoxyphenylmethylene)(tricyclohexylphosphine)ruthenium(II) (HG1) for 16 h in hexane. The product (3) was subjected to FT/IR analysis and showed no significant differences compared with that obtained with the previous products (1) and (2).

The amount of Ru linked to graphene was evaluated by thermogravimetric analysis (*Fig. 1.8*). The analyses were conducted in air flow to allow the Ru to oxidize in the form of ruthenium oxide (RuO_2). Ruthenium(IV)oxide is a (nearly black) purple crystalline solid at room temperature. It can be prepared by direct synthesis at 1000°C from the elements, or by pyrolysis of halides of ruthenium. From the residue was possible to calculate the moles of RuO_2 and therefore the amount of bonded catalysts.

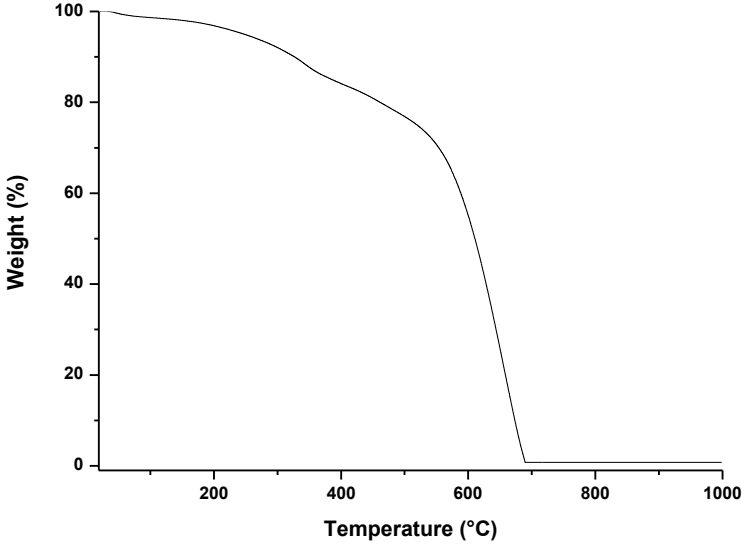

Figure 2.46: TGA curve of functionalization MWCNTs (3).

The residual at 1000°C for the functionalized catalyst observed was

0.8%. Unfortunately, this quantity turns out to be too small for a system self-healing and thus it was decided not to conduct the tests of metathesis.

2.3.2.2 FUNCTIONALIZATION OF THE GRAPHITE WITH 1,3-DIPOLAR CYCLOADDITION REACTION

The same procedure of functionalization of the MWCNTs through 1,3-dipolar cycloaddition reaction was adopted for the functionalization of the graphite HEG (high exfoliated graphite).

- **First step**: ***functionalization of the graphite with 4-hydroxyphenyl glycine and octyl aldehyde***

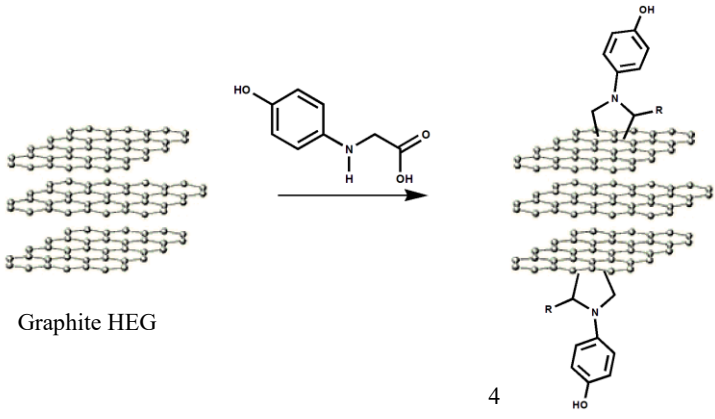

Graphite HEG

4

Figure 2.47: First step: functionalization of the graphite with 4-hydroxyphenyl glycine and octyl aldehyde.

Addition of 4-hydroxyphenyl glycine and octyl aldehyde to a

suspension of graphite in DMF, followed by heating at 130 °C for 5 days, resulted in the incorporation of phenol-functionalized pyrrolidine rings on the surface of the graphite. The product of this procedure was characterized by FT/IR and thermogravimetric analysis.

FT/IR spectroscopy (*Fig. 2.48*) exhibited the expected aromatic C-C stretch at 1634 cm^{-1} and the increase in the signal to ca. 2900 cm^{-1} from the alkyl portions of the attached unit and of aromatic C-C bending at 715 cm^{-1}.

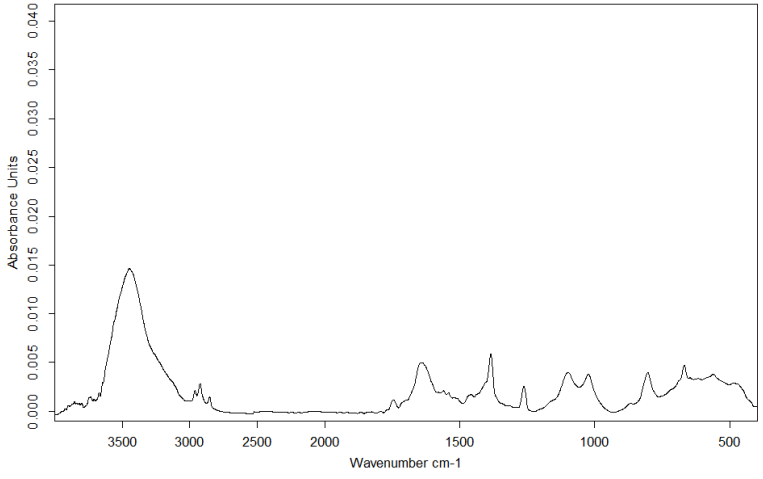

Figure 2.48: Spectrum FT/IR of functionalization of graphite with 4-hydroxyphenyl glycine and octyl aldehyde.

The profile of the TGA is shown in *Fig. 2.49*.

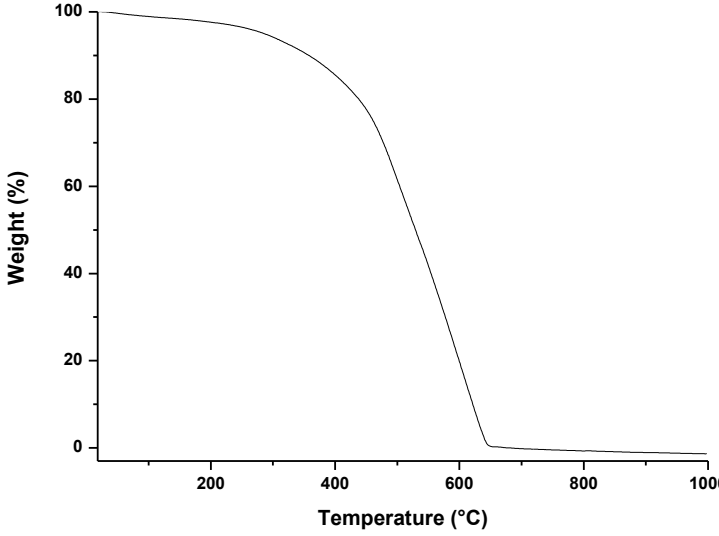

Figure 2.49: TGA curve of functionalization of graphite with 4-hydroxyphenyl glycine and octyl aldehyde.

Elemental analysis of (1) revealed the presence of nitrogen (0.2%). This amount was too small to be able to continue with the functionalization.

It was also tested a different graphite but did not lead to the desired results. The amount of nitrogen elemental analysis was found to be 1.10 %, still too low for our purposes.

2.4 EXPERIMENTAL PART

SECTION 2.1

FUNCTIONALIZATION OF GRAPHENE OXIDE WITH CATALYSTS ACTIVE IN THE METATHESIS POLYMERIZATION

- **Preparation of graphene oxide (GO)**

The graphene oxide (GO) was prepared with the Staudenmaier's method [1]. This procedure starts with the oxidation of graphite (G) to GO using concentrated acids (concentrated sulfuric acid H_2SO_4 in combination with fuming nitric acid HNO_3 and potassium chlorate $KClO_3$). A 2000-mL three-neck flask was flushed with gaseous N_2 and then immersed into an ice bath. 30 g of G was added to a homogeneous mixture of 200 mL of nitric acid and 400 mL of sulfuric acid under vigorous agitation. After the uniform dispersion of G powders, obtained by stirring for some minutes, 250 g of potassium chlorate were added very slowly to minimize the risk of explosion. The reaction mixture was allowed to go on for 120 h at room temperature. The resulting dark green slurry was poured into a copious amount of a 5 wt % HCl aqueous solution and then centrifuged at 10.000 rpm for 15 min (Hermle Z 323 K). The GO powders were further washed with a 5 wt % HCl aqueous solution (2 x 100 mL) and deionized water and finally vacuum dried in an oven

at 60 °C for 48 h.

- **Quantitative evaluation of the -COOH groups on GO**

The acidity of the GO was determined performing a typical acid-base titration. Amount of carboxyl and total acidic site on the GO were quantitatively chemical analyzed by titration. 50 mg of GO were dispersed in 50 ml of NaOH (0.05 M) and the suspension was sonicated for 30 min to obtain the complete reaction between acid group and the base and to remove CO_2. The excess of NaOH was titrated with HCl (0.05 M) and the variation of pH was registered after addition of 1ml of acid. The equivalent volume (V_{eq}) that allows to determine the moles consumed and the title was obtained from the point of inflection. The title obtained for difference was 14.1 mmol/g.

$$GO - OH + NaOH \rightarrow GO - O^{-}Na^{+} + H_2O + NaOH_{exc}$$
$$NaOH_{exc} + HCl \rightarrow NaCl + H_2O$$

A second titration was performed at the aim of valuated the only carboxylic acid groups using a weak base $NaHCO_3$. 50 mg of GO were dispersed in 50 ml of $NaHCO_3$ (0.05 M) and were sonicated for 30 min and 50 ml of acid solution (HCl 0.05M) were added into the flask. The excess of HCl was slowly titrated with NaOH (0.05 M) and the variation of pH was registered after subsequent addition of 1 ml of acid. The value of the title was found to be 5.5 mmol/g.

$$GO - COOH + HCO_3Na$$
$$\rightarrow GO - COO^-Na^+ + H_2O + CO_2 + NaHCO_{3\,exc}$$
$$NaHCO_{3\,exc} + HCl \rightarrow (H_2O + CO_2) + NaCl + HCl_{exc}$$
$$HCl_{exc} + NaOH \rightarrow NaCl + H_2O$$

- **Functionalization of graphene oxide with ruthenium based catalysts**

Grubbs catalysts 1st (G1) and 2nd generation modified ($G2_{o\text{-tol}}$) and Hoveyda-Grubbs catalysts 1st (HG1) and 2nd generation (HG2) were covalently bonded to the graphene oxide sheets. *Fig. 2.5* shows the chemical formulas of the catalysts which were covalently bonded to the GO.

- **First step:** ***formation of graphene acyl chloride***

6200 mg of dried GO were added in a 500 mL Schlenk flask together with 300 mL of thionyl chloride ($SOCl_2$) under nitrogen. The suspension was stirred for 48 h at reflux under nitrogen. The excess of thionyl chloride was evaporated under vacuum. FTI/R spectrum (KBr pellet) of the product shows the signals at ν = 2920 cm^{-1} (s), 2849 cm^{-1} (s),1720 cm^{-1} (s),1090 cm^{-1} (s), 590 cm^{-1}(w) confirming the successful functionalization.

- **Second step:** ***esterification reaction of the GO***

In the same flask 20 ml (0.36 mmol) of ethylene glycol and 250 mL of dry THF were added. The reaction was stirred for 36 h at 70 °C under nitrogen. The mixture was filtered and the residue was washed with 300 ml of methanol, and, finally, dried under vacuum, giving 5.1 g of product. FT/IR spectrum (KBr pellet) of the product shows the signals at ν = 2920 cm^{-1} (s), 2849 cm^{-1} (s), 1743 cm^{-1} (s), 1116 cm^{-1} (w), 1020 cm^{-1} (w) confirming the successful of the second step.

- **Third step:** ***functionalization of GO with 5-acid chloride 2-norbornene***

10 ml (721 mmol) of 5-norbornene-2-carboxylic acid and 33 mL of thionyl chloride were added under nitrogen in a 250 mL Schlenk flask and stirred at reflux for 24 h. The excess of thionyl chloride was evaporated in vacuum and 5.1 g of GO-Gly, 70 mL of CH_2Cl_2, 4 mL of anhydrous dimethylformamide and 4 mL of triethylamine were added to the same flask. The mixture was stirred under nitrogen for 48 h at reflux. The product was isolated by filtration and the residue was washed with 300 mL of methanol and 300 ml of CH_2Cl_2. 4.8 g of product GO-Norbornene were obtained, after drying under vacuum overnight. FT/IR spectrum (KBr pellet) of the product shows the signals at ν: 2960 cm^{-1} (s), 2920 cm^{-1} (s), 2849 cm^{-1} (s), 1743 cm^{-1} (s), 1260 cm^{-1} (s), 1116 cm^{-1} (s), 1020 cm^{-1} (s), 750 cm^{-1} (s) confirming the successful of the third step.

- **Fourth step:** ***functionalization of GO with Ru-based catalysts***

In dry box 1200 mg of GO-Norbornene and 400 mg of Ru-based catalyst (G1, HG1, Dichloro[1,3-Bis(2-methylphenyl)-2-imidazolidinylidene](benzylidene) (tricyclohexylphosphine)ruthenium(II) (G2o-tol)) were added under nitrogen to 150 mL of dry hexane in a reaction flask. The mixture was stirred at room temperature under nitrogen for 16 h. The suspension was filtered and washed with 500 mL of CH_2Cl_2. The products were obtained: 1120 mg GO-G1, 1140 mg GO-G2*o*-tol, 1140 mg GO-HG1 and 1000 mg GO-HG2, after drying under vacuum.

- **ROMP of 2-norbornene**

The experiments were conduct with 3 mg of GO-catalyst in 99 ml of dry THF and stirred of about 1 ml of monomer in a 250 mL Schlenk flask. The reaction was stopped by adding 1 ml of ethyl-vinyl ether and the obtained polymers were coagulated in few ml of methanol. The polymers were filtered and washed with CH_2Cl_2. The products were obtained, after drying under vacuum.

- **ROMP of 5-ethylidene-2-norbornene (ENB)**

The polymerizations were carried out in bulk. In a typical experiment 5 mg of GO-catalyst was mixed with a stirred in about 1ml of monomer in a 4 ml vial. The reactions were stopped by adding 1 mL ethyl-vinyl ether and the obtained polymers were coagulated in few ml of methanol. The polymers were filtered and washed with CH_2Cl_2. The products were obtained, after drying under vacuum.

- **Microcapsule manufacture**

Microcapsules were prepared by *in situ* polymerization in an oil-in-water emulsion. At room temperature (20–24°C), 200 ml of deionized water and 50 ml of 2.5 wt% aqueous solution of ethylene maleic anhydride (EMA) copolymer were mixed in a 1000 ml beaker. Under agitation, 5.00 g urea, 0.50 g ammonium chloride and 0.50 g resorcinol were dissolved in the solution. The pH was raised from about 2.60 to 3.50 by drop-wise addition of sodium hydroxide (NaOH) and hydrochloric acid (HCl). Two drops of 1-octanol were added to eliminate surface bubbles. A slow stream of 60 ml of DCPD was added to form an emulsion and allowed to stabilize for 10 min. After stabilization, 12.67 g of 37 wt% aqueous solution of formaldehyde was added. The emulsion was covered and heated at a rate of 10 °C/min to the target temperature of 55°C. After 4h of continuous agitation the mixer and hot plate were switched off. Once cooled to ambient temperature, the suspension of microcapsules was

separated under vacuum with a coarse-fritted filter. The microcapsules were rinsed with deionized water and air dried for 24/48h.

SECTION 2.2

PROTECTION OF CATALITIC SITE WITH POLYMERIC GLOBULAR SHELL

- **Preparation of gHG2**

The preparation of Hoveyda Grubbs catalysts II generation (HG2) supported on GO sheet was described in the previous section. The amount of HG2 linked to graphene sheet (gHG2) was evaluated [1] by thermogravimetric analysis (TGA) obtained from the residual of RuO_2 at 1000 °C and by ICP-OES (Inductively Coupled Plasma and Optical Emission Spectrometry) analysis. The results obtained using these two different techniques were substantially the same. The amount of the Ru-catalyst that is successfully immobilized on graphene sheets has been found to be 4.94×10^{-7} mol/mg.

- **Preparation of Polynorbornene-GO-HG2 (PolyNBE-GO-HG2)**

- **Ratio HG2:2-norbornene = 1:50**

Initially a molar ratio of HG2 (covalently bonded to graphene sheets) and 2-norbornene 1:50 was used to obtain polynorbornene around the catalytic sites. The molar ratio was calculated using thermogravimetric determination of the amount of HG2 bonded to the graphene sheets.

In the reaction flask was added 2-norbornene (8.8 mg, $9.4 \cdot 10^{-5}$ mol) and GO-HG2 (5.0 mg corresponding to 1.9×10^{-6} mol of ruthenium) in the CH_2Cl_2 dry (10 ml). After 25 minutes, the solvent was removed *in vacuo*. The final product, consisting of Hoveyda Grubbs II generation catalyst protected by polymeric globular shell (PolyNBE-GO-HG2), was washed with hexane to remove the excess of monomer (yield 37.7 mg).

The PolyNBE-GO-HG2 obtained was tested in the metathesis reaction of 2-norbornene to verify the reactivity of the catalytic sites. In the same reaction flask was added 20 ml of CH_2Cl_2 and 2-norbornene (88.5 mg, $9.4 \cdot 10^{-4}$ mol). The mixture was stirred for 25 minutes. At the end, the solvent was removed in vacuo. The increment of initial weight of PolyNBE-GO-HG2 from 37.7 mg a 95.7 mg confirms the activity of the catalyst. The product obtained should have the catalytic site still “alive” since it has not been deactivated by termination reaction. To confirm the activity of the catalytic site an ulterior third polymerization was conducted. In the

same reaction flask was added 20 ml of CH_2Cl_2 and 2-norbornene (87.3 mg, $9.3 \cdot 10^{-4}$ mol). The mixture was stirred for 25 minutes. After this time, the solvent was removed in vacuo. The weight of the PolyNBE-GO-HG2 was incremented from 95.7 mg a 120.0 mg, confirming that the catalytic site is still actives.

These tests have confirmed that it is possible to obtain a catalytic site protected from a polymer globular shell still able to provide further polymerization reactions.

Thus, the PolyNBE-GO-HG2 was synthesized to carry out the metathesis tests in the self-healing epoxy systems.

In the reaction flask was added the 2-norbornene (44.2 mg, $4.7 \cdot 10^{-4}$ mol) and the GO-HG2 (25.1 mg corresponding to 9.4×10^{-6} mol of ruthenium) in the CH_2Cl_2 dry (20 ml) for 25 min. After this time, the solvent was removed in vacuo. The final product (PolyNBE-GO-HG2) was washed with hexane to remove the excess of monomer (yield 66.2 mg).

The self-healing epoxy matrix composite was prepared by mixing an epoxy precursor (Bisphenol A diglycidyl ether, trade name EPON 828 - acronym E, 4 g) with a reactive diluent (1,4-Butanediol-diglycidylether - Acronym B, 1 g) at a concentration of 80%: 20% (by wt) epoxide to flexibilizer giving the EB2 sample. The PolyNBE-GO-HG2 was added at the EB2 system and the mixture was stirred for 1 hour at 90°C. After this time the PolyNBE-GO-HG2 was not well dispersed, so it was sonicated for 20 minutes at 80 °C and even after this treatment the PolyNBE-GO-HG2 the dispersion was not optimal. Thus, the polymer globular shell then was reduced changing the molar ratio of HG2 (covalently bonded to graphene sheets) and

2-norbornene at 1:10.

- **Ratio HG2:2-norbornene = 1:10**

A molar ratio of HG2 (covalently bonded to graphene sheets) and 2-norbornene 1:10 was used to obtain a smaller amount of polynorbornene around the catalytic sites, at the aim to favor the dispersion of this in the epoxy matrix composite.
The protection of catalytic sites was carried out adding in the reaction flask the 2-norbornene (11.3 mg, 1.2×10^{-4} mol) and the GO-HG2 (25.0 mg corresponding to 1.2×10^{-5} mol of ruthenium) in the CH_2Cl_2 dry for 25 min. After this time, the solvent was removed *in vacuo*. The final product consisting of Hoveyda Grubbs II generation catalyst protected by polymeric globular shell (PolyNBE-GO-HG2) was washed with hexane to remove the excess of monomer (yield 37.7 mg).

- **Epoxy mixture**

The epoxy matrix composite was prepared by mixing an epoxy precursor (Bisphenol A diglycidyl ether, trade name EPON 828 - acronym E) with a reactive diluent (1,4-Butanediol-diglycidylether - Acronym B) at a concentration of 80%: 20% (by wt) epoxide to flexibilizer giving the EB2 sample. This reactive diluent has proven to be effective to reduce the viscosity of epoxy precursors [23] and [24]

allowing to improve handling and ease of processing and to optimize consequently performance properties. The curing agent investigated for this study was an anionic initiator Phenol, 2,4,6-tris[(dimethylamino) methyl] (Trade name Ankamine K54 - acronym A). The curing agent Ancamine K54 was added at a concentration of 10% (by wt) with respect to the mixture EB2 giving the sample EB2A.

- **Protected Ru-functionalized graphene Sheets based epoxy mixture**

Protected Ru-functionalized Graphene Sheets based epoxy mixture was obtained by dispersing PolyNBE-GO-HG2 in the epoxy matrix EB2A. In particular, the epoxy specimen EB2A + 0.326% PolyNBE-GO-HG2 was prepared by dispersing PolyNBE-GO-HG2 at a concentration of 0.326% (by wt) with respect to the mixture EB2, by mechanical agitation in the liquid epoxy mixture EB2 at the temperature of 90 °C and kept at this temperature for 1 h using an oil bath and then adding the curing agent Ancamine K54. The mixture thus obtained was cured in a two-stage process. The first stage was carried out at a temperature of 80 °C for 3 h, while the second stage was carried out at 140 °C for 2 h.
Between the first and the second stage, three intermediate stages were always analyzed, each of which envisaged a holding time of 15 min at each of the temperatures of 90 °C, 100 °C and 110 °C.

- **Evaluation of catalytic activity by FT/IR analysis**

Infrared spectroscopy provides a useful way to identify metathesis products and therefore catalyst activity. Indeed, to verify complete dispersion and dissolution of the catalyst, and that its catalytic activity remained unchanged, infrared spectroscopic investigation was carried out.

SECTION 2.3.1

FUNCTIONALIZATION OF THE MULTIWALLED CARBON NANOTUBES WITH ARYLDIAZONIUM SALTS VIA ELECTROCHEMICAL MODIFICATION

- **First step**: ***electrochemical modification of the MWCNTs with 4-bromobenzenediazonium salt***

The electrochemical modification was used to attach 4-bromophenyl group covalently to MWCNTs and was carried out in a microcell (capacity ~ 500 μL) with platinum counter and pseudoreference electrodes. A tungsten needle probe was used to make contact with the electrodes on the substrate surface, which enabled the functioning of the MWCNTs as the working electrode. Reductive coupling of 4-bromobenzenediazonium tetrafluoroborate, $BrC_6H_4N_2^+BF_4^-$ (10 mM,

54 mg, $2.0 \cdot 10^{-1}$ mmol) with MWCNTs (502 mg) was performed with 0.1 M lithium perchlorate ($LiClO_4$, 110 mg, $6.5 \cdot 10^{-1}$ mmol) in N, N-dimethylformamide (DMF, 20 ml) at a potential of – 1.3 V versus Pt and an intensity of current of 10 mA. We work in the absence of oxygen and in nitrogen flow. The potential was applied for a time of 3 h. The product (1) obtained was washed with water (H_2O) and ethanol (CH_3CH_2OH) to remove the residue diazonium salt. The product (1) was dried in vacuum overnight, yields 470 mg. The formation of product (1) was confirmed through the alkaline fusion with metallic Na. The product (1) was treated with metallic Na in ratio 1:1 in a melting pot at 250°C on oxidative flame, up to complete decomposition, according to the reaction:

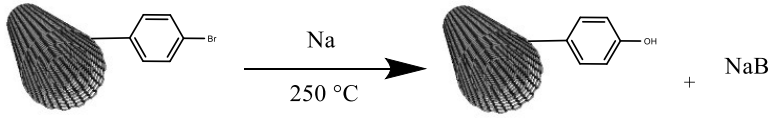

(1)

The melting pot was cooled and at the residue was added H_2O, then the mixture was filtered. The solution recovered was acidified with HNO_3 diluted. At this solution was added some drops of an aqueous solution of $AgNO_3$ to allow the precipitation of AgBr. It was possible to observe the formation of a yellow-white solid precipitate, corresponding to AgBr.

- **Second step**: ***formation of lithium organic derivate of MWCNTs***

The lithium organic derivate of the MWCNTs was formed by reaction of bromophenyl-MWCNTs with *n*-butyl lithium reagent in hexane. The molar ratio of MWCNTs-Ph-Br and Li-organic was 1:1. In a reaction Schlenk flask of 100 ml was added under nitrogen 470 mg of MWCNTs-Ph-Br (product (1), $2.0 \cdot 10^{-1}$ mmol), 50 ml of dry hexane and 1.95 ml ($2.0 \cdot 10^{-1}$ mmol) of solution of *n*-butyl-lithium ($CH_3CH_2CH_2CH_2Li$, *n*-BuLi). The solution of *n*-BuLi used was prepared diluting 2.1 ml of commercial *n*-BuLi 2.5 M in 50 ml of dry hexane. The mixture was stirred for 3 h at - 78 °C. The solution was filtered under nitrogen and the product was recuperated in a glove box. Recovered solution was characterized by ^{1}H-NMR (*Fig. 4*) to verify the presence of byproduct bromobutane. The MWCNTs-Ph-Li obtained was 322 mg.

- **Third step**: ***functionalization of the MWCNTs with 5-norbornene-2-carboxaldehyde***

The reaction was carried out adding in a Schlenk flask of 100 ml under nitrogen, 322 mg of MWCNTs-Ph-Li (product (2)), 0.1 ml ($8.4 \cdot 10^{-1}$ mmol) of 5-norborbornene-2-carboxaldehyde and 50 ml of hexane. The mixture was stirred for 2 h at room temperature. After this time the solution obtained was acidified adding 2 ml of H_2O and 2 ml of HCl 2M and stirred for another 30 minutes. The solution was filtered and washed with H_2O up to the pH was neutral, and then

washed with ethanol and diethyl ether. The product (3) obtained was dried in vacuum overnight, yields 308 mg. It was characterized by FT/IR analysis (KBr pellet): the signal of the C=O stretch (1630 cm^{-1}) derived from the aldehyde was decreased.

- **Fourth step**: ***functionalization of the MWCNTs with Ru-based catalyst***

The catalyst was linked to the MWCNTs functionalized through the previously steps reported by reacting in a Schlenk flask the 308 mg of product (3) with 102.3 mg ($1.6 \cdot 10^{-1}$ mmol) of HG2 catalyst (1,3-Bis-(2,4,6-trimethylphenyl)-2-imidazolidinylidene)dichloro(*o*-isopropoxyphenyl-methylene)-ruthenium(II), in 50 ml of dry hexane, stirring for 16 h. The solution was filtered and washed with chloroform ($CHCl_3$). The product (4) obtained was dried in vacuum over night and was 269 mg. This was characterized by FT/IR analysis (KBr pellet): the spectrum not shows significant differences compared with that obtained for the previous product (3).

- **Metathesis tests**

The functionalized nanotubes with the catalyst (product (4)) were tested in reactions of ring opening metathesis polymerization (ROMP) of 2-norbornene and 5-ethylidene-2-norbornene.

- **ROMP of 2-norbornene**

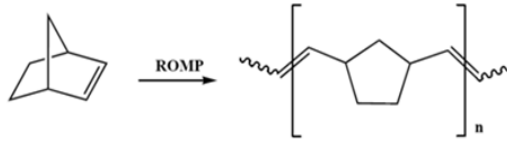

In a reaction flask of 250 ml was added 925 mg (9.8 mmol) of 2-norbornene, 3.3 mg ($6.2 \cdot 10^{-1}$ mmol) of product (4) and 99 ml of tetrahydrofuran (THF) dry. The solution was stirred at room temperature for 1 hour. The polymerization was stopped with some drop of ethylvinylether and the polymer coagulated in about 150 ml of CH_3CH_2OH (ethanol). The product obtained was dried overnight in vacuum and was 68 mg. The activity of the catalyst was $1.12 \cdot 10^4$ $\frac{Kg}{mol^2 * h}$.

- **ROMP of 5-etiliden-2-norbornene**

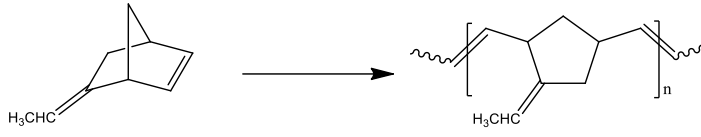

The polymerization was conduct in bulk. In a vial of 4 ml was added 1120 mg (9.3 mmol) of 5-ethyliden-2-norbornene and 5.4 mg (1.0 mmol) of product (4). The mixture was stirred for 24 hours. The polymerization was stopped with some drop of ethylvinylether and the polymer coagulated in about 50 ml of CH_3CH_2OH (ethanol). The product obtained was dried overnight in vacuum and was 33 mg.

SECTION 2.3.2

FUNCTIONALIZATION OF THE MWCNTs WITH 1,3-DIPOLAR CYCLOADDITION REACTION

- **First step**: ***functionalization of the MWCNTs with 4-hydroxyphenyl glycine and octyl aldehyde***

MWCNTs (0.424 g), octyl aldehyde (28 ml, 180 mmol), and *N*-(4-hydroxyphenyl) glycine (0.706 g, $4.22 \cdot 10^{-6}$ mmol) were dispersed in 250 ml of DMF in a 500 ml round-bottom flask. The mixture was stirred at 130 °C under nitrogen for 5 days with further addition of 0.300 g ($1.8 \cdot 10^{-6}$ mmol) aliquots of *N*-(4-hydroxyphenyl) glycine once every 24 h. At the end of this process, the product was collected by filtration and was then washed thoroughly with CH_2Cl_2 (300 ml), THF (150 ml), and methanol (150 ml), and finally dried under vacuum overnight.

- **Second step**: ***functionalization of the MWCNTs with 5-norbornene-2-carboxylic***

5-norbornene-2-carboxylic acid and thionyl chloride were added under nitrogen in schlenk flask and stirred at reflux for 24 h. The excess of thionyl chloride was evaporated in vacuum and 0.484 g of (1), 50 ml of CH_2Cl_2, 1 ml of anhydrous dimethylformamide and 1 ml of triethylamine were added to the same flask. The mixture was

stirred under nitrogen for 48 h at reflux. The product was isolated by filtration and the residue was washed with 500 ml of methanol, 200 ml of THF and 300 ml of CH_2Cl_2. 0.380 g of product (2) were obtained, after drying under vacuum overnight.

- **Third step**: ***functionalization of the MWCNTs with Ru-based catalyst***

0.380 g of (2) and 0.130 g of dichloro(*o*-isopropoxyphenylmethylene)(tricyclohexylphosphine)ruthenium(II) (HG1) were added under nitrogen to 50 ml of dry hexane in a 100 ml schlenk flask. The mixture was stirred at room temperature under nitrogen for 16 h. The suspension was filtered and washed sequentially with 400 ml of methanol, 400 ml of CH_2Cl_2 and 400 ml of hexane. The product (3) 0.350 g was obtained, after drying under vacuum.

FUNCTIONALIZATION OF THE GRAPHITE WITH 1,3-DIPOLAR CYCLOADDITION REACTION

- **First step**: ***functionalization of the HEG with 4-hydroxyphenyl glycine and octyl aldehyde.***

Graphite HEG (0.500 g), octyl aldehyde (33 ml, 211 mmol), and *N*-(4-hydroxyphenyl) glycine (0.832 g, $4.97 \cdot 10^{-6}$ mmol) were dispersed in 300 ml of DMF in a round-bottom flask. The mixture was stirred at 130 °C under nitrogen for 5 days with further addition of 0.320 g ($1.9 \cdot 10^{-6}$ mmol) aliquots of *N*-(4-hydroxyphenyl) glycine once every 24 h. At the end of this process, the product was collected by filtration and was then washed thoroughly with CH_2Cl_2 (300 ml), THF (150 ml), and methanol (150 ml), and finally dried under vacuum overnight.

Conclusion

The covalent functionalization of the carbon filler allows to reduce significantly the amount of Ru-based catalyst used in the aeronautical system to obtain the self-healing ability of these materials.

In particular, Hoveyda Grubbs catalysts bonded to the graphene oxide (GO-HG1 and GO-HG2) are able to trigger self-healing reaction, based on the ROMP of 5-ethylidene-2-norbornene (ENB) that can be used as healing agents in self-healing resins, with the same catalytic activity of the catalysts not bonded to the graphene sheets.

The next protection of the catalytic site with a polymeric globular shell has proven to be very effective in preventing the deactivation of the catalyst during the high temperature of the curing cycle also using very low concentration of PolyNBE-gHG2 (lower than 0.5% by weight). This strategy could represent a revolutionary approach to manufacture new efficient and inexpensive auto-repair systems in many fields of the structural functional materials. The possibility to integrate the very interesting properties of carbon based-nanoparticles inside thermosetting self-healing materials also represents one of the most pursued targets to meet many industrial requirements such as to enhance mechanical and electrical properties.

Alternative approaches, as the functionalization of the carbon nanofiller via electrochemical modification or via 1,3 dipolar cycloaddition, although permit to preserve the unique properties of this carbon nanofiller, i.e. the electrical conductivity, reduce

considerably the catalytic activity.

REFERENCES

[1] C. N. Yeh, K. Raidongia, J. Shao, Q.-H. Yang and J. Huang. *Nat. Chem.* **2015**, 7, 166–170.

[2] J. W. Kim, D. Kang, T. H. Kim, S. G. Lee, N. Byun, D. W. Lee, *et al. ACS Nano* **2013**, 7, 8082– 8088.

[3] J. Luo, L. J. Cote, V. C. Tung, A. T. Tan, P. E. Goins, J. Wu, J. Huang. J. Am. Chem. Soc. **2010**, 32, 17667–17669.

[4] A. M. Dimiev, L. B. Alemany and J. M. Tour. *ACS Nano,* **2013**, 7, 576–588.

[5] S. Zhang, Y. Shao, H. Liao, M. H. Engelhard, G. Yin, Y. Lin. *ACS Nano,* **2011**, *5*, 1785−1791.

[6] S. Ganguli, A. K. Roy, D. P. Anderson. *Carbon*, **2008**, 46, 806-817.

[7] H. M. Ju, S. H. Huh, S. H. Choi, H. L. Lee. *Mater Lett,* **2010**, 64, 357-360.

[8] H. Feng, R. Cheng, X. Zhao, X. Duan, J. Li. *Nat Commun,* **2013**, 4, 1-7.

[9] J A. Johnson, C. J. Benmore, S. Stankovich, R. S. Ruoff. *Carbon*, **2009**, 47, 2239-2243.

[10] H. P. Boehm. *Carbon,* **1994**, 32, 759-769.

[11] C. Costabile, M. Sarno, F. Grisi, N. Latorraca, P. Ciambelli, P. Longo. *J Polym Res,* **2014**, 21, 1-9.

[12] C. Costabile, F. Grisi, G. Siniscalchi, P. Longo, M. Sarno, D. Sannino, et al. J *Nanosci Nanotechnol*, **2011**, 11, 10053-10062.

[13] L. Guadagno, M. Raimondo, K. Lafdi, A. Fierro, S.

Rosolia, M. R. Nobile. *AIP Conf Proc,* **2014**, 1599, 386-389.

[14] M. R. Nobile, M. Raimondo, K. Lafdi, A. Fierro, S. Rosolia, L. Guadagno. *Polym Compos,* **2015**, 1152-1160.

[15] L. Guadagno, M. Raimondo, C. Naddeo, P. Longo, A. Mariconda, W. H. Binder. *Smart Mater Struct,* **2014**, 23.

[16] E. N. Brown, M. R. Kessler, N. R. Sottos, S. R. White. *J. Microencapsul.,* 20, 719–730, **2003**.

[17] M. Raimondo, P. Longo, A. Mariconda and L. Guadagno. *Adv. Comp. Mater.*, 1-11, **2014**.

[18] M. Raimondo, P. Longo, A. Mariconda, L. Guadagno. *Adv Compos Mater,* **2014**.

[19] A. Mariconda, P. Longo, A. Agovino, L. Guadagno, A. Sorrentino, M. Raimondo. "Synthesis of ruthenium catalysts functionalized graphene oxide for self-healing applications". *Polymer*, 69, 330-342, **2015**.

[20] L. Guadagno, A. Mariconda, A. Agovino, M. Raimondo, P. Longo. "Protection of graphene supported ROMP catalyst through polymeric globular shell in self-healing materials". *Composite Part B*, 1-9, **2016**.

[21] L. Guadagno, P. Longo, M. Raimondo, C. Naddeo, A. Mariconda, V. Vittoria, et al. "Use of Hoveyda-Grubbs' second generation catalyst in self-healing epoxy mixtures". *Composite Part B*, 42(2), 296-301, **2011**.

[22] M. Raimondo, P. Longo, A. Mariconda, L. Guadagno. "Healing agent for the activation of self- healing function at low temperature". *Adv Compos Mater*, 24(6), 519-529, **2015**.

[23] L. Guadagno, M. Raimondo, K. Lafdi, A. Fierro, S. Rosolia,

M. R. Nobile. “Influence of nanofiller morphology on the viscoelastic properties of CNF/epoxy resins”. *AIP Conf Proc,* 1599, 386-389*,* **2014**.

[24] M. R. Nobile, M. Raimondo, K. Lafdi, A. Fierro, S. Rosolia, L. Guadagno. “Relationships between nanofiller morphology and viscoelastic properties in CNF/ epoxy resins”. *Polym Compos*, **2015**, 36(6), 1152-1160.

[25] K. Balasubramanian, M. Friedrich, C. Jiang, Y. Fan, A. Mews, M. Burghard and K. Kern. “Electrical transport and confocal raman studies of electrochemically modifier individual carbon nanotubes”. *Advanced Materials*, 15, No. 18, September 16, **2003**.

[26] R. Saito, G. Dresselhaus, M. S. Dresselhaus, *Physical Properties of Carbon Nanotubes*, mperial College Press, London, **1998**.

[27] M. A. Reed, *Molecular Electronics*, Academic Press, London, **2000**.

[28] T. W. Odom, J. L. Huang, P. Kim, C. M. Lieber, *J. Phis. Chem. B*, 104, 2794, **2000**.

[29] J. M. Bonard, N. Weiss, H. Kind, T. Stockli, L. Forro, K. Kern, A. Chatelain, *Adv. Mater.*, 13, 184, **2001**.

[30] M. Knez, M. Sumser, A. M. Bittner, C. Wege, H. Jeske, S. Kooi, M. Burghard, K. Kern. “Electrochemical modification of individual nano-objects”. Journal of Electroanalytical Chemistry, 522, 70-74, **2002**.

[31] P. Longo, C. Costabile, F. Grisi, G. Siniscalchi, O. Ciambelli, M. Sarno, C. Leone and D. Sannino. *Nanotech*, 2, 531-

533, **2009**.

[32] Yao Z., Braidy N., Botton G. A., Adronov A. *J. Am. Chem. Soc.*, **2003**, *125*, 16015-16024.

[33] Liu Y. Q., Adronov A. *Macromolecules*, **2004**, *37*, 4755-4760.

[34] Lehman J. H., Terrones M., Mansfield E., Hurst K. E., Meunier V. *Carbon*, **2011**, *49*, 2581-2602.

CHAPTER 3

NON COVALENT FUNCTIONALIZATION OF THE CARBON NANOFILLER

3.1 π - STACKING INTERACTION OF THE CARBON NANOFILLER WITH PYRENE

In the previous section it was described the possibility of functionalize the carbon nanomaterials at the aim to link the ROMP catalysts and use they in structural materials for engineering applications having self-healing ability. Through this way the graphite, graphene or CNTs, must be individually functionalized by several reactions step for bind the Ru-based catalysts.

On the other hand, the use of carbon nanofiller (graphite, graphene and CNTs) are currently highly considered in the field of structural materials, due to their unique properties, in terms of conductivity and resistance [1], that make them particularly suitable for improving electrical and mechanical properties of the materials in which are dispersed. Their outstanding sensitivity to chemical doping [2,3] coupled with their very small size, reveals a vast potential for many applications.

As described so far (see section 2.3.1), the conductibility of the carbon materials is due to the delocalization of π electrons that is forced to move above and below the planes of the carbon atom, since these electrons are free to move, so they are able to conduct electricity. As already mentioned, any perturbation of the structure of the graphitic plane resulting in drastic reduction of the conductivity of the carbon material.

So, it was searched for a way that would allow of anchor the ROMP catalysts on the nanofiller and, at the same time, to maintain the structure of these substantially intact.

This can be achieved through the use of a molecule that is able to bind to the aromatic system of the nanofiller without disturbing the structure.

The interaction that allows to realize this system is an non covalent interaction, such as of type π - stacking. The molecules suitable for this purpose must have an aromatic system that is able to bind to the graphitic plane; for example the polycyclic aromatics, such as pyrene, could serve as anchors for selective, non-covalent functionalization of nanofiller [4]. Through some synthetic step it is possible to functionalize the pyrene with the Ru-based catalysts and then anchor the pyrene-catalyst system on the carbon filler. Once obtained the pyrene-catalyst may be, through π – stacking interaction, capable of functionalizing any substrate that can give such interaction. This makes this system extremely versatile and above all allows you to optimize the synthesis times. In this way it is possible non only supported the catalysts for the self-healing ability of the materials but also use the itself carbon nanomaterial as filler to

improve the properties of the materials.

3.1.1 SINTHESY OF PYRENE-Ru-BASED CATALYST

- **First step:** ***synthesis of 4-(1-Pyrenyl)-butyroyl chloride***

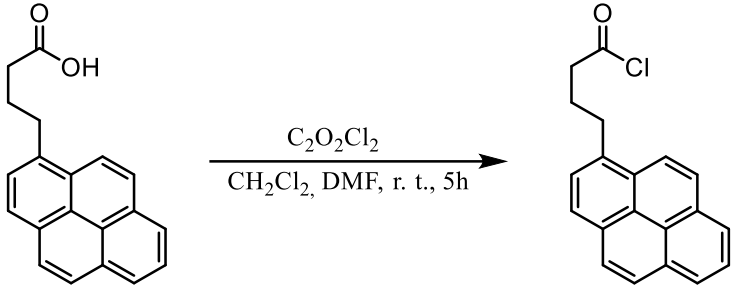

1

Figure 3.1: Chlorination of the 4-(1-pyrenyl)-butyroyl chloride.

The first synthetic step consists in a chlorination reaction that convert the 4-(1-pyrenyl)-butyric acid in the corresponding acyl chloride (product (1), *Fig. 3.1*). The conversion of the acid in the corresponding acyl chloride was need to give a more reactive substrate for the next esterification reaction. The reaction was conduct with oxalyl chloride as source of Cl, and the product obtained was stored in inert environmental because it is moisture sensitive. The product (1) obtained was characterized by ^{1}H (*Fig.*

3.4) and ^{13}C-NMR (*Fig. 3.5*) in $CDCl_3$ and the spectrum was compared with those of the 4-(1-pyrenyl)-butyric acid (^{1}H-NMR in the *Fig. 3.2* and ^{13}C-NMR in the *Fig. 3.3*). The achievement of the reaction was confirmed by the disappeared in the ^{1}H-NMR spectrum of the signal at about 10.5 ppm related to the H of the group COOH, in the ^{13}C-NMR the signal of the C=O at 178 ppm shift at 174 ppm due to formation of acyl chloride Cl, and the signal of the CH_2 next to C=O group shifts at 46 ppm. The signals related to the aromatic H and C and to two CH_2 remain essentially unchanged.

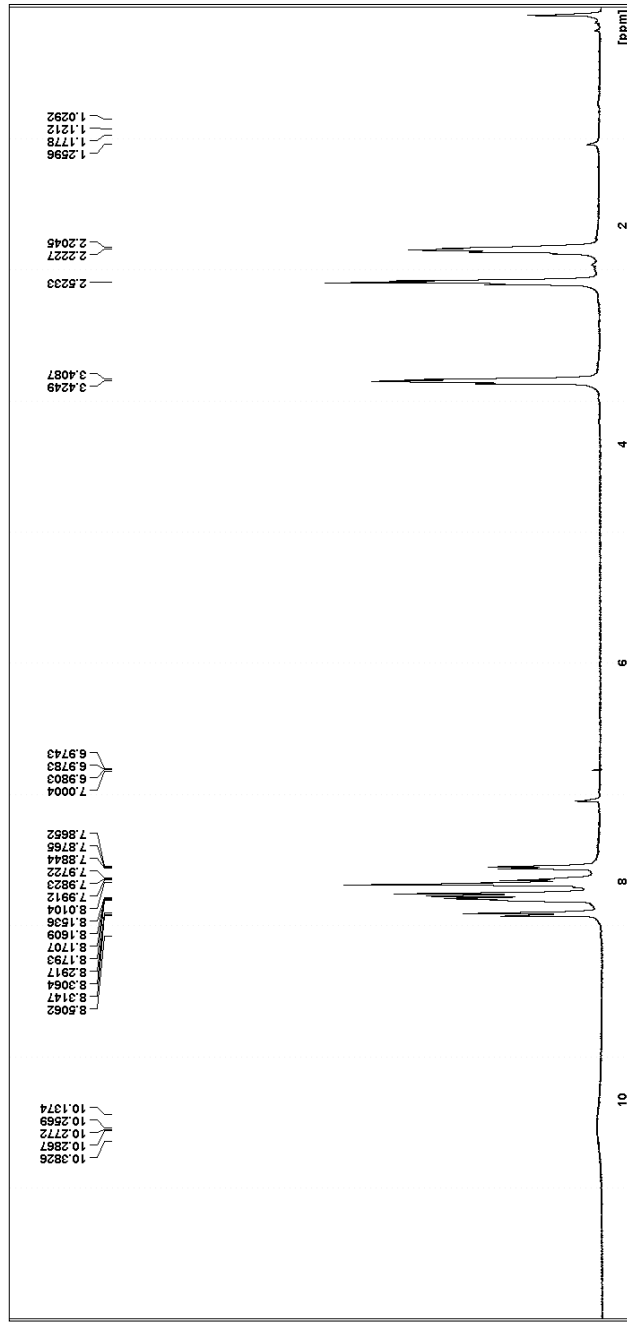

Figure 3.2: ^{1}H-NMR ($CDCl_3$) pyrene butiric acid.

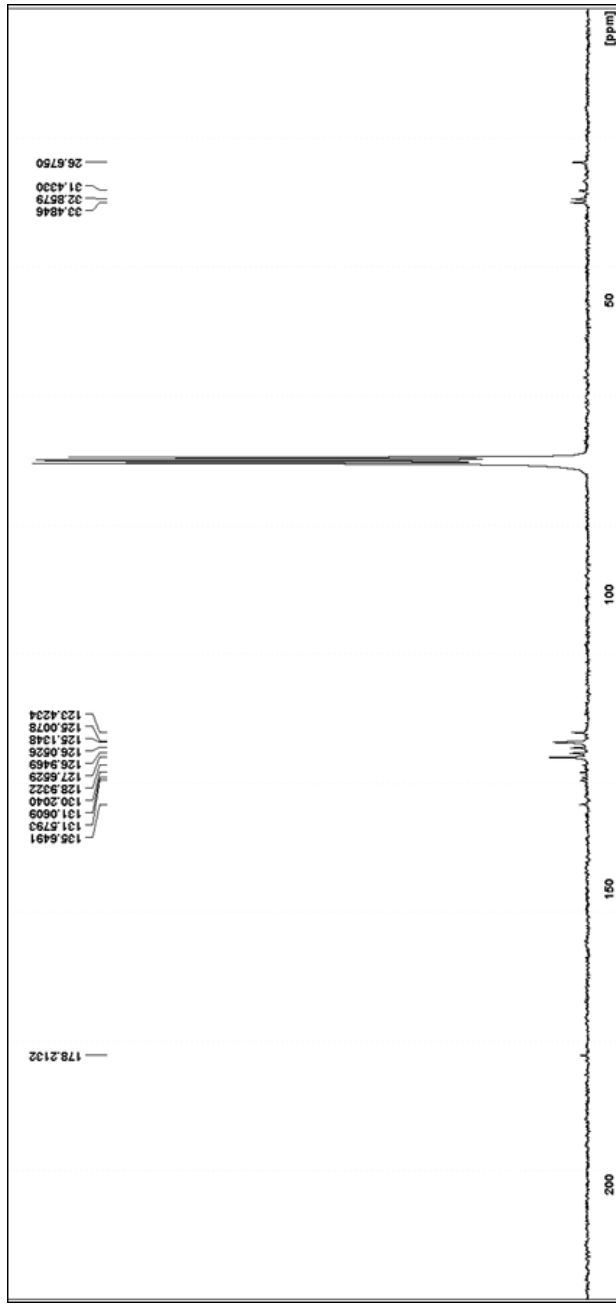

Figure 3.11: ^{13}C-NMR ($CDCl_3$) pyrene butyric acid.

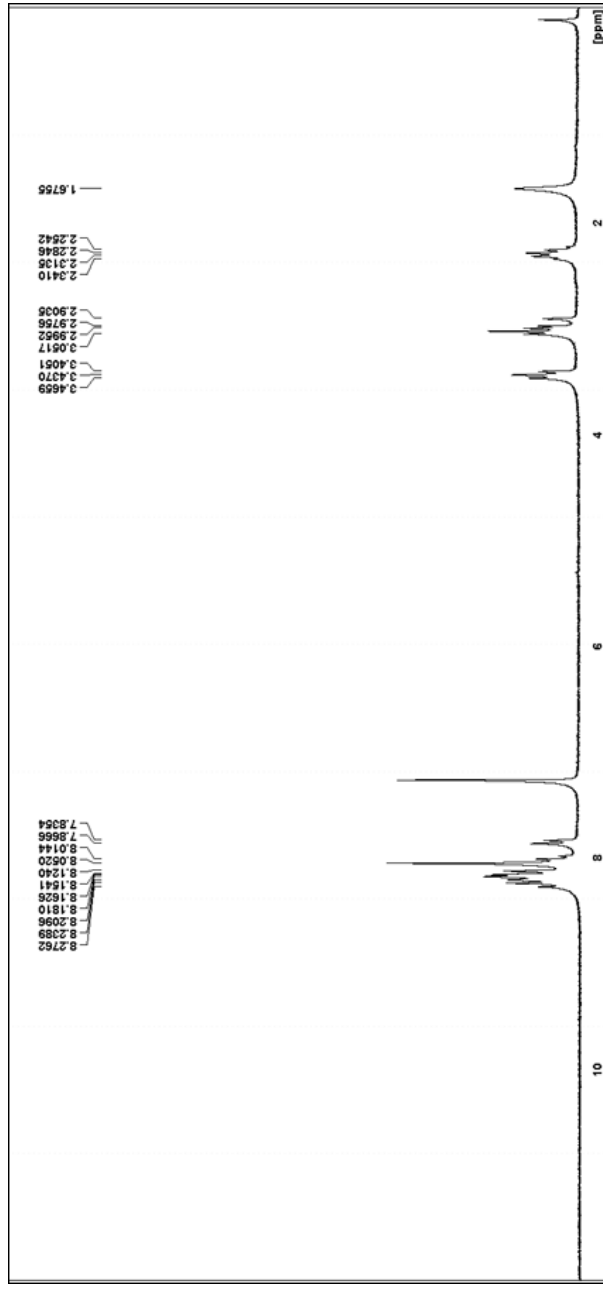

Figure 3.12: ^{1}H-NMR ($CDCl_3$) pyrene chloride.

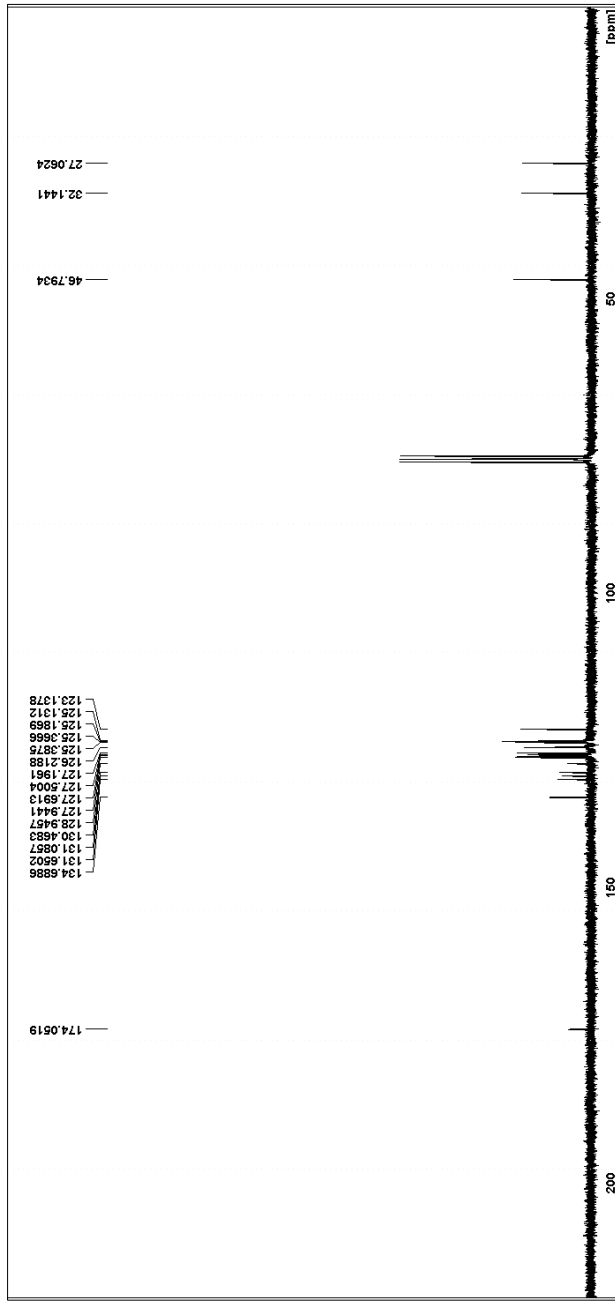

Figure 3.13: ^{13}C-NMR ($CDCl_3$) pyrene chloride.

- **Second step:** ***synthesis 4-Pyren-1-yl-butyric acid bicyclo[2.2.1]hept-5-en-2-ylmethyl ester***

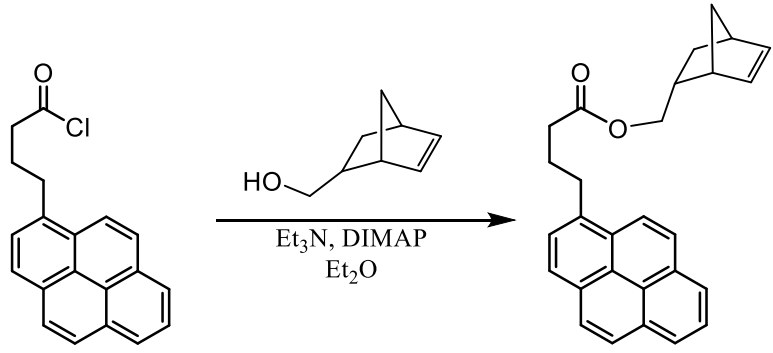

1 **2**

Figure 3.14: Esterification of 4-pyren-1-yl-butyroyl chloride.

The product (1) was react with 2-norbornen-5-yl-methanol to form the ester (product (2), *Fig. 3.6*). This is a reaction of esterification between an acyl chloride and a primary alcohol. The product (2) obtained was characterized by FT/IR analysis (*Fig. 3.7*), ^{1}H-NMR (*Fig. 3.8*) and ^{13}C-NMR (*Fig. 3.9*).

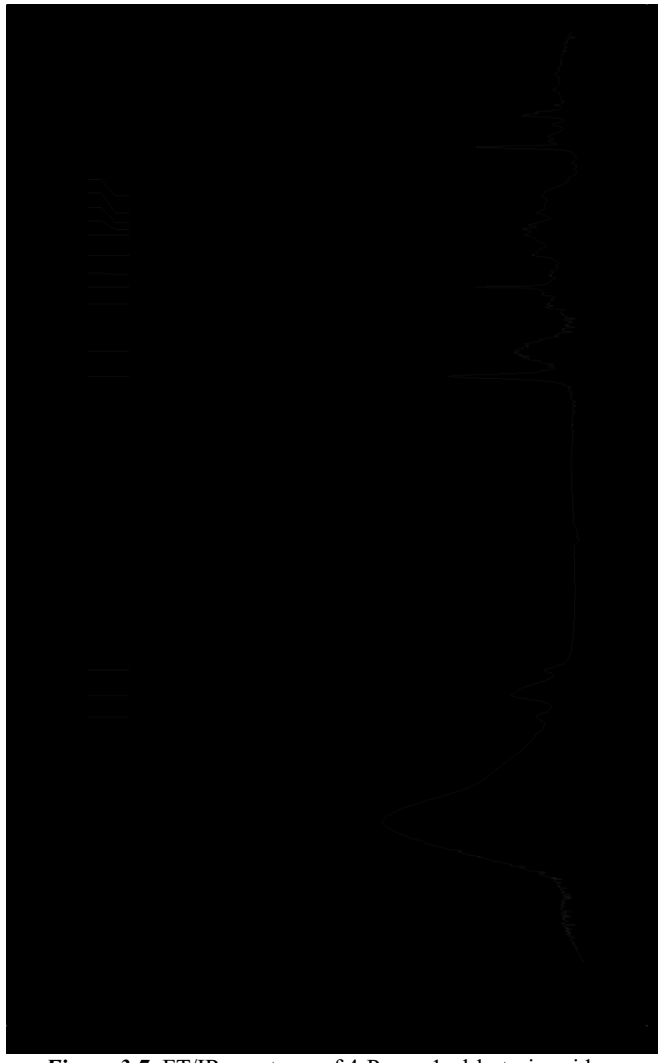

Figure 3.7: FT/IR spectrum of 4-Pyren-1-yl-butyric acid bicyclo[2.2.1]hept-5-en-2-ylmethyl ester.

In the spectrum of *Fig. 3.7* is possible observe the signal at 1731 cm^{-1} related to the stretching of the ester group. The signals at 3051, 2964 and 2867 cm^{-1} are attributable to the C-H, the another signals depend

of the absorbance of saturated and unsaturated groups present in the product (2). The reagent used, 5-norbornene-2-methanol, was in eso/endo mixture and therefore both ^{1}H-NMR and ^{13}C-NMR appear more complex.

In the ^{1}H-NMR (*Fig. 3.8*) in $CDCl_3$ at about 6 ppm there are the signals of the protons on the double bond of the norbornene, the spectrum at higher fields is complicated due to the H of the norbornene.

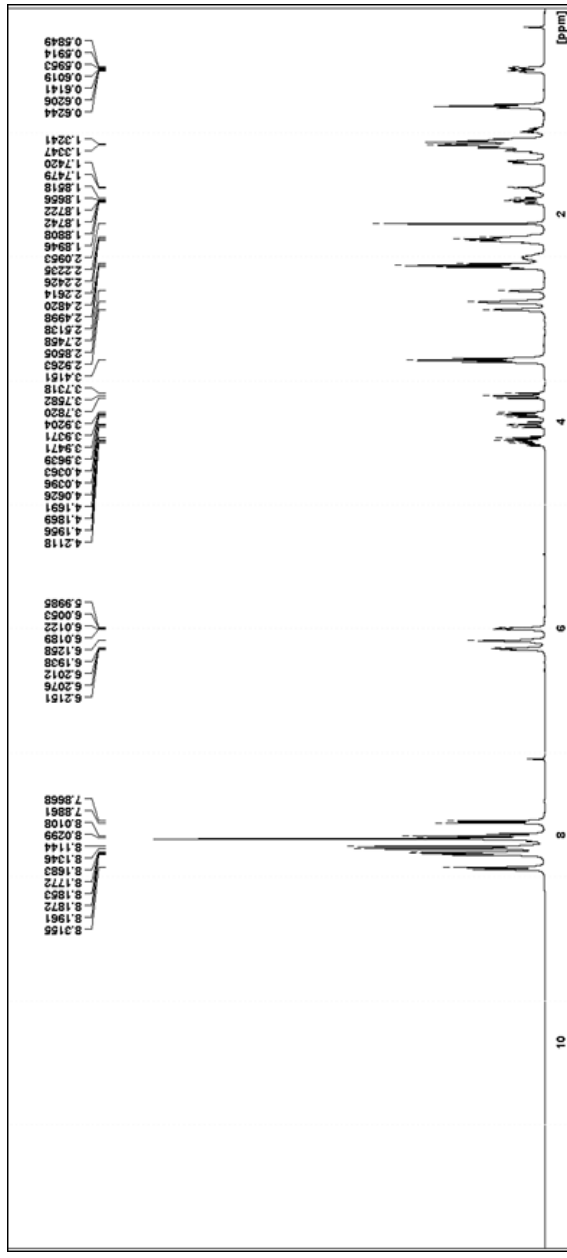

Figure 3.15: ^{1}H-NMR ($CDCl_3$) of 4-Pyren-1-yl-butyric acid bicyclo[2.2.1]hept-5-en-2-ylmethyl ester.

In the ^{13}C-NMR (*Fig. 3.9*) $CDCl_3$ we can observe the signal at 68 ppm related to the double bond of the norbornene, the signal at about 50 ppm of the O-CH_2 and other signals in the saturated region related to the C of the ring of the norbornene, the signal at 173.7 ppm has undergone a slight shift.

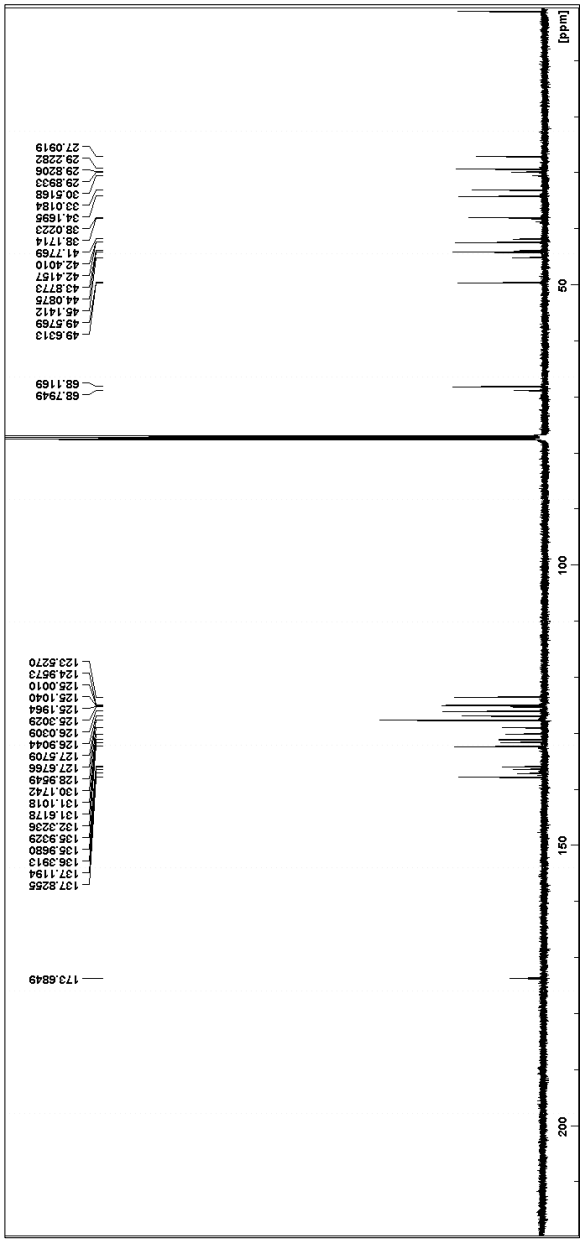

Figure 3.9: ^{13}C-NMR ($CDCl_3$) of 4-Pyren-1-yl-butyric acid bicyclo[2.2.1]hept-5-en-2-ylmethyl ester.

- **Third step:** ***synthesis of pyrene-Hoveyda-Grubbs II generation catalyst***

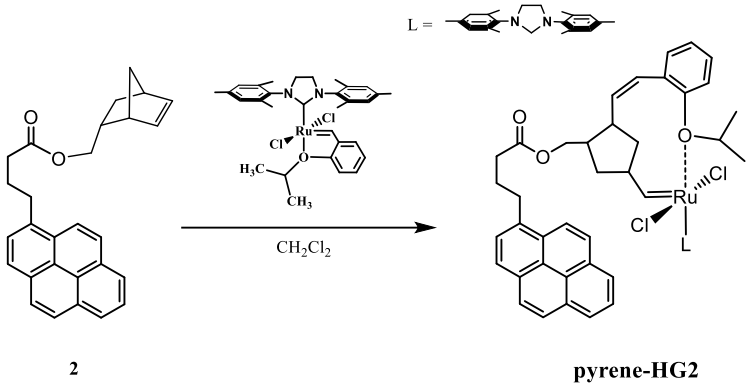

Figure 3.16: Metathesis reaction that bind the Hoveyda Grubbs II generation catalyst to the pyrene.

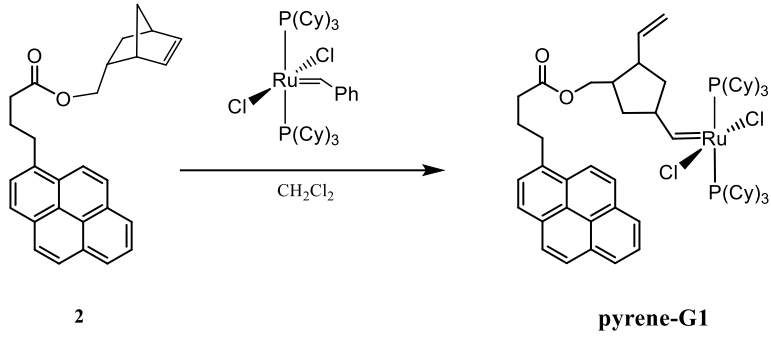

Figure 3.17: Metathesis reaction that bind the Grubbs I generation catalyst to the pyrene.

The catalyst was bound to the pyrene by a first metathesis reaction on a monomer previously linked to the pyrene (product (2)), the pyrene-catalyst isolated is a stable catalytic species and can be use in the functionalization of carbonfiller. The catalysts linked to the pyrene was Hoveyda Grubbs II generation (*Fig. 3.10*) and Grubbs I generation (*Fig. 3.11*), this were chosen because the HG2 is the

catalyst with the best activity ($1.83 \cdot 10^6$ for the GO-HG2 and $3.46 \cdot 10^6$ for the HG2, as reported in the section 2.1.4), while the G1 is the catalyst with less steric hindrance of substituents. The reaction was conduct in inert environment at room temperature for 16 hours. The product pyrene-HG2 was washed with diethyl ether while for the pyrene-G1 nothing wash was effectuated because the catalysts of the 2° generation are more stable for the presence of the NHC ligand instead the phosphinic ligand, characteristic of the 1° generation catalysts, are more subjected to the decomposition process and thus we preferred avoid this step.

The solid products recovered pyrene-HG2 and pyrene-G1 was characterized by FT/IR spectrum, ^{1}H-NMR and ^{13}C-NMR. The FT/IR spectrums of pyrene-HG2 (*Fig. 3.12*) and of pyrene-G1 (*Fig. 3.13*) don't shows significant difference respect to the spectrum of product (2).

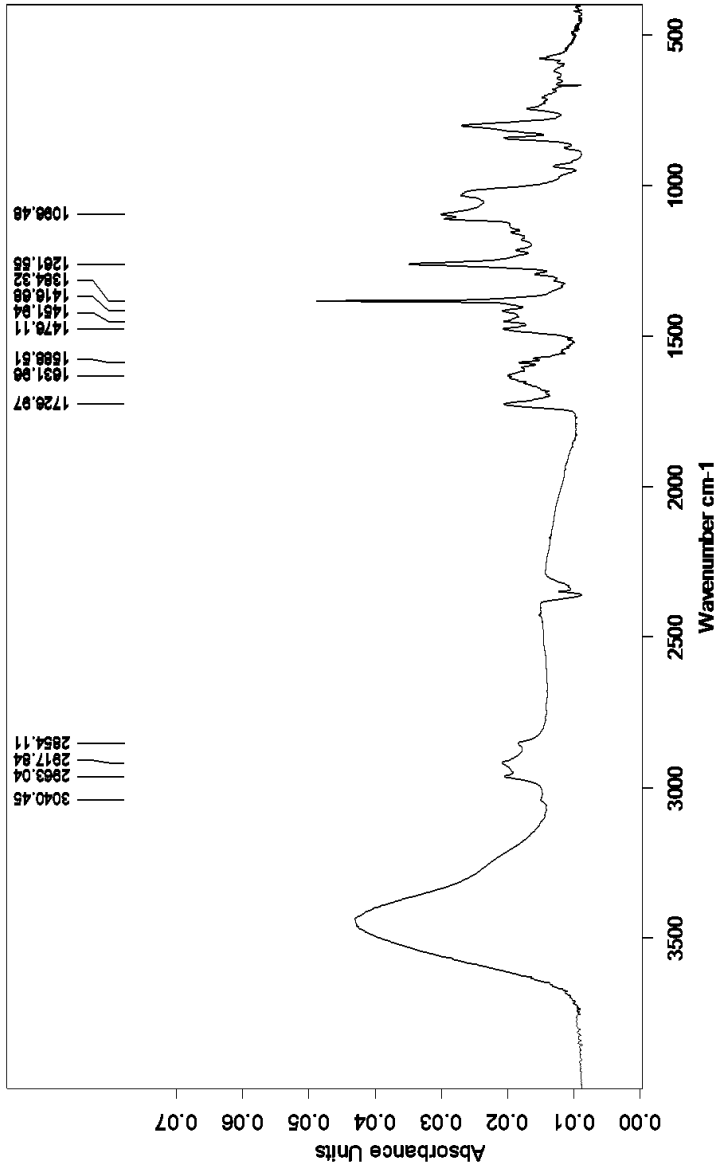

Figure 3.12: FT/IR spectrum of pyrene-HG2.

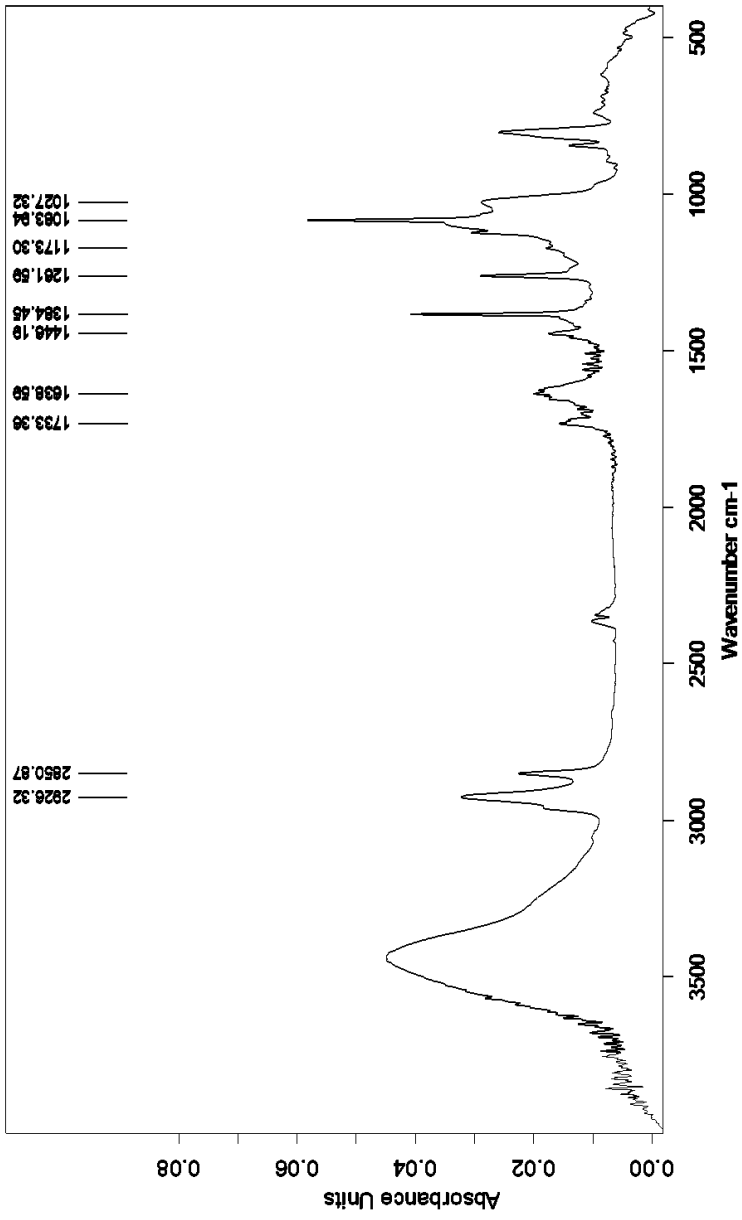

Figure 3.13: FT/IR spectrum of pyrene-G1.

In the ^{1}H-NMR (*Fig. 3.14*) in $CDCl_3$ of the pyrene-HG2 it is possible to observe the signal at 16.5 ppm, characteristic of the H alkylidenic bonded to Ru of the Hoveyda Grubbs catalyst, the signals at 6 ppm disappears and in the aromatic region the spectrum is more complex. In the ^{13}C-NMR (*Fig. 3.15*) in CD_2Cl_2 it is observed the signal of the C alkylidenic at 212 ppm, the signal at 76 ppm of the OCH_2, and other signals related to the aromatic and aliphatic C of the complex.

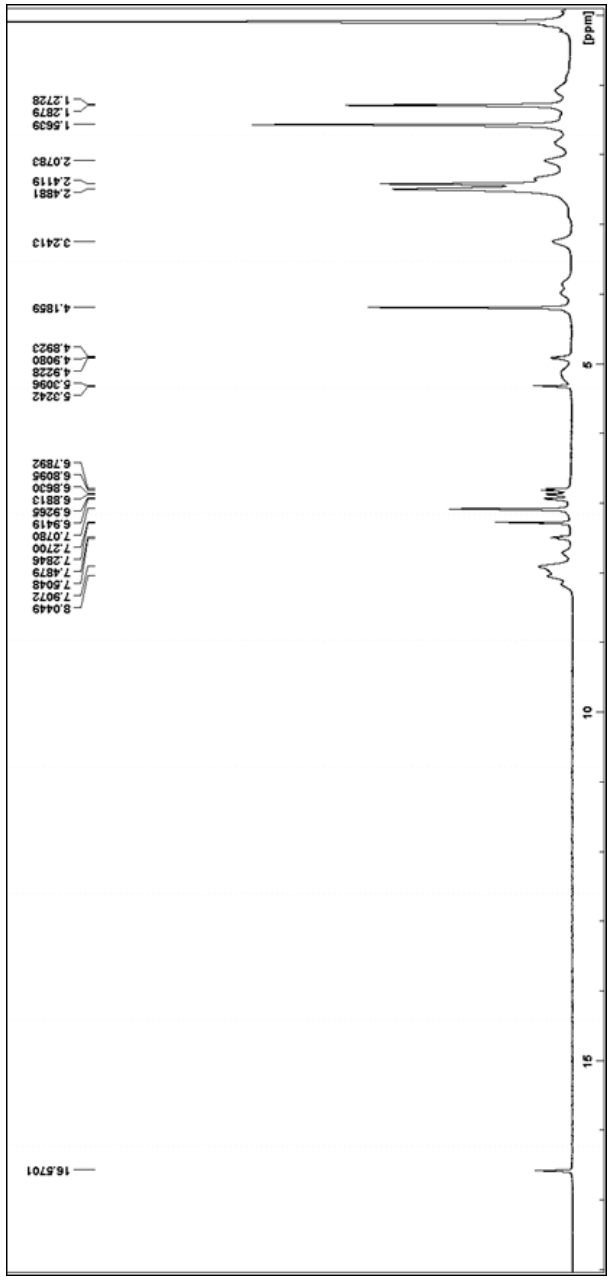

Figure 3.14: ^{1}H-NMR ($CDCl_3$) of pyrene-HG2.

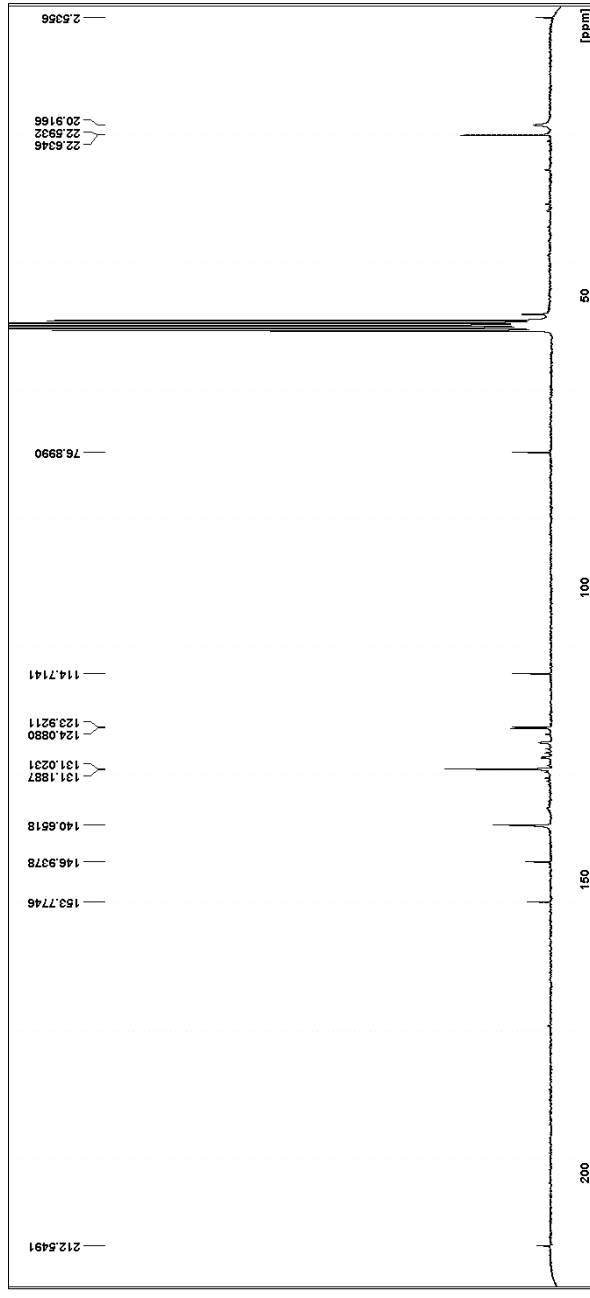

Figure 3.15: ^{13}C-NMR (CD_2Cl_2) of pyrene-HG2.

In the ^{1}H-NMR (*Fig. 3.16*) in $CDCl_3$ of the pyrene-G1 we observe the signal at 20 ppm of the H alkylidenic bond to the Ru of the Grubbs catalyst, the signals at 6 ppm disappears and in the aromatic and aliphatic region the spectrum is more complex. The ^{13}C-NMR (*Fig. 3.17*) in $CDCl_3$ shows all the expected signals for the pyrene-G1.

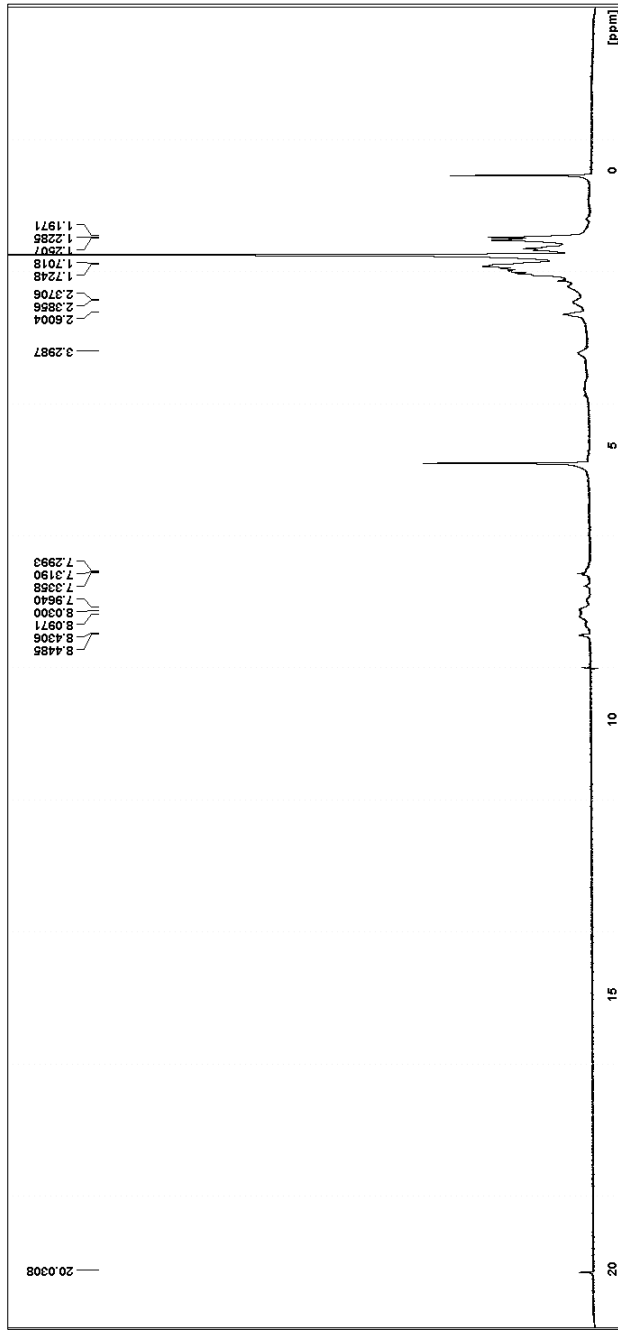

Figure 3.16: ^{1}H-NMR ($CDCl_3$) of the pyrene-G1.

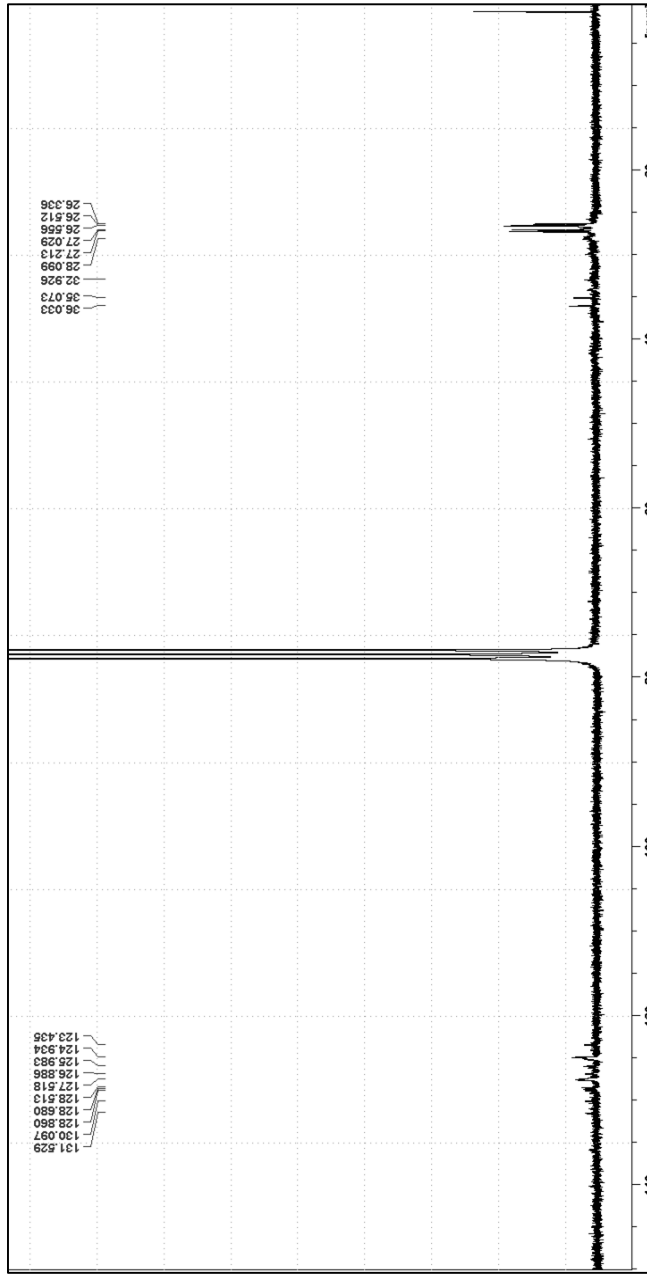

Figure 3.17: ^{13}C-NMR ($CDCl_3$) of the pyrene-G1.

The catalytic systems synthetized was tested before the attack on the carbon filler in the metathesis of 2-norbornene and 5-ethyliden-2-norbornene.

3.1.1.1 METATHESIS TEST OF PYRENE-HG2 AND PYRENE-G1

The catalyst activity of the pyrene-HG2 and pyrene-G1 was evaluated in the Ring Opening Metathesis Polymerization (ROMP) of 2-norbornene and 5-ethylidene-2-norbornene. The ROMP of 2-norbornene are shown in *Scheme 3.1*.

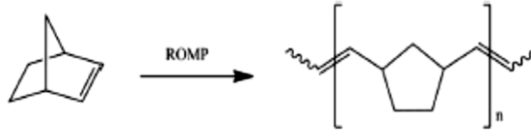

Scheme 3.1: Ring Opening Metathesis Polymerization of 2-norbornene.

The reaction conditions applied were the same used for the metathesis test for the GO-catalysts and catalysts described in the section 2.1.4. The catalytic activity obtained for the pyrene-HG2 was $4.70 \cdot 10^4$ $\frac{Kg}{mol^2 * h}$. Comparing this value with the activity of the catalyst HG2 not bonding ($3.46 \cdot 10^6 \frac{Kg}{mol^2 * h}$) or bonding on GO ($1.83 \cdot 10^6 \frac{Kg}{mol^2 * h}$) we can observe that the activity has been reduced of two orders of magnitude. For the pyrene-G1 the activity obtained was $4.72 \cdot 10^7 \frac{Kg}{mol^2 * h}$, while the activity of GO-G1 was $1.96 \cdot 10^6$ and

for G1 was $8.88 \cdot 10^6$, in this case we can observe a little increment of the activity. This behavior can be explained considering that the pyrene-HG2 was washed with diethyl ether, instead the pyrene-G1 was isolated through the removal of the solvent in vacuum, without washing step. Probably in the product pyrene-G1 there is traces of G1 not bonding to the pyrene.

The same behavior of pyrene-catalyst was observed in the ROMP of 5-ethyliden-2-norbornene, shows in the *Scheme 3.2*.

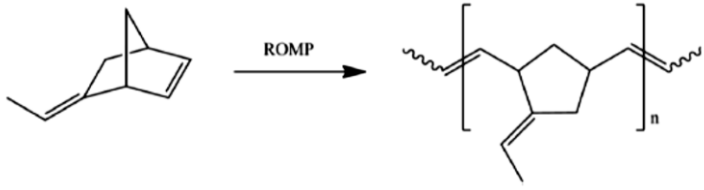

Scheme 3.2: Ring Opening Metathesis Polymerization of 5-ethyliden-2-norbornene.

The conversion obtained for the pyrene-HG2 was 6.4 % and for pyrene-G1 was 98.1 %.

3.1.2 FUNCTIONALIZATION OF CARBON NANOFILLER WITH PYRENE-CATALYST THROUGH π – STACKING INTERACTION

The carbon filler was functionalized through π – stacking interaction with the pyrene-catalyst obtained in order to support the catalyst on the surface and test them in self-healing systems. The π - stacking

interaction between the pyrene-catalyst and the carbon filler is very simple to realize, just stir them in the CH_2Cl_2 dry at room temperature for few hours and then remove the solvent through filtration.

3.1.2.1 FUNCTIONALIZATION OF MWCNTs WITH PYRENE-Ru-BASED CATALYSTS

At first the pyrene-catalyst synthesized was used to test the effects on the activity of the π-stacking interaction with the multiwalled carbon nanotubes (MWCNTs). The products MWCNTs-pyrene-HG2 and MWCNTs-pyrene-G1 was characterized by FT/IR and thermogravimetric analysis and tested in the metathesis reactions. The synthetic step of functionalization of MWCNTs with pyrene-HG2 is show in *Fig. 3.18*.

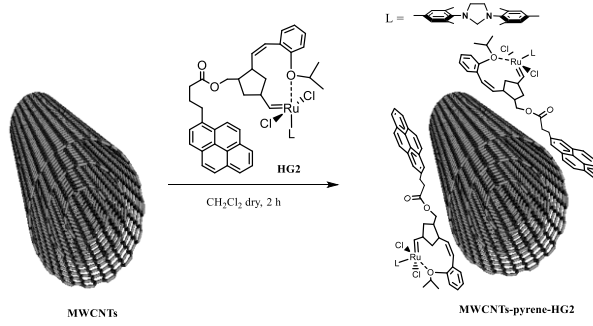

Figure 3.18: Preparation of MWCNTs-pyrene-HG2.

Comparing the FT/IR spectrum of the MWCNTs-pyrene-HG2 (*Fig. 3.19*) with that pyrene-HG2 (*Fig. 3.12*) it can be observed the reduction of the signal at 1731 cm^{-1} of the ester groups.

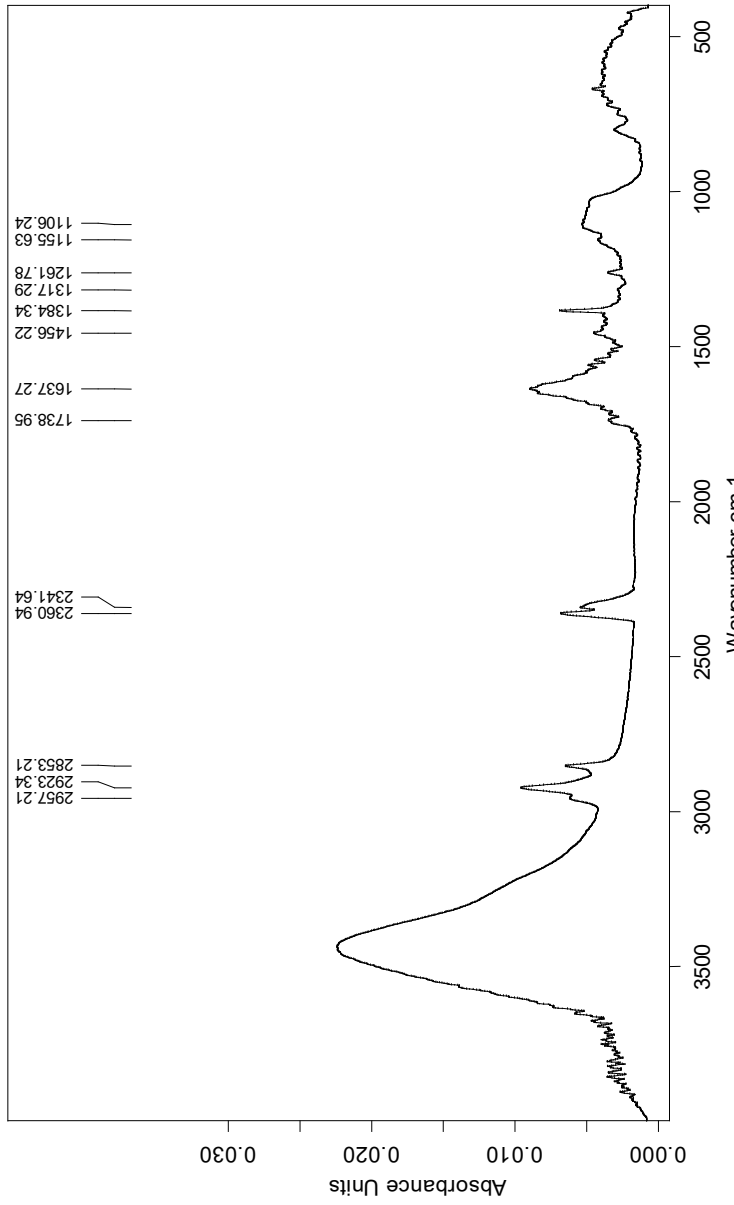

Figure 3.19: FT/IR spectrum of MWCNTs-pyrene-HG2.

The stretching of ester groups is now affected by the nearness of the aromatic plane of the MWCNTs due of the π – stacking interaction, highlighting that the interaction was established.

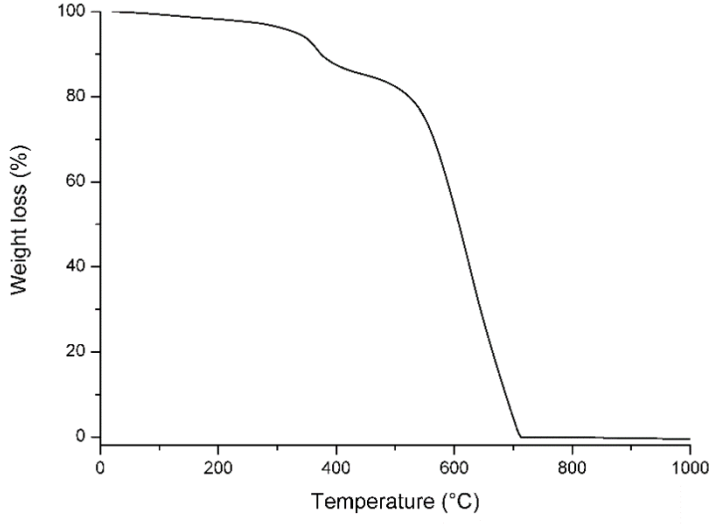

Figure 3.20: Thermogram in air at 1000 °C of MWCNTs-pyrene-HG2.

In the thermogram of MWCNTs-pyrene-HG2 (*Fig. 3.20*) can be observe a weight loss of about 15 % up to 350 °C due to phenomenon of decarboxylation of the ester function –COO-, the more labile groups, between 350°C at 700 °C the loss is approximately 84 % due to the degradation of the remaining structure.

In the *Fig. 3.21* is show the functionalization of the MWCNTs with pyrene-G1.

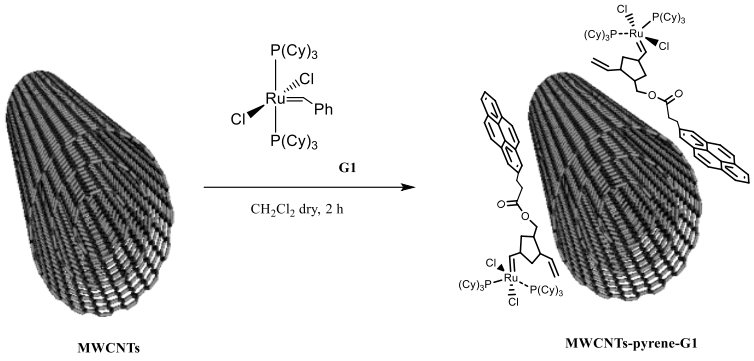

Figure 3.21: Preparation of MWCNTs-pyrene-G1.

The FT/IR spectrum of the MWCNTs-pyrene-G1 (*Fig. 3.22*) shows the disappear of the signal at 1733 cm^{-1}, as already described for the MWCNTs-pyrene-HG2. The thermogram of MWCNTs-pyrene-G1 (*Fig. 3.23*) show essentially the same losses of the MWCNTs-pyrene-HG2.

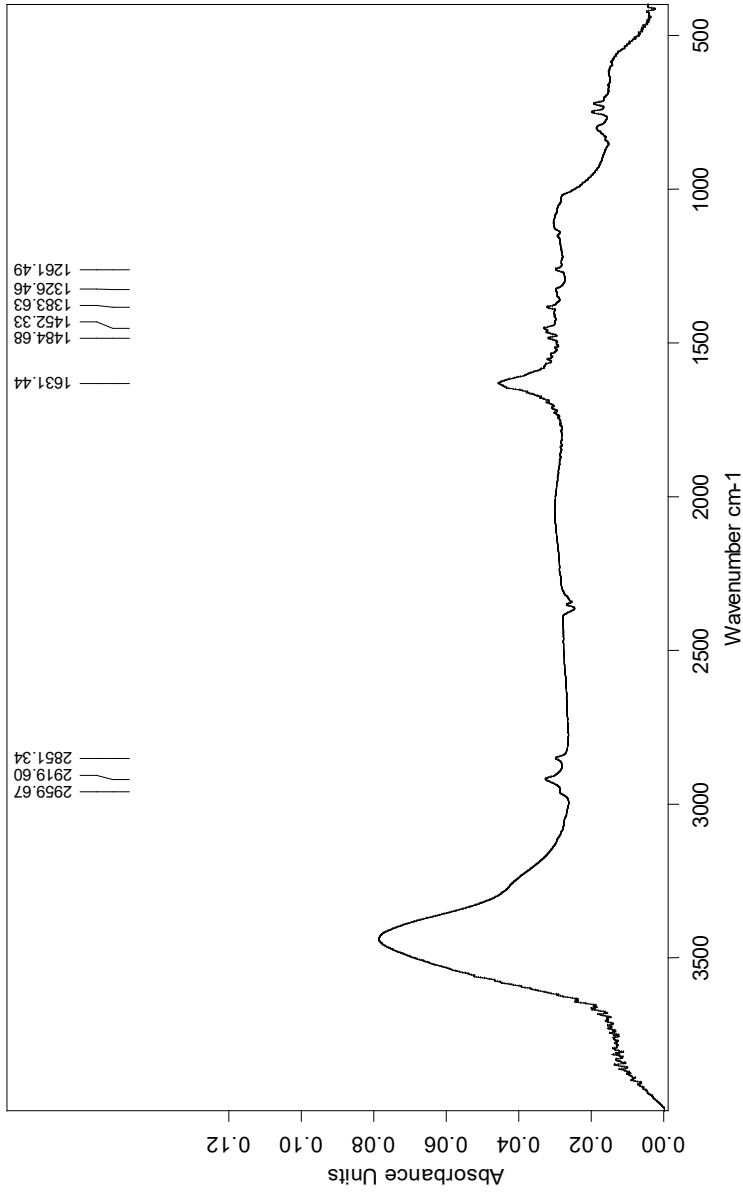

Figure 3.22: FT/IR spectrum of MWCNTs-pyrene-G1.

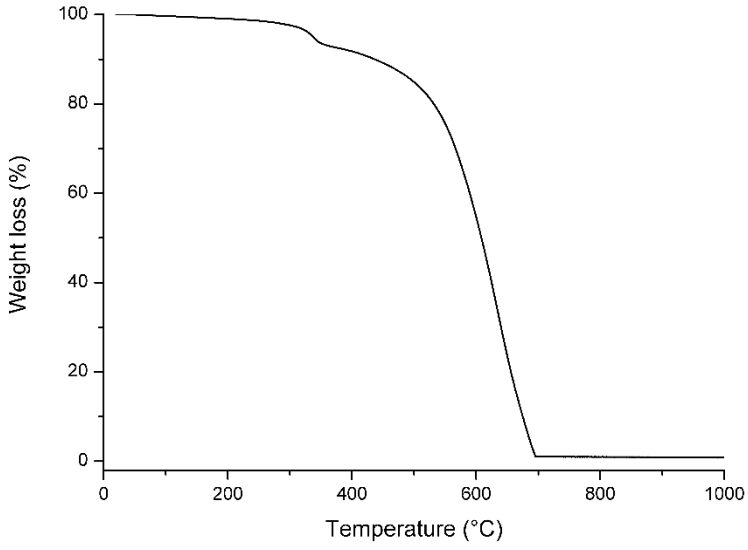

Figure 3.2183: Thermogram in air at 1000 °C of MWCNTs-pyrene-G1.

In the thermogram can be observe a weight loss of about 5 % up to 320 °C due to phenomenon of decarboxylation of the ester function –COO-, the more labile groups, between 320°C at 700 °C the loss is approximately 94 % due to the degradation of the remaining structure.

The MWCNTs-pyrene-HG2 and MWCNTs-pyrene-G1 was tested in the ROMP of 2-norbornene and 5-ethyliden-2-norbornene to evaluate as the activity of the catalytic site has been modified by π - stacking interaction with the nanofiller.

3.1.2.2 METATHESIS TEST OF MWCNTs-PYRENE-HG2 AND MWCNTs-PYRENE-G1

- **ROMP of 2-norbornene with MWCNTs-pyrene-HG2 and MWCNTs-pyrene-G1**

The ROMP of 2-norbornene (shown in *Scheme 3.1*) with MWCNTs-pyrene-HG2 unexpectedly did not lead to any product, instead for the MWCNTs-pyrene-G1 the activity evaluated was $7.43 \cdot 10^2$ $\frac{Kg}{mol^2 * h}$, five orders less respect pyrene-G1. These results have led us to think that the interaction that is created is so strong that the catalytic site is inaccessible to the monomer. To verify the identity of the interaction established between the catalyst and the nanofiller we had conduct an investigation with the catalyst HG2 and a type of molecules that replicate the behavior of the nanofiller, because the carbon nanofiller is insoluble. The molecules choice is the pyrene itself, since the four aromatic ring can simulate the graphitic plane.

- **ROMP of 5-ethyliden-2-norbornene with MWCNTs-pyrene-HG2 and MWCNTs-pyrene-G1**

The MWCNTs-pyrene-catalyst was tested also in the ROMP of the

5-ethyliden-2-norbornene. The results obtained reflect the same behavior observed for the polymerization of the 2-norbornene. The conversion obtained was 0.44 % for the MWCNTs-pyrene-HG2 and 0.46 % for the MWCNTs-pyrene-G1. Also in this case the activity of the catalyst is very low for the same reason explained above.

3.1.2.3 STUDY OF THE INTERACTION BETWEEN GRAPHITE AND CATALYST USING PYRENE

The pyrene is a chromophore, more specifically, a molecule that emits light radiation during a transition from a higher electronic level to a smaller one. Generally, all unsaturated groups may be defined as chromophores, as well as polyenic systems, aromatic rings, etc. Some chromophoric groups are called fluorophores if after the absorbance of photons of a certain wavelength exhibit fluorescence, emitting the absorbed radiation to a differ wavelength than the incident radiation.

Thanks to this property of the pyrene we analyze the interaction pyrene/catalyst through the fluorescence analysis to observe the influence that the catalyst effects on the absorbance of the aromatic plane. The profile pictures obtained was reported in the *Fig. 3.24*. The sample was irradiated at λ_{ex} 338 nm, the excitation frequency of the pyrene.

The pyrene, in solution of chloroform ($CHCl_3$), shows an intense

absorbance at λ 478 nm (red profile in *Fig. 24n*) while the catalyst HG2 don't shows nothing absorbance (black profile in the *Fig. 3.24*). The mixture of pyrene/HG2 at molar ratio 1:1 in $CHCl_3$ lead the shift of the absorbance of the pyrene at λ 499 nm (blue profile in the *Fig. 3.24*). The change in absorbance is evidence proof that the catalyst establishes a strong interaction with the aromatic network that does not allow at the monomer to reach the catalytic site and justifies the low activity of the system MWCNTs-pyrene-catalyst system. Moreover, the aromatic rings present on the catalyst could in turn establish a non-covalent π - stacking interaction with the graphitic plane of the carbon nanofiller, further reinforcing the interaction that is generated.

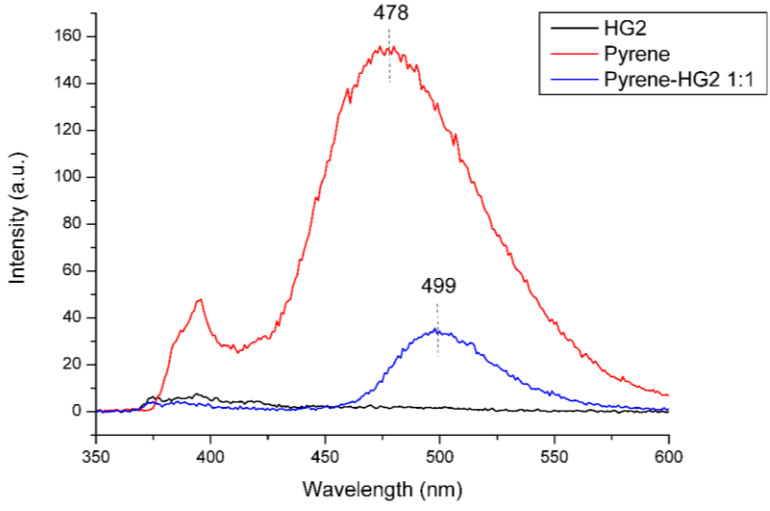

Figure 3.24: Fluorescence spectra of HG2, pyrene and pyrene-HG2 molar ratio 1:1 at λ_{ex} 338 nm.

As ulterior confirms of the strong interaction π - stacking between the nanofiller and the pyrene-catalysts was conduct an exhaustive extraction in boiling decaline (decahydronaphtalene, boiling point ~186 °C) of the sample MWCNTs-pyrene. If the pyrene remained attacked to the nanofiller, in the soluble fraction there should be no pyrene, this can be verified by performing a fluorescence analysis on the recovered solution as soluble fraction. *Fig. 3.25* shows the fluorescence spectrum of the soluble fraction in which we can observe the absence of the characteristic absorbance of pyrene at λ 478 nm. Therefore, we can conclude that the interaction between the MWCNTs and the pyrene is particularly strong, thus the monomer doesn't reach the catalytic site.

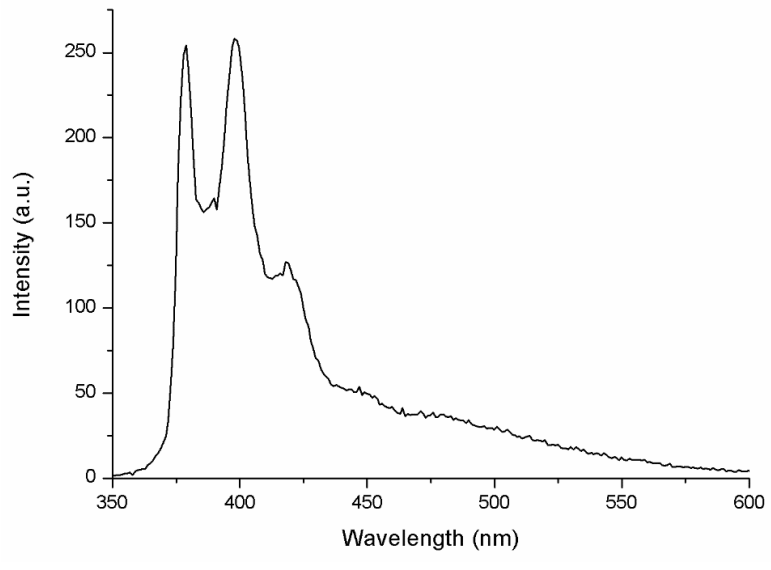

Figure 3.25: Fluorescence spectra of soluble fraction MWCNTs-pyrene in boiling decaline.

3.1.2.4 FUNCTIONALIZATION OF GRAPHITE WITH PYRENE-Ru-BASED CATALYSTS

- **Synthesis of graphite-pyrene-norbornene**

For the functionalization of the graphite, given the results obtained for the MWCNTs, we reversed the order of the last two steps of the preparation (phase 3 and phase of step of the mixing of pyrene-catalyst with the nanofiller to generate the π - stacking interaction). Therefore, before we functionalized the graphite with the product (2) and then bound the catalyst. The graphite was mixed with the product (2) (pyrene-norbornene) in CH_2Cl_2 for 2 hours and the graphite-pyrene-norbornene (*Fig. 3.26*) obtained was characterized by FT/IR (*Fig. 3.27*).

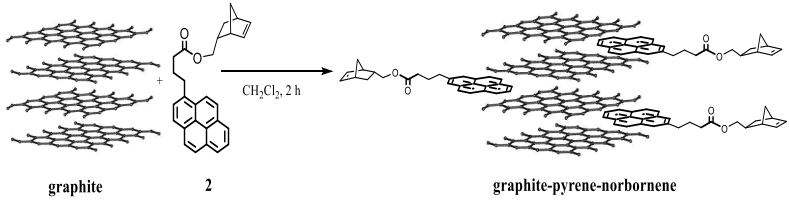

Figure 3.26: Functionalization of graphite with pyrene-norbornene.

In the spectrum the signal of the -COO-, that was at 1731 cm^{-1} in the spectrum of product (2) in *Fig. n*, shift at 1576 cm^{-1} due to the influence of the non-covalent interaction, instead the signal at 844

cm^{-1} and 721 cm^{-1} disappears.

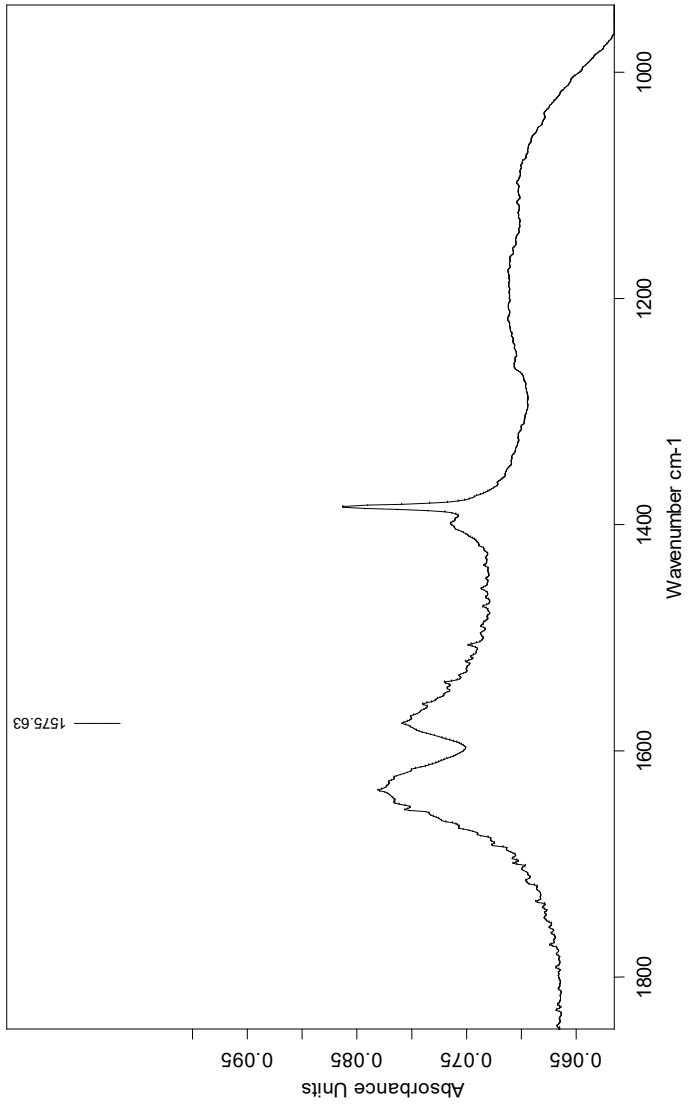

Figure 3.27: FT/IR spectrum of graphite-pyrene-norbornene, zoom of area 1850-950 cm^{-1}.

- **Synthesis of graphite-pyrene-HG2**

The product graphite-pyrene-norbornene, after establishing the π - stacking interaction, was react with HG2 catalyst. The reaction was carried out in N_2 with dry hexane for 16 hours at room temperature. This is the same procedure adopted for the functionalization of GO with the Ru-based catalysts.

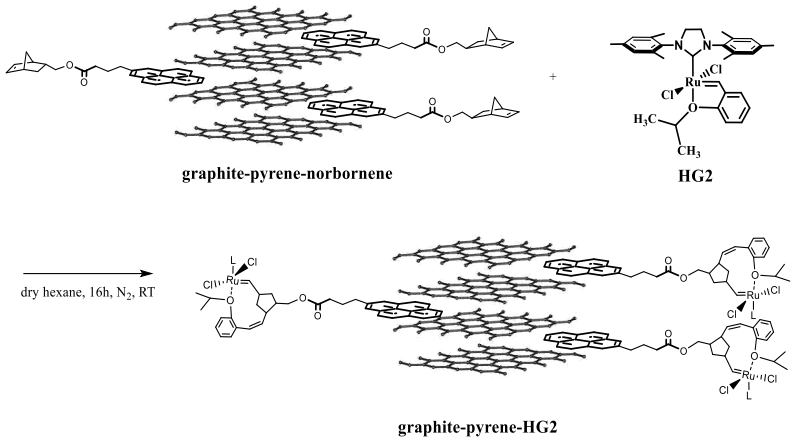

Figure 3.2198: Functionalization of graphite-pyrene-norbornene with HG2.

The product obtained was characterized by FT/IR analysis (*Fig. 3.29*) and thermogravimetric analisys. The FT/IR spectrum is substantially the same of the previous product graphite-pyrene-norbornene (*Fig. 3.27*).

The thermogram of *Fig. 3.30* shows the same profile of the MWCNTs-pyrene-HG2, with a weight loss of about 25 % up to 430 °C, and 74 % between 430 °C and 860 °C.

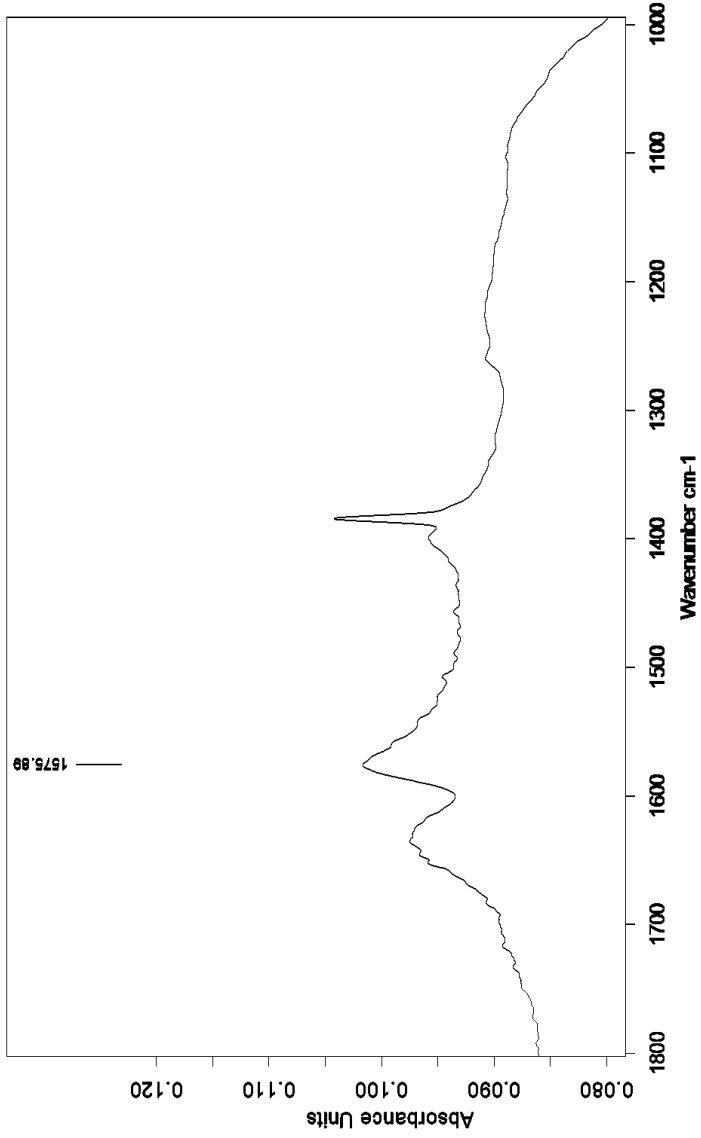

Figure 3.29: FT/IR spectrum of graphite-pyrene-HG2, zoom of area 1800-1000 cm^{-1}.

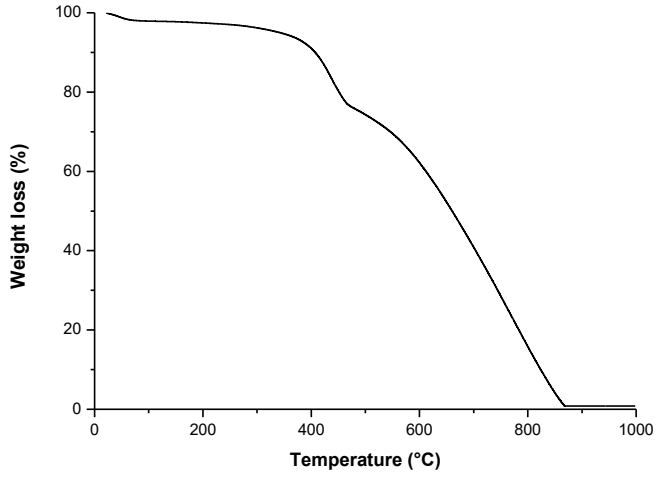

Figure 3.30: Thermogram of graphite-pyrene-HG2.

3.1.2.5 METATHESIS TEST OF GRAPHITE-PYRENE-HG2

- **ROMP of 2-norbornene**

The graphite-pyrene-HG2 was tested in the polymerization of 2-norbornene, by using the same reaction conditions reported above. The activity obtained was $5.0 \cdot 10^1 \frac{Kg}{mol^2 * h}$. Also with the graphite the π - stacking interaction was very strong and the monomer had difficulty to arrive at catalytic site, thus the activity was drastically reduced. The inversion of the reaction steps didn't have nothing effect on the catalytic activity, the π - stacking interaction that was generate between the graphite and the pyrene-norbornene after the

attack of the catalyst is again very strong.

3.2 ADDITIONAL USES OF PYRENE-Ru-BASED CATALYSTS

As described in the introduction the use of carbon nanofillers are currently highly considered in the field of structural materials for improving their electrical and mechanical properties. This application shows a real problem regards the dispersion in the materials because, it has been seen by previous studies, these tend to form aggregates visible to the naked eye and then the dispersion of this fillers are non-homogeny. The idea proposed initially was of use a polymer bound to the filler that acts as a compatibilizing agent and encourages a homogenous distribution of carbon nanofiller in the materials. This was realized with the polynorbornene obtained to the ROMP of 2-norborene with GO-catalyst (described in the section 2.1.4). Preliminary test has showed that this strategy improves the dispersion of the filler but needs modify the structure of the pristine graphite, and then consequently are lost some characteristic properties of the filler. The new synthetic approach through the π - stacking interaction, described for the functionalization of the carbon nanofiller with the Ru-based catalysts, leaves intact the structure of the filler and can be used for this purpose. The pyrene-catalyst complex can be used as catalyst for the synthesis of a polymer, so the polymer obtained have a terminal pyrene that is able, thanks at its

aromatic system, to bind the polymer on the carbon filler via π - stacking interaction. The great advantage of this strategy is the possibility of link any polymer on any filler capable to establish the non-covalent interaction of type π - stacking.

3.2.1 SYNTHESIS OF POLYMER-PYRENE

The synthesis of polymer involves a Ring Opening Metathesis Polymerization (ROMP) of a monomer by a Ruthenium catalyst-pyrene. The catalytic complex chosen for this test was the pyrene-HG2 (*Fig. 3.10*) synthetized as describe above in the section 3.1.1. We have seen that the pyrene-HG2 system is deactivated when placed on the graphitic plane (such as graphite or MWCNTs), but this results didn't limit its use as catalyst.

The monomers used are 2-norbornene and cyclooctadiene, the polymers produced are polynorbornene and polybutadiene, and through hydrogenation of latter we also obtained the polyethylene.

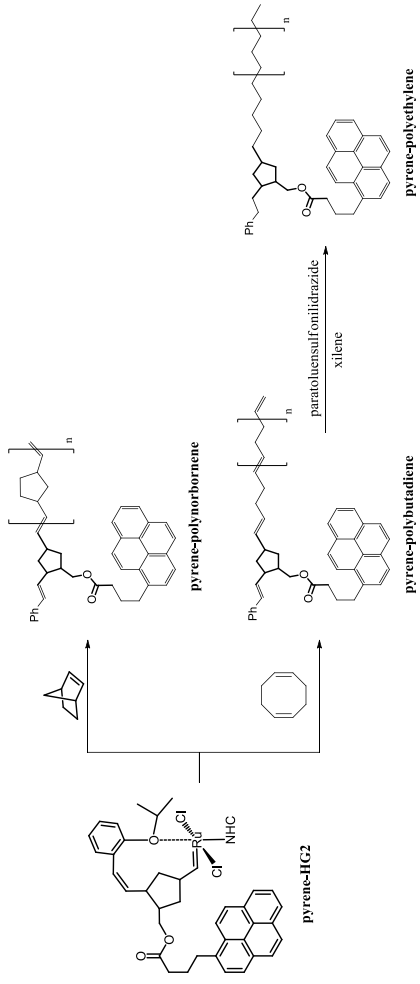

Figure 3.20: Synthesis of polymer-pyrene by pyrene-HG2.

Polymerizations were carried out in a solution of dry CH_2Cl_2 using a molar ratio pyrene-HG2/ monomer of 1: 100. Once upon obtained the polymers-pyrene, they were dissolved in a suitable solvent and establish π - stacking interaction with carbon filler (*Fig. 3.30*)

through simple stirring in CH_2Cl_2 dry for 2h. The filler tested was the graphite in weight ratio of 1:1.

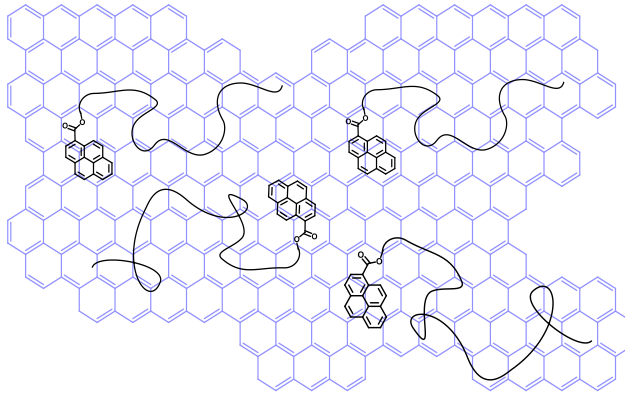

Figure 3.21: graphitic plane with a polymer-pyrene linked by π - stacking interaction.

An interesting peculiarity was that when the graphite was added to the solution, this remain well dispersed also without mixing, instead the graphite precipitates on the bottom when added to a solution in absence of pyrene. The polymer-pyrene obtained was dried in vacuum and characterized by TEM (Electronic Transmission Microscopy).

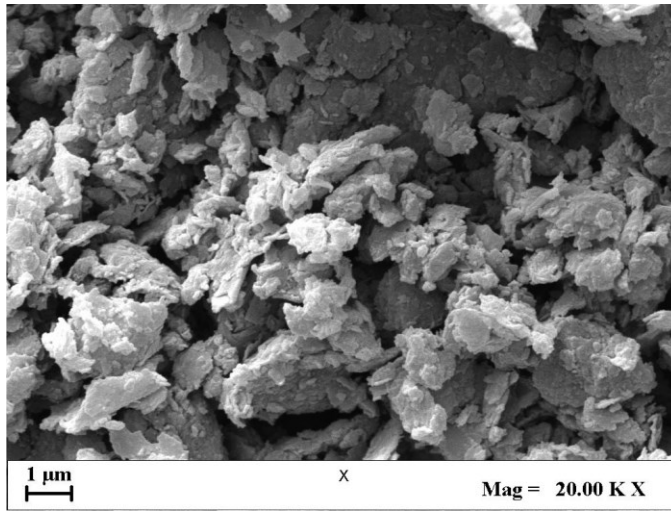

a.

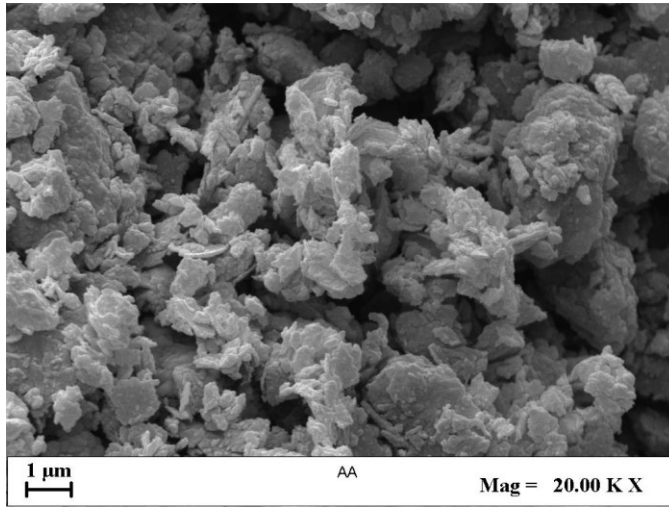

b.

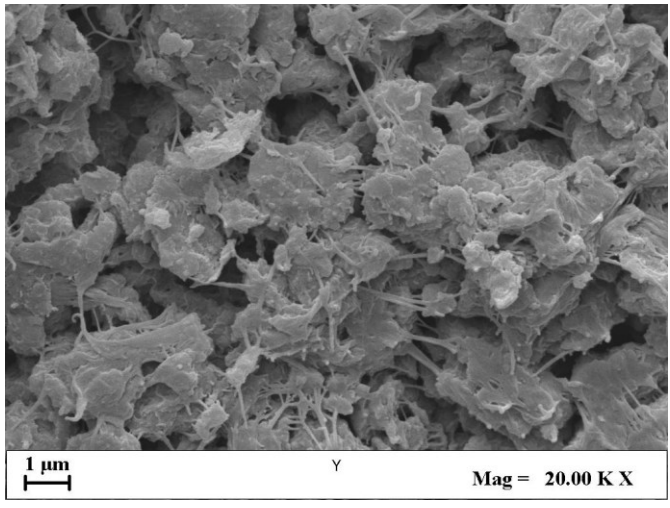

c.

Figure 3.22: TEM (Electronic Transmission Microscopy) images of a) graphite, b) graphite-polybutadiene-pyrene and c) graphite-polybutadiene.

From the comparison of the images in *Fig. 3.31* it can be seen that in the sample *b* the polymer is perfectly adhered to the surface of the graphite, which has a very similar appearance to that of the graphite of sample *a*. In the sample *c* there isn't adhesion between the polymer and the graphite surface, while are predominant the interactions between the polymeric chains themselves, so that they form separate visible filaments.

Therefore, the use of a pyrene allows both to link the polymer to the filler without modify the structure, and then use the polymer as compatibylizing agent, and to obtain a better distribution of polymer itself in the chosen filler.

At the aim to evaluate the nature of the interaction between the polymer-pyrene and graphite an exhaustive extraction of pyrene-polynorbornene-graphite in boiling xylene was performed. No

product soluble is recovered demonstrating that the π - stacking interaction between graphite and polymer is very strong.
This strategy allows to link any polymer on any carbon filler.

3.3 ELECTRICAL PROPERTIES OF THE PYRENE-CARBON NANOFILLER

The functionalization of the carbon filler through π - stacking interaction was performed principally at the aim of preserve the characteristic of the filler and then use they in the nanocomposite. The covalent modifications, as well as the insertion of ionic groups on the surface of carbon nanomaterial, produces hybridized sp^3 carbon, resulting in loss of electrical conductivity of the nanofillers. Instead, non-covalent modifications do not alter the characteristics of the nanofiller because preserve the sp^2 hybridization of carbon atoms.
Therefore, the conductivity of the carbon filler shouldn't have been modified after the functionalization with pyrene. This last was evaluated effecting some tests with the MWCNTs functionalized with 1-pyrene butyric acid.

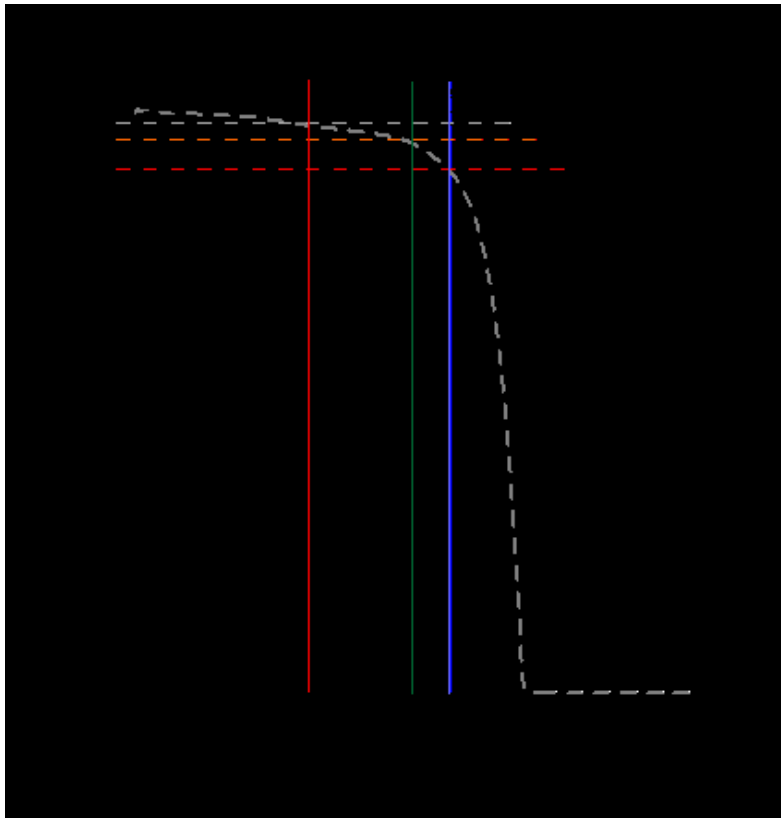

Figure 3.23: Thermogravimetric analysis of MWCNTs (black line) and MWCNTs-pyrene butiric acid (dashed line).

In *Fig. 3.35* are reported the thermogravimetrics curves in air for MWCNTs (black line) and MWCNTs functionalized with 1-pyrene-butyric acid (dashed line). It is worth to note that pristine MWCNTs are stable up to about 520 ° C and at this temperature the MWCNTs-pyrene show a weight loss of approximately 10 wt%. This means that, in the case of functionalized filler, there is an incidence by weight strictly due to functional groups attached to carbon nanotubes

quantified at 10 wt%.

3.3.1 TEST OF CONDUCIBILITY IN THE NANOFILLED COMPOSITES

The MWCNTs functionalized was dispersed in the epoxy matrix to obtain nanofilled composites. The epoxy matrix is prepared by mixing an epoxy precursor, tetraglycidylmethylenedianiline (TGMDA), with an epoxy reactive monomer 1-4 butanedioldiglycidyl ether (BDE) that acts as a reactive diluent allowing to reduce the moisture content and to facilitate the dispersion step of nanofiller [5-8]. At a concentration of 80 %: 20 % (by wt). The DDS hardener agent is added at a stoichiometric concentration with respect to all the epoxy rings (TGMDA and BDE). Epoxy blend and DDS are mixed at 120°C and the MWCNTs functionalized with 1-pyrenebutyric acid are added and incorporated into the matrix at loading concentrations of 0.05 %, 0.1 %, 0.32 %, 0.5 %, 0.64 % and 1 % by weight by using a ultrasonication for 20 min. All the mixtures are cured by two-stage curing cycles: a first isothermal stage is carried out at the lower temperature of 125°C for 1 hour and then a second isothermal stage at higher temperatures up to 200°C for 3 hours.

In such composites the electrical properties are related to the morphology of conductive network formed by filler particles sufficiently close to allow, in the limit of a certain cut-off distance,

the electrical conduction via tunneling since an inevitable thick insulating polymer layer wraps around the outer shells of MWCNTs thus isolating them electrically [9].

In particular, for low values of filler, the percolation network is not formed and the composite exhibits an electrical conductivity of the order of pS/m, typical of insulating materials. Otherwise, as soon as the filler concentration exceeds a critical value (i.e. ϕ_c, electrical percolation threshold, EPT) the conductivity increases sharply (by several orders of magnitude) following the classical power law:

$$\sigma = \sigma_0(\phi - \phi_c)^t$$

where σ_0 is the intrinsic conductivity of the filler and t is a critical exponent depending on the dimensionality of the percolating structure. *Fig. 3.36* shows the DC volume conductivity (i.e. σ), measured at room temperature, as a function of the filler concentration (wt %) for the MWCNTs and MWCNTs-pyrene. The weight concentrations refer exclusively to the multiwalled nanotubes. Since the contribution of the functional groups has been subtracted, a slight misalignment between the concentrations of the two fillers is present.

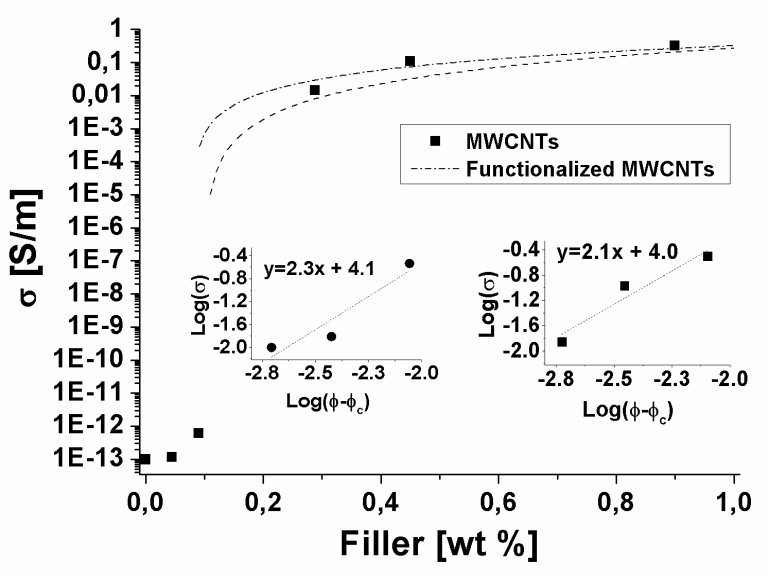

Figure 3.24: DC volume conductivity of the nanocomposites versus filler weight percentage. The inserts show the log-log plot of the electrical conductivity as a function of (ϕ-ϕ_c) with a linear fit for composites reinforced with pristine and functionalized MWCNTs.

The experimental characterization doesn't reveal remarkable difference, as concerns the EPT, achieved with the two fillers since for both the respective values fall in the similar restricted range, i.e. [0.1-0.32] wt % and [0.1-0.28] wt %. Instead, an appreciable improvement for the electrical conductivity of the composites for each filler concentration above the EPT is observed. Higher values also of an order of magnitude (0.015 S/m against 0.109 S/m at 0.5 wt % and 0.45wt%, respectively) are achieved with a 10 wt % in less of conductive filler. Finally, the characteristic parameters of the percolation law can be estimated from the curves (inserts of *Fig. 37*),

reporting the log-log plots of the experimental conductivity vs. filler concentration. In particular, the value for the critical exponent t can be obtained as the slope of the linear fit. The estimated values, i.e. 2.3 and 2.1 for both pristine and functionalized MWCNTs reinforced composites respectively, are found to agree with universal values, indicative of a 3-D organization of the percolating structure typically obtained with 1-D type of filler.

3.4 EXPERIMENTAL PART

SECTION 3.1.1
SINTHESY OF PYRENE-Ru-BASED CATALYST

- **First step:** ***synthesis of 4-Pyren-1-yl-butyroyl chloride (1)***

To a suspension of 4-(1-pyrenyl) butyric acid (2.0 g, 6.94 mmol) in ca. 225 ml of dry CH_2Cl_2 was added neat oxalyl chloride (2.1 ml, ca. 21 mmol) and two drops of DMF. No significant change was observed during the dropwise addition of $(COCl)_2$, but complete dissolution of the acid was observed upon addition of DMF. The resultant gold-yellow solution was stirred at room temperature for 5 h, and the volatiles were removed in vacuum. Diethyl ether (22 ml) and hexane (ca. 45 ml) were added to the resulting light brown solid, and the resulting suspension was stirred for ca. 10 min. The supernatant was decanted using a cannula, and the solid was whashed with hexane (15 ml). The resultant off-white solid was dried under vacuum (1.60 g, 76 % yield).
The ^{1}H-NMR spectrum of the pyrene butyric acid (250 MHz, $CDCl_3$) shows the following signals: δ 10.28 (1H), 8.51(d, 1H),

8.17 (dd, 1H), 7.99 (m, 2H), 7.88(d, 1H), 3.42 (t, 2H), 2.52 (m, 2H), 2.22 (m, 2H), 1.25 (s, 1H). The ^{13}C-NMR spectrum of the pyrene butyric acid (400 MHz, $CDCl_3$) shows the following signals: δ 178.21, 135.65, 131.58, 131.06, 130.20, 128.93, 127.65, 126.95, 126.05, 125.13, 125.01, 123.42, 33.48, 32.86, 31.43, 26.68.

The ^{1}H-NMR spectrum of the pyrene chloride (250 MHz, $CDCl_3$) shows the following signals: δ 8.28 (d, 1H), 8.20 (d, 1H), 8.18 (d, 1H), 8.14 (d, 1H), 8.13, (1H), 8.04 (2H), 8.01 (dd, 1H), 7.87 (d, 1H), 3.47 (t, 2H), 3.05 (t, 2H), 2.34 (m, 2H), 1.67 (s, 1H). The ^{13}C-NMR spectrum of the pyrene chloride (250 MHz, $CDCl_3$) shows the following signals: δ 174.05, 134.68, 131.65, 131.08, 130.47, 128.94, 127.94,127.69, 125.70, 127.20, 126.21, 125.37, 125.13, 123.14, 46.79, 32.14, 27.06.

- **Second step:** ***synthesis of 4-Pyren-1-yl-butyric acid bicyclo[2.2.1]hept-5-en-2-ylmethyl ester***

An oven-dried Schlenk flask containing 2-norbornen-5-ylmethanol (200 µl, 1.63 mmol), triethylamine (450 µl, 3.23 mmol) and a crystal of DMAP in ca. 50 ml of diethyl ether was chilled to 0 °C. Dropwise addition of a solution of 4-(1-pyrenyl)butyroyl chloride (500 mg, 1.63 mmol) in diethyl ether (25 ml) caused immediate turbidity. The resulting mixture was allowed to warm to room temperature and stirred for 8 h. After

this time, the mixture was poured over deionized water, and the organic layer separated. The aqueous layer was extracted with diethylether (3 · 10 mL) and the organics were dried over $MgSO_4$. Rotary evaporation afforded crude product as a yellow oil, further purified by column chromatography on silica gel (hexanes/ethyl acetate 5:1). The pure product was isolated in a mixture of endo- and exo- isomers.

The ^{1}H-NMR spectrum of the pyrene-norbornene (400 MHz, $CDCl_3$) shows the following signals: δ

8.31, 8.20, 8.19, 8.18, 8.13, 8.03, 8.01, 7.87, 6.21, 6.12, 6.01, 4.21, 4.06, 4.03, 3.96, 3.92, 3.76, 3.41, 2.93, 2.85, 2.74, 2.51, 2.26, 2.09, 1.90, 1.75, 1.33.

The ^{13}C-NMR spectrum of the pyrene-norbornene (400 MHz, $CDCl_3$) shows the following signals: δ 173.68, 137.82, 136.4, 135.93, 132.32, 131.62, 131.10, 130.17, 128.95, 127.68, 126.9, 126.03, 125.30, 125.20, 125.00, 123.53, 68.79, 68.12, 49.63, 45.14, 44.08, 43.89, 42.41, 41.78, 38.17, 38.02, 34.17, 33.02, 30.52, 29.89, 29.23, 27.09.

- **Thirt step:** ***synthesis of pyrene-Ru catalyst***

.

Pyrene-HG2: The product (2) (195 mg, $4.94 \cdot 10^{-1}$ mmol) and the HG2 catalyst were added under nitrogen to 130 ml of dry CH_2Cl_2 in a reaction flask. The mixture was stirred at room temperature under nitrogen for 18 h. The suspension was filtered and washed adding in

the reaction flask diethyl ether (5 x 20 ml). At each addition the mixture was mixing for 30 minutes, made decanted and the solvent was removed with a Pasteur. After was dried in vacuum and the product pyrene-HG2 obtained was 203 mg.

The ^{1}H-NMR spectrum of the pyrene-HG2 (400 MHz, $CDCl_3$) shows the following signals: δ 16.57 (s, 1H), 8.04, 7.09, 7.50, 7.48, 7.28, 7.08, 6.94, 6.88, 6.81, 6.79, 5.32, 4.92, 4.18, 3.24, 2.48, 2.41, 2.08, 1.56, 1.29. The ^{13}C-NMR spectrum of the pyrene-HG2 (250 MHz, CD_2Cl_2) shows the following signals: δ 212.55, 153.77, 146.94, 140.65, 131.19, 124.09, 123.92, 114.71, 76.90, 22.63, 20.92.

Pyrene-G1: For the synthesis of pyrene-G1 in a reaction flask was added under nitrogen the product (2) (52.8 mg, $1.34 \cdot 10^{-1}$ mmol), the G1 catalyst (106.6 mg, $1.29 \cdot 10^{-1}$ mmol) and CH_2Cl_2 (40ml). The mixture was stirring for 18 h at room temperature and dried in vacuum. The product pyrene-G1 obtained was 176 mg.

The ^{1}H-NMR spectrum of the pyrene-G1 (400 MHz, $CDCl_3$) shows the following signals: δ 20.03 (s, 1H), 8.45, 8.43, 8.10, 8.03, 7.96, 7.34, 7.32, 7.30, 3.30, 2.60, 2.38, 2.37, 1.72, 1.70, 1.26, 1.23, 1.20.

The ^{13}C-NMR spectrum of the pyrene-G1 (400 MHz, $CDCl_3$) shows the following signals: δ 131.53, 130.10, 128.86, 128.68, 128.51, 127.52, 126.89, 125.98, 124.93, 123.44, 36.03, 35.07, 32.93, 28.10, 27.21, 27.03, 26.56, 26.51, 26.34.

- **ROMP of 2-norbornene with pyrene-HG2**

The polymerization was carried out in a reaction flask of 250 ml with 99 ml of dry THF, 2-norbornene (958.1 mg, $1.02 \cdot 10^{-2}$ mol) and pyrene-HG2 (2.9 mg, $2.84 \cdot 10^{-3}$ mmol). The mixture was stirred for about 17 hours at room temperature. The polymerization was stopped with some drops of ethylvinyl ether and the polymer was coagulated in ethanol. The polymer obtained, after drying under vacuum overnight, was 20 mg.

- **ROMP of 2-norbornene with pyrene-G1**

The polymerization was carried out in a reaction flask of 250 ml with 99 ml of dry THF, 2-norbornene (924.6 mg, 9.8 mmol) and pyrene-HG2 (3.2 mg, $2.80 \cdot 10^{-3}$ mmol). The mixture was stirred for 15 minutes at room temperature. The polymerization was stopped with some drops of ethylvinyl ether and the polymer was coagulated in ethanol. The polymer obtained, after drying under vacuum overnight, was 325 mg.

- **ROMP of 5-ethyliden-2-norbornene with pyrene-HG2**

The polymerization was carried out in bulk in a vial of 4 ml with 5-

ethyliden-2-norbornene ($1.04 \cdot 10^3$ mg, 8.67 mmol) and pyrene-HG2 (5.0 mg, $4.89 \cdot 10^{-3}$ mmol). The mixture was stirred for about 6 hours at room temperature. The polymerization was stopped with some drops of ethylvinyl ether and the polymer was coagulated in ethanol. The polymer obtained, after drying under vacuum overnight, was 61 mg.

- **ROMP of 5-ethyliden-2-norbornene with pyrene-G1**

The polymerization was carried out in bulk in a vial of 4 ml with 5-ethyliden-2-norbornene ($1.15 \cdot 10^3$ mg, 9.58 mmol) and pyrene-G1 (4.9 mg, $4.29 \cdot 10^{-3}$ mmol). The mixture was stirred for about 25 seconds at room temperature. The polymerization was stopped with some drops of ethylvinyl ether and the polymer was coagulated in ethanol. The polymer obtained, after drying under vacuum overnight, was $1.13 \cdot 10^3$ mg.

SECTION 3.1.2.1

FUNCTIONALIZATION OF MWCNTs WITH PYRENE-Ru-BASED CATALYSTS

- **Functionalization of MWCNTs with pyrene-HG2**

The π – stacking interaction between the pyrene-HG2 and the MWCNTs was obtained mixing in the reaction flask the pyrene-HG2 (200 mg, $1.96 \cdot 10^{-1}$ mmol) and the MWCNTs ($1{,}006 \cdot 10^{3}$ mg) in the CH_2Cl_2 dry (50 ml). The blend was stirred for 2 hours at room temperature. The product was filtered, washed with CH_2Cl_2 (~ 30 ml) and dried for overnight in vacuum. The product obtained was ≈ $1{,}092 \cdot 10^{3}$ mg.

- **Functionalization of MWCNTs with pyrene-G1**

The π – stacking interaction between the pyrene-G1 and the MWCNTs was obtained mixing in the reaction flask the pyrene-G1 (176 mg, $1.54 \cdot 10^{-1}$ mmol) and the MWCNTs (889 mg) in the CH_2Cl_2 dry (60 ml). The blend was stirred for 2 hours at room temperature. The product was filtered, washed with CH_2Cl_2 (~ 30 ml) and dried for overnight in vacuum. The product obtained was ≈ 998 mg.

SECTION 3.1.2.2

3.1.2.2 METATHESIS TEST OF MWCNTs-PYRENE-HG2 AND MWCNTs-PYRENE-G1

- **ROMP of 2-norbornene with MWCNTs-pyrene-HG2**

The polymerization was carried out in a reaction flask of 250 ml with 99 ml of dry THF, 2-norbornene (903.7 mg, $9.60 \cdot 10^{-3}$ mol) and MWCNTs-pyrene-HG2 (3.5 mg, $8.42 \cdot 10^{-5}$ mmol). The mixture was stirred for about 17 hours at room temperature. The polymerization was stopped with some drops of ethylvinyl ether and coagulation in ethanol did not give any products.

- **ROMP of 2-norbornene with MWCNTs-pyrene-G1**

The polymerization was carried out in a reaction flask of 250 ml with 99 ml of dry THF, 2-norbornene (927.3 mg, 9.85 mmol) and pyrene-HG2 (3.2 mg, $3.05 \cdot 10^{-4}$ mmol). The mixture was stirred for about 5 hours at room temperature. The polymerization was stopped with some drops of ethylvinyl ether and the polymer was coagulated in ethanol. The polymer obtained, after drying under vacuum overnight, was ~ 11 mg.

- **ROMP of 5-ethyliden-2-norbornene with MWCNTs-pyrene-HG2**

The polymerization was carried out in bulk in a vial of 4 ml with 5-ethyliden-2-norbornene ($1.01 \cdot 10^3$ mg, 8.38 mmol) and MWCNTs-pyrene-HG2 (5.0 mg, $4.77 \cdot 10^{-4}$ mmol). The mixture was stirred for about 17 hours at room temperature. The polymerization was stopped with some drops of ethylvinyl ether and the polymer was coagulated in ethanol. The polymer obtained, after drying under vacuum overnight, was ~ 4 mg.

- **ROMP of 5-ethyliden-2-norbornene with MWCNT-pyrene-G1**

The polymerization was carried out in bulk in a vial of 4 ml with 5-ethyliden-2-norbornene ($1.08 \cdot 10^3$ mg, 9.03 mmol) and MWCNTs-pyrene-G1 (4.9 mg, $4.68 \cdot 10^{-4}$ mmol). The mixture was stirred for about 4 hours and 30 minutes at room temperature. The polymerization was stopped with some drops of ethylvinyl ether and the polymer was coagulated in ethanol. The polymer obtained, after drying under vacuum overnight, was ~ 5 mg.

SECTION 3.1.2.4

FUNCTIONALIZATION OF GRAPHITE WITH PYRENE-Ru-BASED CATALYSTS

- **Synthesis of graphite-pyrene-norbornene**

In a vial of 20 ml was added the graphite (200 mg), pyrene-norbornene (102 mg, $2.59 \cdot 10^{-1}$ mmol) and dry CH_2Cl_2 (10 ml). The mixture was stirring for 2 hours at room temperature and then was filtered and washed with dry CH_2Cl_2 (~ 100 ml). The product was recovered and dried in vacuum overnight. The product obtained was 175 mg.

- **Synthesis of graphite-pyrene-HG2**

In a Schlenk reaction flask of 50 ml was added 175 mg of graphite-pyrene-norbornene (corresponding to 100 mg of pyrene-norbornene, $2.53 \cdot 10^{-1}$ mmol), HG2 (30.6 mg, $4.88 \cdot 10^{-2}$ mmol) and dry hexane (30 ml). The mixture was stirring in N_2 for 16 hours at room temperature and then was filtered and washed with CH_2Cl_2 (~ 100 ml). The product was recovered and dried in vacuum overnight. The product obtained was 160 mg.

SECTION 3.1.2.5

METATHESIS TEST OF GRAPHITE-PYRENE-HG2

- **ROMP of 2-norbornene with graphite-pyrene-HG2**

The polymerization was carried out in a reaction flask of 250 ml with 99 ml of dry THF, 2-norbornene (921.6 mg, 9.79 mmol) and graphite-pyrene-HG2 (3.5 mg, $2.10 \cdot 10^{-4}$ mmol). The mixture was stirred for about 15 minutes at room temperature. The polymerization was stopped with some drops of ethylvinyl ether and the polymer was coagulated in ethanol. The polymer obtained, after drying under vacuum overnight, was ~ 26 mg.

SECTION 3.2.1

SYNTHESIS OF POLYMER-PYRENE

- **Synthesis of polynorbornene-pyrene**

In a reaction flask of 250 ml was added the pyrene-HG2 (78.6 mg, 0.072 mmol) and the 2-norbornene (678 mg, 7.2 mmol) in 135 ml of dry CH_2Cl_2. The mixture was stirring for 2 h at room temperature. The polymerization was stopped with some drop of ethylvinyl ether and the solvent has been removed in vacuum.

- **Synthesis of polybutadiene-pyrene**

The synthetic procedure is the same reported for the polynorbornene-pyrene. The reagent used was pyrene-HG2 (129.6 mg, 0.12 mmol), cyclooctadiene ($1.294 \cdot 10^3$ mg, 12 mmol) and 150 ml of dry CH_2Cl_2.

- **Synthesis of polyethylene-pyrene**

In a reaction flask was added the polybutadiene-pyrene (300 mg), 30 ml of xylene and p-toluenesulfonyl hydrazide (1.5 g, 8.05 mmol). The mixture was stirred at 100 °C for 18 h. The product was filtered and washed with xylene and diethyl ether, and after dried in vacuum was 275 mg.

- **Synthesis of polynorbornene**

In a reaction flask of 250 ml was added the HG2 (29.1 mg, 0.046 mmol) and the 2-norbornene (473 mg, 4.64 mmol) in 85 ml of dry CH_2Cl_2. The mixture was stirred for 16 h at room temperature. The polymerization was stopped with some drop of ethylvinyl ether and the solvent has been removed in vacuum.

- **Synthesis of polybutadiene**

The synthetic procedure is the same reported for the polynorbornene. The reagent used was HG2 (31.7 mg, 0.051 mmol), cyclooctadiene (547 mg, 5.06 mmol) and 95 ml of dry CH_2Cl_2.

- **Synthesis of polyethylene**

In a reaction flask was added the polybutadiene-pyrene (200 mg), 20 ml of xylene and p-toluenesulfonyl hydrazide (1 g, 5.37 mmol). The mixture was stirring at 100 °C for 18 h. The product was filtered and washed with xylene and diethyl ether and after dried in vacuum.

- **Interaction pyrene-polymer and graphite**

The polymer was dissolved in chloroform, for each 100 mg of polymer was used 20 ml of solvent, the ratio between graphite and polymer was 1:1 by weight. Once upon the polymer was completely dissolved was added the graphite and the solution was stirred for 16 h. The solvent was removed in vacuum.

SECTION 3.3

ELECTRICAL PROPERTIES OF THE PYRENE-CARBON NANOFILLER

- **Synthesis of MWCNTs-pyrene butyric acid**

In the reaction flask was added the 1-pyrene-butyric acid (100 mg, $3.46 \cdot 10^{-1}$ mmol) and the nanofiller (≈ 1 g) in the CH_2Cl_2 dry (50 ml). The blend was stirred for 2 hours at room temperature. The product was filtered, washed with CH_2Cl_2 (30 ml) and dried overnight in vacuum. The product obtained was ≈ 1.080 g.

CONCLUSION

A non-covalent functionalization of the carbon nanofiller with pyrene allow to preserve the excellent properties of the filler and to optimize the time of reaction thanks the versatility of the complex pyrene-Ru-based catalyst, that can be linked on any substrate able to give the π – stacking interaction.

Furthermore, such type functionalization is useful to reduce the phenomenon of agglomeration of filler when it is dispersed within the polymeric matrix thus improving the manufacturing process.

The application of carbon nanofillers has the purpose of improve electrical and mechanical properties of the materials, but show a real problem regards the non-homogeneous dispersion. The pyrene-catalyst allows to obtain materials in which carbon nanofiller is homogeneously dispersed through the use of a polymer as compatibilizer. The polymer has a terminal pyrene that is able to bind the polymer on the surface of carbon filler without modifying the structure of the graphitic plane. In this way any polymer can be linked to any carbon filler preserving the properties of the latter.

Moreover, in presence of the complex pyrene-carbon filler, an improvement of the electrical conductivity, even of an order of magnitude, is observed above the electrical percolation threshold.

REFERENCES

[1] S. Iijima. *Nature*, 56, 354, **1991**.

[2] J. Kong, M. Franklin, C. Zhou, M. Chapline, S Peng, K. Cho and H. Dai. *Science*, 622, 287, **2000**.

[3] J. Kong, M. Chapline and H. Dai. *J. Am. Chem. Soc.*, 3838, 123, **2001**.

[4] F. J. Gòmez, R. J. Chen, D. Wang, R. M. Waymouth and H. Dai. *Chem. Commun*, 190-191, **2003**.

[5] L. Guadagno, M. Raimondo, U. Vietri, L. Vertuccio, G. Barra, B. De Vivo, P. Lamberti, G. Spinelli, V. Tucci, R. Volponi. *RSC Advances,* 5(8), 6033-6042, **2015**.

[6] L. Guadagno, M. Raimondo, V. Vittoria, L. Vertuccio, C. Naddeo, S. Russo, B. De Vivo, P. Lamberti, G. Spinelli, V. Tucci. *RSC Advances*, 4(30), 15474-15488, **2014**.

[7] M.R. Nobile, M. Raimondo, K. Lafdi, A. Fierro, S. Rosolia, L. Guadagno. *Polymer Composites*, 36(6), 1152-1160, **2015**.

[8] L. Guadagno, M. Raimondo, L. Vertuccio, M. Mauro, G. Guerra, K. Lafdi, B. De Vivo, P. Lamberti, G. Spinelli, V. Tucci. *RSC Advances*, 5(46), 36969-36978, **2015**.

[9] B. De Vivo, P. Lamberti, G. Spinelli, V. Tucci. *Journal of Applied Physics*, 115(15), 154311, **2014**.

CHAPTER 4

RADICAL POLYMERIZATION OF STYRENE FOR SELF-HEALING APPLICATIONS

4.1 POLYMERIZATION OF THE STYRENE AT ROOM TEMPERATURE WITH Cu(0) CATALYST

The living controlled radical polymerization of styrene at room temperature is rarely reported. Cu(0) mediated radical polymerization of styrene at room temperature was investigated for the self-healing of materials. Despite the mechanism of Cu(0) mediated controlled radical polymerization is still debated in literatures [2-5], Cu(0) mediated controlled radical polymerization catalyst has shown its advantages respect to other living controlled radical polymerizations [2,6]: low reaction temperature (room temperature), small amount of catalyst, ultrafast polymerization and high molecular weight with narrow molecular weight distributions of the obtained polymers. Cu(0) mediated controlled radical polymerization is an atom transfer radical polymerization, in which Cu(0) is the active catalytic species. In particular, Cu(0) in the initiator reaction forms Cu(I), this last disproportionate to form Cu(0) and Cu(II). The Cu(0) is also able to reduce the excess of Cu(II) to

regenerate active Cu(I) [3-5], then the Cu(0) is restored.

The use of Cu(0) as the living controlled radical polymerization catalyst directly is interesting, since it is cheaper and easier to be handled than Cu(I) or Cu(II) complexes. Besides, Cu(0) is highly active and the polymerization could be conducted at room temperature.

The innovation proposed in this work regards also the type of initiator used: i.e.: the methyl-2-bromopropionate (MBP, *Fig. 4.1*), instead of classic peroxydic derivate, that is more difficult to manipulate. The ligand used was N,N,N',N'',N''-pentamethyldiethylentriamine (PMDETA, *Fig. 4.2*).

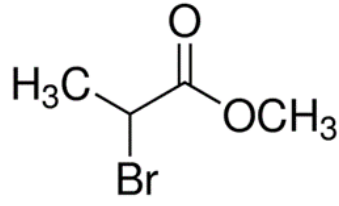

Figure 1: methyl-2-bromopropionate

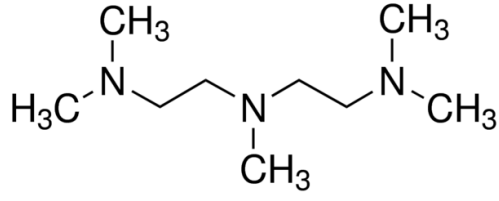

Figure 4.2: N,N,N',N'',N''-pentamethyldiethylentriamine

The reaction conditions were modulated at the molar ratios of Styrene: MBP: Cu(0): PMDETA = 200: 1: 1: 1; Cu(0) powder with

a particle size of 60-80 nm was used as primary activating species. The schematic representation of the reaction of polymerization of the styrene is shown in *Fig. 4.3*.

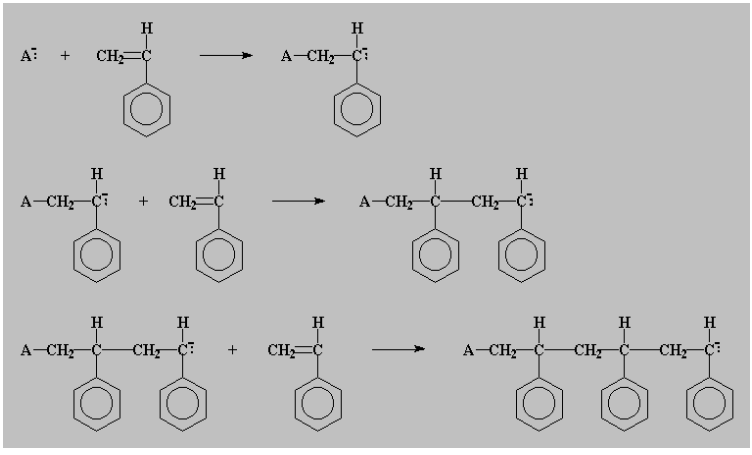

Figure 4.3: Schematic representation of the reaction of polymerization of the styrene ($A:^-$ is the initiator).

As described previously, the healing agent converts in a polymer that have a high degree of crosslinking because must allow to improve the mechanical properties of the material in which are incorporated. For this purposes it was choosen to perform the radical polymerization with a mixture of styrene and divinylbenzene that allows to obtain a crosslinked polymer (*Fig. 4.4*). The addition of the divynilbenzene permits to combining at the same time the self-

healing ability with the improvement of the resistance of the material.

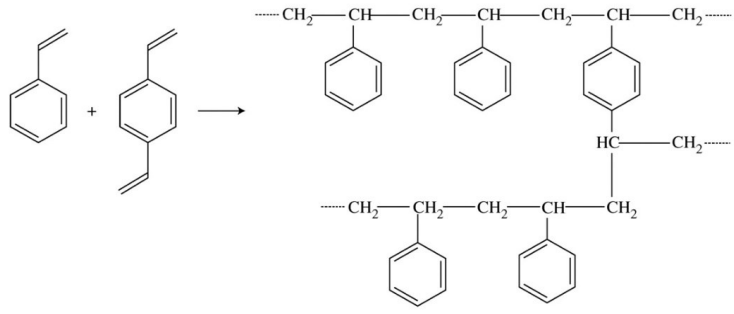

Figure 4.4: Polystyrene-divinylbenzene

The efficiency of the catalytic system was also verified at 70 °C and at 0 °C, to test the resistance of the catalysts at different conditions. This polymerization was carried out treating the system Cu(0)-PMDETA in DMF for 2 hours at the temperature selected and then adding the monomer. The polymerizations gave a conversion of 11.2 % at 0 °C and 15.0 % at 70 °C. The exhaustion extraction in boiling decaline of the Polystyrene-divinylbenzene 7:3 allows us to determine the percentage of crosslinked polymer. The result obtained was 97 % of insoluble fraction. The Mn and Mw/Mn values were determine by GPC and was $M_n = 20550$ and $M_w/M_n = 2.15$.

The results obtained made this new catalytic system a promising candidate for the self-healing application.

4. 2 EXPERIMENTAL PART

- **Polymerization of styrene at room temperature**

In a 25 mL flask was added the solvent dimethylformamide (DMF, 5.00 mL), catalyst Cu(0) (27.6 mg, 0.435 mmol) and ligand N,N,N',N'',N''-pentamethyldiethylentriamine (PMDETA, 87 µL, 0.418 mmol). The mixture was stirred for 10 minutes, then was added the initiator methyl-2-bromopropionate (45 µL, 0.435 mmol) and 10 mL of monomers (distilled styrene, 7 mL, 60.9 mmol; distilled divinylbenzene, 3 mL, 21.1 mmol; the distillation of styrene and divinylbenzene was conduct with CaH_2). The solution was deoxygenated by bubbling with nitrogen for 20 minutes. The reaction flask then was placed in a stirred oil bath equipped with a thermostat at 25 °C. The suspension was stirred for 16 h under nitrogen. After this time the flask was cooled by ice water. Afterward, the flask was opened, and the contents were dissolved in 25 mL of tetrahydrofuran (THF) and passed through a small basic Al_2O_3 chromatographic column to remove any unreacted Cu(0) catalyst and Cu(II) compound. The resultant solution was precipitates into about 150 mL of cold methanol under stirring. The polymer was isolated by filtration and dried under vacuum overnight. The product obtained was 2.30 g. The monomer conversion was 25 %.

- **Polymerization of the styrene at 70 °C**

In a 25 mL reaction flask was added the solvent dimethylformamide (DMF, 5.00 mL), catalyst Cu(0) (27.6 mg, 0.435 mmol) and ligand N,N,N',N'',N''-pentamethyldiethylentriamine (PMDETA, 88 μL, 0.421 mmol). The solution was deoxygenated by bubbling with nitrogen for 20 minutes and then was heating at 70 °C in a stirred oil bath equipped with a thermostat for 2 h. After this time, the mixture was reported at room temperature and was added the initiator methyl-2-bromopropionate (47.5 μL, 0.348 mmol) and 10 mL of monomers (distilled styrene, 10 mL, 87.0 mmol). The suspension was stirred for 16 h under nitrogen at 25 °C. After this time the flask was cooled by ice water. Afterward, the flask was opened, and the contents were dissolved in 25 mL of tetrahydrofuran (THF) and passed through a small basic Al_2O_3 chromatographic column to remove any unreacted Cu(0) catalyst and Cu(II) compound. The resultant solution was precipitates into about 150 mL of cold methanol under stirring. The polymer was isolated by filtration and dried under vacuum overnight. The product obtained was 1.36 g. The monomer conversion was 15 %.

- **Polymerization of the styrene at 0 °C**

In a 25 mL reaction flask was added the solvent dimethylformamide (DMF, 5.00 mL), catalyst Cu(0) (27.6 mg, 0.435 mmol) and ligand N,N,N',N'',N''-pentamethyldiethylentriamine (PMDETA, 88 μL,

0.421 mmol). The solution was deoxygenated by bubbling with nitrogen for 20 minutes and then was cooled in ice water bath at 0 °C for 2 h. After this time, the mixture was reported at room temperature and was added the initiator methyl-2-bromopropionate (47.5 μL, 0.348 mmol) and 10 mL of monomers (distilled styrene, 10 mL, 87.0 mmol). The suspension was stirred for 16 h under nitrogen at 25 °C. After this time the flask was cooled by ice water. Afterward, the flask was opened, and the contents were dissolved in 25 mL of tetrahydrofuran (THF) and passed through a small basic Al_2O_3 chromatographic column to remove any unreacted Cu(0) catalyst and Cu(II) compound. The resultant solution was precipitates into about 150 mL of cold methanol under stirring. The polymer was isolated by filtration and dried under vacuum overnight. The product obtained was 1.02 g. The monomer conversion was 11.2 %.

CONCLUSION

The self-healing of damage materials could be obtained thought radical polymerization rather than metathesis reaction, so that to use a Cu(0) based catalyst, very less expensive than the Ru catalysts.
The radical polymerization of the styrene-divynilbenzene at room temperature, rarely reported in literature, allows to obtain a crosslinked polymer, capable to improve the properties of the materials in which the self-healing reaction occur.

REFERENCES

[1] X. Zhang, Y. Wu, J. Huang, X. Miao, Z. Zhang and X. Zhu, *Chinese Journal of Polymer Science* Vol. 31, No. 4, 702-712, **2013**.

[2] V. Percec, T. Guliashvili, J. S. Ladislaw, A. Wistrand, A. Stjerndahl, M. J. Sienkowska, M. J. Monteiro and S. Sahoo, *J. Am. Chem. Soc.*,128-143, 14156, **2006**.

[3] K. Matyjaszewski, S. Coca, S. G. Gaynor, M. L. Wei and B. E. Woodworth. *Macromolecules*, 23-30, 7348, **1997**.

[4] K. Matyjaszewski, N. V. Tsarevsky, W. A. Braunecker, H. Dong, J. Huang, W. Jakubowski, R. Nicolay, W. Tang and J. A. Yoon. *Macromolecules*, 22-40, 7795, **2007**.

[5] C. Y. Lin, M. L. Coote, A. Gennaro and K. Matyjaszewski. *J. Am. Chem. Soc.*, 130-138, 12762, **2008**.

[6] B. M. Rosen and V. Percec. *Chem. Rev.*,109-111, 5069, **2009**.

MATERIALS AND TECHNIQUES

- MATERIALS

All chemical products (reagent quality) were purchased from Sigma Aldrich Company and were used without further purification.

All reactions involving air sensitive reactants were carried out in oven-dried glassware under nitrogen atmosphere with anhydrous solvents, using standard Schlenk techniques and glovebox techniques. All filtration techniques are carried out at the air.

Hexane was distilled from sodium/benzophenone. CH_2Cl_2 was dried on CaH_2, tetrahydrofuran (THF) on lithium aluminum hydride ($LiAlH_4$) and freshly distilled before use.

The graphene oxide GO used was prepared starting from the high surface area graphite (G) (trade name Synthetic Graphite 8427) from Asbury Graphite Mills Inc., with a minimum carbon wt % of 99.8 and a surface area of 330 m^2/g. The latter is oxidized by the Staudenmaier method, which involves treatment with H_2SO_4, HNO_3 and $KClO_3$ for 120 hours at room temperature [1].

This treatment allows both obtain oxidized groups, such as epoxy, oxydryl, carbonyl and carboxyl groups, to be introduced on each single layer and at the same time leads to graphite exfoliation.

MWCNT are produced via the catalytic carbon vapor deposition (ccvd) process. Nanotubes which exit the reactor are then purified to greater than 95% carbon.

Cross-linked fraction of metathesis polymer was determined, according to the ASTM method D2765-84, as the percent of the

original weight of the sample extracting for 6 h in boiling decahydronaphthalene (decaline, a mixture of cis and trans isomers). The extraction was followed by drying at 150 °C in a vacuum oven.

- TECHNIQUES

Thermogravimetric analysis (TGA) was carried out in air using a Netzsch TG 290 F1 thermal analyzer. The temperature range was 25–1000 °C at a heating rate of 10 °C min^{-1}. The weight loss was recorded as a function of the temperature.

FT/IR spectra were obtained at a resolution of 2.0 cm^{-1} with a FT/IR (BRUKER Vertex 70 and Tensor 27) spectrometer equipped with deuterated triglycine sulfate (DTGS) detector and a KBr beam splitter, using KBr pellets prepared with a 6-atm press. The frequency scale was internally calibrated to 0.01 cm^{-1} using a He-Ne laser. 32 scans were signal averaged to reduce the noise.

Field emission scanning electron microscopy (FESEM) pictures were obtained with a LEO 1525 microscope. The samples were covered with a 250 Å thick gold film using a sputter coater (Agar mod. 108 A).

Wide-angle X-ray diffraction (WAXD) patterns were obtained by an automatic Bruker D8 Advance diffractometer, in reflection, at 35 KV and 40 mA, using the nickel-filtered Cu Kα radiation (λ = 1.5418 Å). The X-ray diffraction profiles were recorded in the range of 2θ = 2-100 °, by scanning with a pitch of 0.03 ° and with a collection time of one second per point.

The evaluation of the crack-healing efficiency of the composite materials was investigated by using a dynamic mechanical thermoanalyzer (TA instrument-DMA 2980). Solid samples with dimensions

3 x 10 x 35 mm were tested by applying a variable flexural deformation in single cantilever mode. A V-shaped starter notch, 1 mm depth and 2 mm wide, was machined close to the sample extremity (*Fig. 1*). The test protocol combines three different steps. In the first step, the notched sample was analyzed under the dynamic flexural deformations for about 300 s in order to determine the pristine elastic modulus. After that, the oscillation was stopped and a sharp precrack was created in the samples by gently tapping a fresh razor blade into a machined starter notch. An impulsive load of about 20Nwas immediately applied to the specimen in order to produce a crack propagation along the virgin crack plane. At this point, the dynamic monitoring of the sample was conducted at constant temperature, with a displacement amplitude set to 0.1% and a frequency to 1 Hz. Several test conditions were investigated in order to obtain a reasonable picture of the amount and time of recovery without influencing the healing mechanisms.

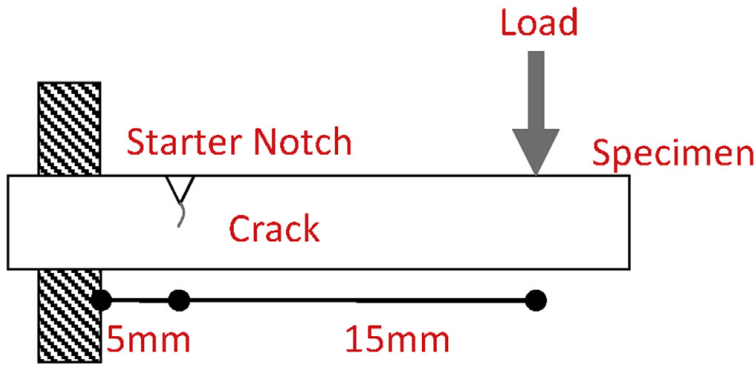

Figure 25:. Test geometry adapted for the healing tests.

Methods The Transmission Electron Microscopy (TEM) characterization was performed on a Jeol 2010 LaBa6 microscope operating at 200 kV. MWCNTs were dispersed (in ethanol) by ultrasonic waves for 30 min. The obtained suspension was dropped on a copper grid (holey carbon).

The electrical characterization of the nanocomposites was performed on disk shaped specimen of about 2mm of thickness and 50mm of diameter. In order to reduce possible surface roughness and to ensure an ohmic contact with the measuring electrodes the samples were coated by using a silver paint with a thickness of about 50 μm and a surface resistivity of 0.001 Ω·cm. The measurement system, remotely controlled by the software LABVIEW®, is composed by a suitable shielded cell with temperature control, a multimeter Keithley 6517A with function of voltage generator (max ±1000V) and voltmeter (max ± 200 V) and an ammeter HP34401A (min current 0.1μA) for samples above the EPT. For those below the percolation threshold the system is composed only by a multimeter Keithley 6517A with function of voltage generator (max ±1000V) and pico-

ammeter (min current 0.1fA).

The fluorescence characterization was conduct with a Fluorescence Spectrophotometer VARIAN CARY ECLIPSE composed by two Czerny-turner monochromators (excitation and emission) with a Xenon light source.

The ultrasonicator used was Hielscher model UP200S-24KHz high power ultrasonic probe.

The ^{1}H and ^{13}C NMR spectra were recorded at room temperature, using a Bruker AVANCE-III 250-300-400 MHz instruments.

[1] M. Mauro, V. Cipolletti, M. Galimberti, P. Longo, G. Guerra; The journal of physical chemistry, 2012, 116, 24809−24813.

General conclusion

The self-healing ability of the engineering material used for the design of the aeronautical components can prolong the life of the material itself thanks the repairing mechanisms that starts at the same moment in which the materials are damages. The healing process takes place by ring opening metathesis polymerization of a microencapsulated healing agent which reacts with a catalysts based on ruthenium: i.e. Grubbs and Hoveyda-Grubbs of 1st and 2nd generation. For aeronautical materials to have this property, the amount of catalyst that needs to be dispersed in them is very high and very expensive, but it is considerably reduced if the catalysts are supported on the carbon nanoparticles, as graphite, graphene or carbon nanotubes. Furthermore, the possibility to integrate the very interesting properties of graphene based-particles inside thermosetting self-healing materials represents one of the most pursued targets for many industrial applications.

The ruthenium catalyst was covalently bonded on the GO and result active in this aeronautic composite material up to 90 °C. The catalytic site protected by polymeric globular shell, that isolate the catalytic systems by very reactive environment such as oxirane rings of epoxy resins, is active up to 140 °C.

The results obtained are very promising considering that, for the developed systems, the amount of the Ru-based catalysts bonded to the graphene sheets is lower than 0.5 % wt with respect to the epoxy mixture; whereas, utilizing powders of Grubbs' catalyst, a high amount (~5% wt) is necessary to activate self-healing mechanisms

in thermosetting resins. This allows to considerably reduce the costs of the composite.

The MWCNTs can be functionalized whit the ROMP catalysts through a covalent mode that leaves intact the graphitic plane, both by electrochemical modification and cycloaddition, but in this case the nearness of the catalytic site to the filler considerably reduce the activity of the catalyst.

The functionalization through π – stacking, using as catalytic complex pyrene-catalyst allows to preserve the extraordinary properties of the filler, as the thermodynamic stability, extremely high charge carrier mobility, mechanical stiffness, and optical properties and furthermore permits of reduced the time of the reaction because can be linked on any filler able to give this non covalent interaction.

Furthermore, the use of the pyrene in the thermosetting resins increases of an order of magnitude the electrical conductibility of the materials.

A new generation of self-healing system can be obtained by substitution of the ruthenium catalyst with a Cu(0) based catalyst, very less expensive. The repairing mechanism would be a radical polymerization of the styrene-divynilbenzene at room temperature, rarely reported in literature.

The carbon-based nanomaterials, due to their unique combinations of chemical and physical properties, are used as fillers in the composite materials for various industrial applications to improve their performances, but the dispersion is very critical because they tend to aggregate when are added to the matrix. A possible solution

is to utilize a polymer as compatibilizer.

The system pyrene-catalyst can be used for the polymerization of selected monomers at the aim to obtain a polymer with a terminal pyrene that allows it to bond on any filler. This polymer, having a pyrene as chain end, can be used in the composite material because allows to have a homogeneous dispersion of the filler in the matrix, as highlighter by the microscopy images.